



Thèse

2009

Open Access

This version of the publication is provided by the author(s) and made available in accordance with the copyright holder(s).

---

Polymeric immunonanoparticles for active tumor targeting: preparation,  
characterization and "in vivo" evaluation

---

Cirstoiu, Adriana

**How to cite**

CIRSTOIU, Adriana. Polymeric immunonanoparticles for active tumor targeting: preparation, characterization and 'in vivo' evaluation. 2009. doi: 10.13097/archive-ouverte/unige:8513

This publication URL: <https://archive-ouverte.unige.ch//unige:8513>

Publication DOI: [10.13097/archive-ouverte/unige:8513](https://doi.org/10.13097/archive-ouverte/unige:8513)

UNIVERSITÉ DE GENÈVE

Section des sciences pharmaceutiques  
Laboratoire de pharmacie galénique  
et biopharmacie

FACULTÉ DES SCIENCES

Professeur Robert Gurny  
Docteur Florence Delie

**Polymeric immunonanoparticles for active tumor targeting:  
Preparation, characterization and *in vivo* evaluation**

THESE

présentée à la Faculté des sciences de l'Université de Genève  
pour obtenir le grade de Docteur ès sciences, mention sciences pharmaceutiques

par

Adriana Cirstoiu

de

Solca (Roumanie)

Thèse N°: 4145

Genève

Atelier de reproduction Repromail

2009

(IMPRIMATUR)

A Emanuel et Gabriela,  
à ma famille



## Remerciements

Je remercie les membres du jury, le Professeur Jörg Kreuter (Johann Wolfgang Goethe-Universität, Frankfurt am Main) et le Professeur Elias Fattal (Université de Paris XI, Châtenay Malabry), pour avoir accepté d'évaluer ce travail de thèse.

Je tiens à adresser mes grands remerciements au Professeur Robert Gurny pour m'avoir donné l'opportunité de réaliser un de mes rêves professionnels et d'accomplir cet intéressant travail de thèse dans d'excellentes conditions. J'exprime également ma grande reconnaissance aux co-directeurs de cette thèse, Dr. Florence Delie et Dr. Franz Buchegger.

Merci beaucoup Robert pour tous vos conseils et vos remarques constructives qui m'ont aidée à améliorer mes compétences dans le domaine de la recherche.

Merci Florence pour ta grande disponibilité, tes bons conseils, tes encouragements, tes corrections, et pour avoir toujours suivi le déroulement et l'avancement de ce travail ; merci aussi pour ton éternel optimisme et pour ne pas m'avoir laissée « me jeter dans l'Arve » dans les moments critiques de la thèse. Par ailleurs, j'ai beaucoup apprécié d'être assistante pour les TPs de pharmacie galénique.

Merci Franz pour les précieux conseils et la vive participation à la réalisation de ce travail.

J'aimerais également exprimer ma reconnaissance au Dr. Leila Bossy Nobs pour m'avoir transmis son savoir faire dans le domaine des immuno-nanoparticules.

Mes remerciements s'adressent au Dr. Norbert Lange et Dr. Xavier Montet pour l'aide précieuse apportée dans la réalisation de l'expérience de bioluminescence.

Merci à Brigitte Delavy pour les nombreux échantillons d'origine animale que nous avons broyé ensemble dans le cadre de l'expérience de biodistribution.

Ma gratitude s'adresse également à tous les membres du Laboratoire de pharmacie galénique, pour la bonne ambiance qui règne dans ce labo.

Particulièrement, merci beaucoup chère Myrtha pour votre grande gentillesse, votre bonne humeur et la capacité de voir toujours le bon côté de choses.

Merci Marco d'avoir toujours veillé sur le bon fonctionnement des appareils et pour les longues discussions au sujet des plantes.

Je remercie les anciennes locataires du labo 492 : Angelica, Magali, Nicoleta, Aude pour les bons moments passés ensemble et les discussions intéressantes sur des sujets professionnels et personnels. Merci Angelica pour ton amitié, ta gentillesse et ton soutien.

Chère Nicoleta, c'était un grand plaisir d'avoir partagé le même bureau avec toi en tant que compatriote, collègue et amie et d'avoir eu la chance de dire chaque matin «Buna ziua ». Mi-ai fost un bun exemplu de curaj si motivatie. Iti multumesc pentru toate discutiile interesante atat profesionale cat si personale.

Cher Pol, merci pour ton amitié, tes bons conseils dans tous les domaines, merci d'avoir partagé avec moi le repas du midi, la bonne salade accompagnée de mozzarella, et aussi, pour les moments de détente à la piscine des Vernets et sur le terrain de badminton. Je te souhaite de finir vite ton travail parce que tu le mérites bien.

Bonne chance Karine sur la dernière ligne droite! C'était sympa d'avoir vu grossir nos ventres en même temps pour une bonne cause.

Je remercie tous mes présents et anciens collègues: Maria Fernanda, Caterina, Gesine, Emilie, Marta, Ludmila, Nawal, Simon, Claudia, Claudia di Tomaso, Marie-Christine, Leila, Doris, Martinus, Bartelemy, Frederic, Rocio, Sergio, Nicolas, Sabine, Marino pour leur amitié et leur bonne humeur.

Je souhaite aux nouvelles venues, Julie et Benedicte, avec les lesquelles j'ai partagé le bureau pendant mes derniers mois de thèse, bonne chance dans leur recherche et que leur travail soit couronné de succès.

Finalement, je tiens à remercier de tout cœur ma famille et mon frère, Adrian, pour leurs soutien et encouragements. Merci spécialement à Emanuel, pour son amour et sa patience. Merci à ma petite Gabriela d'avoir apporté un peu de « sel et poivre », mais, aussi beaucoup de soleil dans ma vie.



## Table of contents

|  |     |
|--|-----|
| <b>Introduction</b> .....  | 10  |
| <b>Chapter I.</b> Differential tumor cell targeting of anti-HER2 (Herceptin <sup>®</sup> ) and anti-CD20 (Mabthera <sup>®</sup> ) coupled nanoparticles.....   | 29  |
| <b>Chapter II.</b> Nanomedicines for active targeting: Physico-chemical characterization of paclitaxel-loaded anti-HER2 immunonanoparticles and <i>in vitro</i> functional studies on target cells.....                  | 48  |
| <b>Chapter III.</b> The benefits of anti-HER2 paclitaxel-loaded immunonanoparticles in treatment of disseminated ovarian cancer overexpressing specific receptors: Therapeutic efficacy and biodistribution in mice..... | 72  |
| <b>Conclusions and Perspectives</b> .....  | 96  |
| <b>Résumé</b> .....  | 100 |
| <b>Abbreviations</b> .....   | 106 |

## Table of Contents

---

---

## Introduction

Despite significant progress in chemotherapy, cancer remains the second leading cause of death after cardiovascular diseases<sup>1</sup>. The main limitation of conventional chemotherapy is the non-specific distribution of drugs to cancerous and normal tissues leading to high toxicity and serious side effects. Also, the low therapeutic index of these agents and the development of multi-drug resistance results in a suboptimal treatment. Recent advances in the understanding of the molecular biology of cancer have been exploited to achieve more selective treatments. In this way, new delivery technologies are in development to improve the therapeutic efficacy of anti-cancer drugs. Drug carrier systems such as polymeric and protein nanoparticles, liposomes, micelles or dendrimers have emerged as promising treatment approaches with several major advantages including improved therapeutic index by preferential localization at the target sites and reduced distribution in healthy tissues, delivery of hydrophobic drugs, high drug loading capacity and controlled release rate, the possibility to escape multi-drug resistance, and combinations of imaging and drug therapy to monitor effects in real time or possibility to attach recognition moieties for active targeting<sup>2,3</sup>.

The strategies using nanocarriers systems for drug delivery at target sites are focused on passive and active targeting. The principle of these approaches is represented in Figure 1.

Passive delivery refers to the transport of nanomedicines into the solid tumor interstitium and cells by passive diffusion or convection<sup>4</sup>. Passive targeting occurs through enhanced permeability and retention (EPR) effect and favors the accumulation of drug within the tumor interstitium more than ten fold higher than in normal tissue<sup>5</sup>. EPR effect is due to leaky tumor vasculature presenting fenestrations between 100 and 800 nm in contrast to endothelial junctions of normal vessels ranging from 5 to 10 nm, and, poor lymphatic drainage. These tumor features favor the extravasation and retention of nanoparticles within the targeted region<sup>6-8</sup>.

The physico-chemical properties of nanomedicines including size as well as surface characteristics dictate their pharmacokinetics and biodistribution since these parameters

determine the uptake of nanomedicines by macrophages present within the organs of the reticulo-endothelial system (RES) such as the liver and spleen.

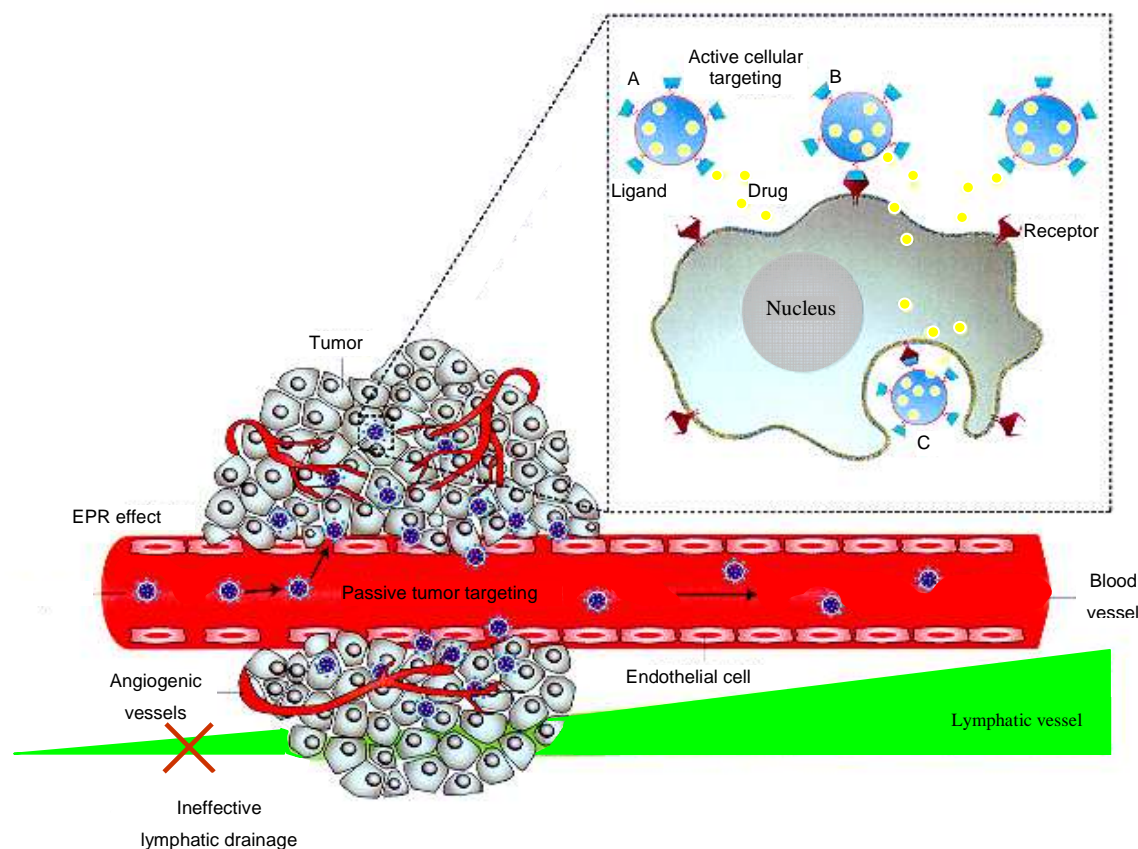


**Figure 1.** Polymeric nanoparticles are shown as representative nanocarriers (circles). Passive tissue targeting is achieved by extravasation of nanoparticles through increased permeability of the tumor vasculature and ineffective lymphatic drainage (EPR effect). Active cellular targeting (inset) can be achieved by functionalizing the surface of nanoparticles with ligands that promote cell-specific recognition and binding. The nanoparticles can (A) release their contents in close proximity to the target cells; (B) attach to the membrane of the cell and act as an extracellular sustained-release drug depot; or (C) internalize into the cell (reproduced from Peer et al.)<sup>9</sup>.

Particles ranging from 50 to 250 nm avoid, on the one hand, the entrapment by hepatic and splenic endothelial fenestrations and, the other hand, the extravasation into healthy tissues, thereby promoting accumulation at target sites. Furthermore, the grafting of their surface with hydrophilic molecules such as poly-ethylene glycols (PEGs) allows a longer circulation time,

and, consequently, an increase in efficacy of resultant “stealth NPs” by escaping macrophage clearance<sup>10,11</sup>.

Cationic liposomes are increasingly being researched due to their favourable interactions with negative charge of phospholipids present in the angiogenic endothelial cells<sup>12,13</sup>.

The external application of physical factors such as a magnetic field or light can lead to an improvement of local accumulation and/or efficacy of superparamagnetic nanocarriers or those containing photosensitizers<sup>14,15</sup>.

Despite extensive research in nanomedicine field, only a few formulations are available on the market for cancer treatment. Albumin bound paclitaxel nanoparticles (Abraxane<sup>®</sup>) approved by FDA in 2005 for the treatment of metastatic breast cancer has improved administration and efficacy of drug. Intratumoral accumulation of paclitaxel (Tx) was found to be 30% higher for Abraxane<sup>®</sup> than Taxol<sup>®</sup>, containing Tx dissolved in a mixture of Cremophor El and ethanol, in a breast xenograft model<sup>16</sup>. A phase III clinical study demonstrated a higher overall response rate (33 % vs 19 %) and a longer time to tumor progression (23 vs 17 weeks) for Abraxane<sup>®</sup> treatment versus free Tx with reduced side effects such as neutropenia and neuropathy<sup>17</sup>. PEG-ylated and non-PEG-ylated liposomal formulations containing doxorubicin (Doxil<sup>®</sup>, Caelyx<sup>®</sup> and Myocet<sup>™</sup>) and daunorubicine (DaunoXome<sup>®</sup>) demonstrated effective therapeutic response in AIDS related Kaposi’s sarcoma, breast and ovarian cancer treatment<sup>18-20</sup>. The stealth liposomes have dramatically prolonged doxorubicin circulation time and enhanced accumulation in tumors<sup>21</sup>.

Active targeting involves the presence of targeting moieties on the nanocarrier surface that recognize and specifically bind to biomarkers over-expressed on cancer cells. Table 1 illustrates some examples of actively targeted particulate systems. This approach combines the potential of nanoparticulate systems to deliver anticancer drugs with the ability of the ligand to target specifically malignant cells. More efficient distribution of the drug to tumor tissue, higher efficacy in earlier stages of cancer and higher drug levels in target cells are expected to be reached and maintained for a longer time<sup>10,22,23</sup>. The advances in sequencing of the human genome and discovery of new tumor biomarkers provide the possibility to identify new targets for cancer therapy<sup>24</sup>. For a successful targeting strategy, the target receptors must be specifically and stably expressed in tumor cells and most not be present or expressed at very low levels in host cells. On the other hand, the lack of immunogenicity, a

long half-life, and a specific interaction with the relevant antigen is required for the molecules used as ligands<sup>23</sup>.

**Table 1.** Examples of actively targeted carrier systems

| Cellular target                         | Ligand                | Active molecule            | Carrier system                  | ref   |
|---|-----------------------|----------------------------|---------------------------------|-------|
| HER2 receptor                           | Anti-HER2 mAbs        | Paclitaxel                 | PEG-PLA NPs                     | 25    |
|   |                       | PE38KDL immunotoxin        | PLGA NPs                        | 26    |
|   |                       | Doxorubicin                | Serum albumin NPs               | 27    |
|   |                       | Antisense oligonucleotides | Serum albumin NPs               | 28    |
|   |                       | Paclitaxel                 | PLGA/montmorillonite NPs        | 29    |
|   |                       | Doxorubicin                | Liposomes                       | 30    |
| CD20 receptor                           | Anti-CD20 mAbs        | -                          | PLA NPs                         | 31    |
|   |                       | Doxorubicin                | Liposomes                       | 33    |
|   |                       | Doxorubicin                | Liposomes                       | 32,33 |
| CD19 receptor                           | Anti-CD19 mAbs        | Doxorubicin                | Liposomes                       | 32,33 |
| Epidermal growth factor receptor (EGFR) | C225 mAbs             | Doxorubicin                | Liposomes                       | 34    |
| Folate receptor                         | Folate                | Paclitaxel                 | Micelles                        | 35    |
|   |                       | Doxorubicin                | Liposomes                       | 36    |
|   |                       | Doxorubicin                | Liposomes                       | 37    |
| Transferrin receptor                    | Transferrin           | Alpha-interferon           | Liposomes                       | 38    |
|   |                       | Paclitaxel                 | Nanoparticles                   | 39    |
| Acid hyaluronic receptor                | Acid hyaluronic       | 5 fluorouracil             | Chitosan NPs                    | 40    |
| Cytokeratins                            | Anti-cytokeratin mAbs | Cystatin protease          | PLGA NPs                        | 41    |
| ASGP receptor                           | Galactosamine         | Paclitaxel                 | $\gamma$ -PGA-PLA nanoparticles | 42    |
| Gp 112 glycoprotein                     | 34A antibody          | Amphotericin B             | Liposomes                       | 43    |
| Carcinoembryonic antigen                | 21B2 antibody         | -                          | Liposomes                       | 43    |
| Surface bound nucleosome                | 2C5 mAbs              | Doxorubicin                | PLGA NPs                        | 44    |
| Thrombomodulin                          | 201B mAbs             | -                          | Cd <sup>125</sup> Te/ZnS NPs    | 45    |

---

Another rationale in the choice of the ligand is related to its possible internalization after a specific interaction with the receptor. This feature is very attractive, as it implies the possibility of delivering the drug directly inside of cancer cells resulting in an improvement of therapeutic outcome. The preservation of internalization capacity of anti-HER2 mAbs after coupling to the carrier devices was demonstrated *in vitro*, when anti-HER2 immunonanoparticles made from either polymeric or serum albumin showed a specific targeting and cellular internalization in HER2 positive cancer cells<sup>31,46-48</sup>. *In vivo*, anti-HER2 immunoliposomes exhibited a six-fold higher intracellular tumor accumulation and a greater therapeutic efficacy compared to uncoated liposomes<sup>49,50</sup>. Anti-CD19 (internalized mAbs) immunoliposomes loaded with doxorubicine resulted in a greater survival compared to the same liposomes coated with anti-CD20 (non-internalized mAbs) in a B-Lymphoma xenograft model.

The intracellular fate of immunonanocarriers after internalization via receptor-mediated endocytosis is schematically presented in Figure 2. The endosomes formed after a specific ligand-receptor interaction will deliver the drug to the cytoplasm by lysosomal activation. Then, depending on its properties, drug reaches targeted organelles. The encapsulated drug may avoid recognition by P-glycoproteins often involved in drug resistance. Finally, the receptors released from the conjugate are metabolized or recycled on the cell surface.

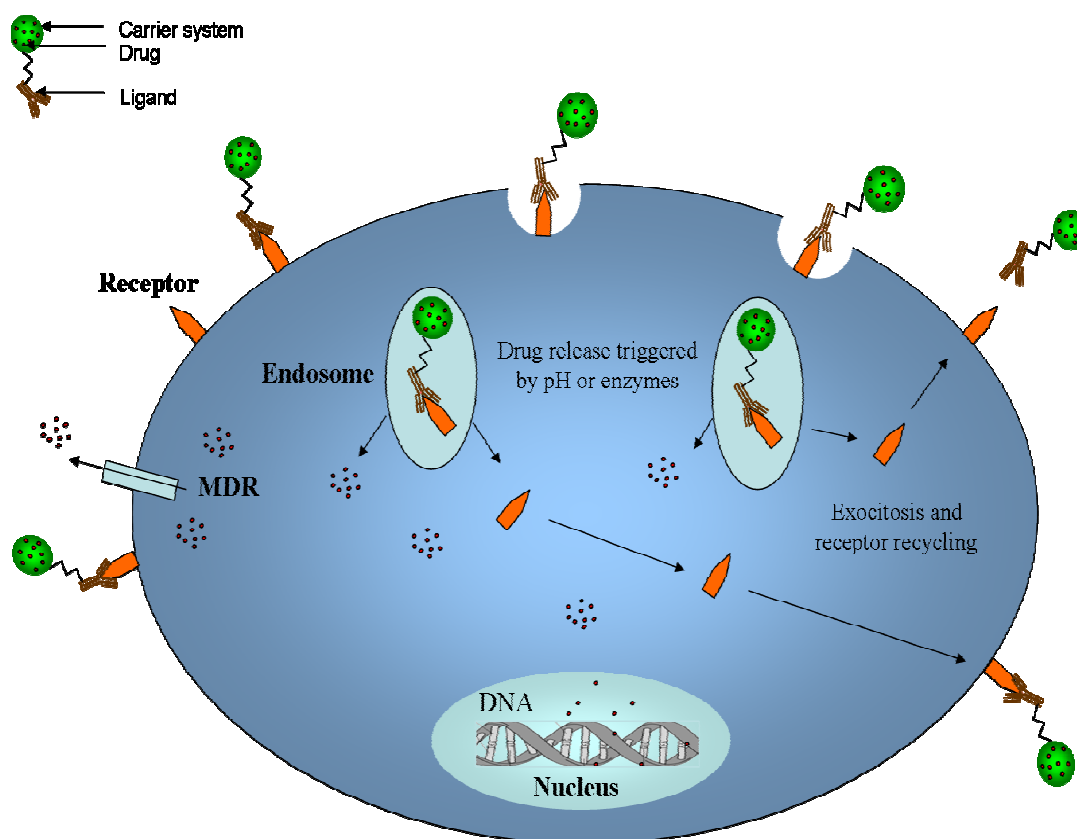


**Figure 2.** Internalization of nanocarriers via receptor-mediated endocytosis.

(Modified from Cho et al.)<sup>51</sup>.

The common biomarkers used for active targeting belong to following classes: i) targets preferentially expressed on endothelial cells of tumor blood vessels related to angiogenesis process (e.g. integrins and negatively charged phospholipids, vascular endothelial growth factor receptors) and ii) targets over-expressed on tumor cells responsible for high proliferation rates (e.g. human epidermal receptor, transferrin and folate receptors)<sup>52</sup>. The molecules used as recognition moieties to target malignant cells include entire or fragmented monoclonal antibodies, lipoproteins, hormones, polysaccharides, folate and transferrin ligands<sup>53</sup>. Some are described below.

---

## Recognition moieties in active targeting

### *Monoclonal antibodies*

Cancer cells are known to express or over-express specific receptors implicated in the cellular mechanism of disease. One key strategy to reach these biomarkers is the development of monoclonal antibodies (mAbs) as “magic bullets that identify their targets themselves without harming the organism”<sup>54</sup>. Furthermore, the invention of the hybridoma technology by Kohler and Milstein in 1975 led to a wide variety of antibody-based targeting strategies developed for cancer therapy<sup>55</sup>. The murine mAbs failed to show efficacy in clinical trials due to human anti-mouse response and their fast clearance from the organism<sup>56</sup>. In order to reduce their immunogenicity, efforts have been focused on the development of chimeric<sup>57</sup>, and humanized derivatives of mAbs<sup>58</sup>. To date, nine molecules have been approved by FDA for cancer treatment (Table 2) with many others currently in clinical studies<sup>59</sup>.

Significant results in cancer treatment have been obtained using mAbs alone or in combination with chemotherapeutics or radiotherapy in different types of cancers<sup>60,61</sup>.

MAbs are the first and still most frequently used molecules for active targeting due to their high selectivity and specificity.

One approach to achieve immunotargeting is represented by mAbs drug-conjugates<sup>62,63</sup>. Mylotarg<sup>®</sup> containing calicheamicin bound to humanized IgG4 anti-CD33 mAbs was approved for the treatment of acute myeloid leukemia<sup>64</sup>. However, the therapeutic effect of drug-conjugates is limited by the coupling of only a few drug molecules per monoclonal antibody molecule in addition to the risk of chemical modification of drug molecules subsequent to ligand binding.

**Table 2.** FDA-approved mAbs in oncology<sup>64</sup>

| Product   | Target   | Type                               | Year of approval | Indications                |
|---|----------|------------------------------------|------------------|----------------------------|
| Rituximab (Rituxan <sup>®</sup> )                   | CD20     | Chimeric IgG1                      | 1997             | B-cell lymphoma            |
| Trastuzumab (Herceptin <sup>®</sup> )               | HER2/neu | Humanized IgG1                     | 1998             | Breast cancer              |
| Gemtuzumab (Mylotarg <sup>®</sup> )                 | CD33     | Humanized IgG4-toxin-conjugate     | 2000             | Acute myeloid leukemia     |
| Alemtuzumab (MabCampath <sup>®</sup> )              | CD52     | Humanized IgG1                     | 2001             | Chronic lymphatic leukemia |
| <sup>90</sup> Y-ibritumomab (Zevalin <sup>®</sup> ) | CD20     | Murine IgG1-radionuclide-conjugate | 2002             | B-cell lymphoma            |
| <sup>131</sup> I-tositumomab (Bexxar <sup>®</sup> ) | CD20     | Murine IgG1-radionuclide-conjugate | 2003             | B-cell lymphoma            |
| Bevacizumab (Avastin <sup>®</sup> )                 | VEGF     | Humanized IgG1                     | 2004             | Colorectal cancer          |
| Cetuximab (Erbix <sup>®</sup> )                     | EGFR     | Chimeric IgG1                      | 2004             | Colorectal cancer          |
| Panitumumab (Vectibix <sup>®</sup> )                | EGFR     | Entirely human IgG2                | 2006             | Colorectal cancer          |

Another promising strategy is the conjugation of mAbs to drug-loaded carriers such as liposomes or nanoparticles<sup>29,65-67</sup>. Some advantages of immunocarriers versus drug-conjugates include the ability to deliver high payloads of drug to target sites in the presence of a small number of ligands, the protection of the drug from enzymatic degradation, and the possibility of using the same carrier system to encapsulate different drugs without the need for typical covalent conjugation for each drug molecule<sup>65</sup>. An important challenge of immunocarrier preparation is the efficient attachment of mAbs to the carrier without modification of its affinity or pharmacological activity. The principal methods of mAbs coupling to liposomes and nanoparticles including covalent and non-covalent techniques were recently reviewed by Nobs et al.<sup>68</sup>

Entire or fragmented mAbs such as Fab' and single-chain variable (Fv) were attached to the nanocarriers. Entire mAbs have a higher binding affinity and stability over mAbs fragments

---

and the presence of Fc domain can help to achieve additive or synergistic effects between mAbs used as ligand and encapsulated drug. However, the presence of Fc fragments can induce complement activation and immunogenic responses with rapid clearance of immunocarriers from the body. The use of less immunogenic antibody fragments may prolong the circulation time of immunocarriers and promote a better penetration of tumors<sup>30,43</sup>. Kirpotin et al.<sup>69</sup> reported that the internalization efficacy of anti-HER2 immunoliposomes increased with the increase in surface density of conjugated Fab' fragments before reaching a plateau at 15 Fab/liposome. Nobs et al. demonstrated that the highest amount of antibody on the NP surface (approximately 2500 mAbs molecules per NPs) demonstrated the lowest cellular binding, likely due to antibody inactivation<sup>31</sup>. These results suggest that an optimal number of ligands would be necessary to achieve efficient cellular targeting.

A leading antibody used as ligand for active targeting is trastuzumab directed against HER2 (ErbB2) receptor tyrosine kinase which represents one of the most promising targets for immunotherapy. The HER2 receptor (*c-erbB-2*, *neu*) is over-expressed in 20-30% of breast and ovarian cancers and correlated with a high occurrence of metastasis and angiogenic processes, as well as with a poor prognosis<sup>70</sup>. The surface accessibility, the high level of expression in certain primary and metastatic tumors, and the internalization of this receptor via receptor-mediated endocytosis could promote efficient delivery of drug at target sites and the preferential intracellular accumulation<sup>50,71</sup>.

The efficacy of NPs or liposomes containing chemotherapeutic agents such as Tx, doxorubicine or immunotoxins and functionalized with whole anti-HER2 mAbs or fragments has been widely demonstrated in different cancer cell lines and animal models such as breast and ovarian cancer<sup>26,27,29,67,72</sup>. Also, fluorescent nanoparticles conjugated to anti-HER2 mAbs were constructed for diagnostic and curative effect in ovarian cancer<sup>73,74</sup>.

### *Aptamers*

New ADN or ARN oligonucleotides named aptamers that mimic properties of antibodies have been developed for specific targeting of antigens by an *in vitro* method called systemic evolution of ligands by exponential enrichment (SELEX). Functionalization of nanoparticles with aptamers has increased cellular binding 77-fold when compared to control NPs. Also, the

higher efficacy of aptamer conjugated nanoparticles was demonstrated in a prostate xenograft cancer model <sup>75</sup>. The interesting properties of these new ligands such as their high affinity and specificity, the possibility to design molecules for any antigen, and the lack of immunogenicity provide encouraging perspectives on improvement of cancer treatment.

### *Folic acid and folates*

Folate receptor (FR) is a selective tumor marker frequently overexpressed in a range of tumors such as ovarian, lung, breast, renal, colorectal, brain and neuroendocrine metastases. The high specificity and affinity of the folic acid receptor (FR), the small size of the molecule and the simple conjugation chemistry enable the application of folate targeting technology to FR-positive cancers <sup>76</sup>. Liposomes or polymeric nanoparticles functionalized with folate have been used for selective delivery of chemotherapeutic agents, radio-imaging agents, genes, antisense oligonucleotides, radionuclides. *In vitro* studies have shown that cellular uptake of folate/doxorubicin-loaded liposomes was 45-fold higher than non-targeted liposomes <sup>36</sup>. Also, Tx-loaded nanoparticles functionalized with folate promote enhanced drug target delivery in breast cancer cells *in vitro* <sup>77</sup>. The *in vivo* efficacy of folate-loaded doxorubicin and daunorubicin liposomes was demonstrated in a myeloid leukemia xenograft model <sup>78,79</sup>. However, the presence of FR in normal tissues such as lung, intestine, and kidney limits the selectivity of such treatment.

### *Transferrin*

Transferrin is a serum glycoprotein that ensures the iron transport from blood to the cells after binding to the transferrin receptors and internalization via receptor mediated endocytosis. Due to the increasing needs of cell tumors for iron, an up-regulation of transferrin receptors in cancer is often encountered <sup>80</sup>. The transferrin-doxorubicine or chlorambucil conjugates exhibited a greater cytotoxic effect on a variety of cancer cells including multidrug resistant cell lines <sup>81,82</sup>. Alpha-interferon encapsulated in transferrin-coated liposomes demonstrated a greater anti-proliferative effect against a murine bladder xenograft cancer model due to efficient intracellular delivery of drug via receptor mediated endocytosis <sup>38</sup>. Sahoo et al <sup>39</sup> reported the complete regression of tumors in a murine model of prostate cancer and a higher

survival rate of animals treated with transferrin-conjugated Tx-loaded nanoparticles compared to uncoated NPs or free drug.

Although active targeting using immunonanomedicines represents a promising approach to improve cancer treatment, it is still in early stage of development<sup>83</sup>. The successful clinical application is restrained due to several limitations such as the loss of antibody specificity after chemical conjugation to the nanocarrier system, increased uptake by macrophages of antibody conjugates, appearance of antigenicity after multiple dose applications, or residual accumulation of the polymeric matrix in the organism. The details regarding the fate and toxicity of immunonanomedicines in clinical studies are scarce due to the high diversity of their features, which would imply the need to evaluate each preparation as a new drug formulation<sup>51,83</sup>.

The present work is focused on the development and the evaluation of polymeric immunonanoparticles for active targeting of tumors overexpressing specific receptors.

The preparation and physico-chemical characterization of immunonanoparticles will be described, and the therapeutic efficacy and biodistribution of paclitaxel-loaded anti-HER2 nanoparticles, will be evaluated in a disseminated intraperitoneal xenograft model of ovarian cancer in SCID mice.

---

**Reference List**

1. Heron, M. Deaths: leading causes for 2004. *Natl. Vital Stat. Rep.*, 56, 1-95, 2007.
2. Brigger, I., Dubernet, C. & Couvreur, P. Nanoparticles in cancer therapy and diagnosis. *Adv. Drug Deliv. Rev.* 54, 631-651, 2002.
3. Panyam, J. & Labhasetwar, V. Biodegradable nanoparticles for drug and gene delivery to cells and tissue. *Adv. Drug Deliv. Rev.* 55, 329-347, 2003.
4. Yuan, F. Transvascular drug delivery in solid tumors. *Semin. Radiat. Oncol.*, 8, 164-175, 1998.
5. Maeda, H. The enhanced permeability and retention (EPR) effect in tumor vasculature: The key role of tumor-selective macromolecular drug targeting. *Adv. Enzyme Regul.* 41, 189-207, 2001.
6. Duncan, R. Polymer conjugates for tumor targeting and intracytoplasmic delivery. The EPR effect as a common gateway? *Pharm. Sci. Technol. Today* 2, 441-449, 1999.
7. Maeda, H., Wu, J., Sawa, T., Matsumura, Y. & Hori, K. Tumor vascular permeability and the EPR effect in macromolecular therapeutics. A review. *J. Control. Release*, 65, 271-284, 2000.
8. Maeda, H., Sawa, T. & Konno, T. Mechanism of tumor-targeted delivery of macromolecular drugs, including the EPR effect in solid tumor and clinical overview of the prototype polymeric drug SMANCS. *J. Control. Release*, 74, 47-61, 2001.
9. Peer, D., Karp, J. M., Hong, S., Farokhzad, O. C., Margalit, R. & Langer, R. Nanocarriers as an emerging platform for cancer therapy. *Nat. Nanotechnol.*, 2, 751-760, 2007.
10. Moghimi, S. M., Hunter, A. C. & Murray, J. C. Long-circulating and target-specific nanoparticles: theory to practice. *Pharmacol. Rev.*, 53, 283-318, 2001.

- 
11. Jabr-Milane, L. S., van Vlerken, L. E., Yadav, S. & Amiji, M. M. Multi-functional nanocarriers to overcome tumor drug resistance. *Cancer Treat. Rev.*, 34, 592-602, 2008.
  12. Krasnici, S., Werner, A., Eichhorn, M. E., Schmitt-Sody, M., Pahernik, S. A., Sauer, B., Schulze, B., Teifel, M., Michaelis, U., Naujoks, K. & Dellian, M. Effect of the surface charge of liposomes on their uptake by angiogenic tumor vessels. *Int. J. Cancer*, 105, 561-567, 2003.
  13. Kunstfeld, R., Wickenhauser, G., Michaelis, U., Teifel, M., Umek, W., Naujoks, K., Wolff, K. & Petzelbauer, P. Paclitaxel encapsulated in cationic liposomes diminishes tumor angiogenesis and melanoma growth in a "humanized" SCID mouse model. *J. Invest. Dermatol.*, 120, 476-482, 2003.
  14. Zeisser-Labouebe, M., Lange, N., Gurny, R. & Delie, F. Hypericin-loaded nanoparticles for the photodynamic treatment of ovarian cancer. *Int. J. Pharm.*, 326, 174-181, 2006.
  15. Le Renard, P. E., Buchegger, F., Petri-Fink, A., Bosman, F., Rufenacht, D., Hofmann, H., Doelker, E. & Jordan, O. Local moderate magnetically induced hyperthermia using an implant formed in situ in a mouse tumor model. *Int. J. Hyperthermia*, 25, 229-239, 2009.
  16. Desai, N., Trieu, V., Yao, Z., Louie, L., Ci, S., Yang, A., Tao, C., De, T., Beals, B., Dykes, D., Noker, P., Yao, R., Labao, E., Hawkins, M. & Soon-Shiong, P. Increased Antitumor Activity, Intratumor Paclitaxel Concentrations, and Endothelial Cell Transport of Cremophor-Free, Albumin-Bound Paclitaxel, ABI-007, Compared with Cremophor-Based Paclitaxel. *Clin. Cancer Res.*, 12, 1317-1324, 2006.
  17. Gradishar, W. J., Tjulandin, S., Davidson, N., Shaw, H., Desai, N., Bhar, P., Hawkins, M. & O'Shaughnessy, J. Phase III trial of nanoparticle albumin-bound paclitaxel compared with polyethylated castor oil-based paclitaxel in women with breast cancer. *J. Clin. Oncol.*, 23, 7794-7803, 2005.
  18. O'Brien, M. E. R., Wigler, N., Inbar, M., Rosso, R., Grischke, E., Santoro, A., Catane, R., Kieback, D. G., Tomczak, P., Ackland, S. P., Orlandi, F., Mellars, L., Alland, L. & Tendler, C. Reduced cardiotoxicity and comparable efficacy in a phase III trial of pegylated liposomal doxorubicin HCl (CAELYX/Doxil) versus conventional doxorubicin for first-line treatment of metastatic breast cancer. *Ann. Oncol.*, 15, 440-449, 2004.

- 
19. Gordon, A. N., Fleagle, J. T., Guthrie, D., Parkin, D. E., Gore, M. E. & Lacave, A. J. Recurrent epithelial ovarian carcinoma: a randomized phase III study of pegylated liposomal doxorubicin versus topotecan. *J. Clin. Oncol.*, 19, 3312-3322, 2001.
  20. Stewart, S., Jablonowski, H., Goebel, F. D., Arasteh, K., Spittle, M., Rios, A., Aboulafia, D., Galleshaw, J. & Dezube, B. J. Randomized comparative trial of pegylated liposomal doxorubicin versus bleomycin and vincristine in the treatment of AIDS-related Kaposi's sarcoma. International Pegylated Liposomal Doxorubicin Study Group. *J. Clin. Oncol.*, 16, 683-691, 1998.
  21. Zhang, L., Gu, F. X., Chan, J. M., Wang, A. Z., Langer, R. S. & Farokhzad, O. C. Nanoparticles in Medicine: Therapeutic Applications and Developments. *Clin. Pharmacol. Ther.*, 83, 761-769, 2008.
  22. Allen, T. M. Ligand-targeted therapeutics in anticancer therapy. *Nat. Rev. Cancer*, 2, 750-763, 2002.
  23. Marcucci, F. & Lefoulon, F. Active targeting with particulate drug carriers in tumor therapy: fundamentals and recent progress. *Drug Discov. Today*, 9, 219-228, 2004.
  24. Loo, D. T. & Mather, J. P. Antibody-based identification of cell surface antigens: targets for cancer therapy. *Curr. Opin. Pharmacol.*, 8, 627-631, 2008.
  25. Debotton, N., Parnes, M., Kadouche, J. & Benita, S. Overcoming the formulation obstacles towards targeted chemotherapy: In vitro and in vivo evaluation of cytotoxic drug loaded immunonanoparticles. *J. Control. Release*, 127, 219-230, 2008.
  26. Gao, J., Kou, G., Wang, H., Chen, H., Li, B., Lu, Y., Zhang, D., Wang, S., Hou, S., Qian, W., Dai, J., Zhao, J., Zhong, Y. & Guo, Y. PE38KDEL-loaded anti-HER2 nanoparticles inhibit breast tumor progression with reduced toxicity and immunogenicity. *Breast Cancer Res. Treat.*, 115, 29-41, 2009.
  27. Anhorn, M. G., Wagner, S., Kreuter, J., Langer, K. & von Briesen, H. Specific Targeting of HER2 Overexpressing Breast Cancer Cells with Doxorubicin-Loaded Trastuzumab-Modified Human Serum Albumin Nanoparticles. *Bioconjugate Chem.*, 19, 2321-2331, 2008.
  28. Spankuch, B., Steinhauser, I., Wartlick, H., Kurunci-Csacsco, E., Strebhardt, K., I & Langer, K. Downregulation of Plk1 expression by receptor-mediated uptake of antisense oligonucleotide-loaded nanoparticles. *Neoplasia*, 10, 223-234, 2008.

- 
29. Sun, B., Ranganathan, B. & Feng, S. S. Multifunctional poly(lactide-co-glycolide)/montmorillonite (PLGA/MMT) nanoparticles decorated by Trastuzumab for targeted chemotherapy of breast cancer. *Biomaterials*, 29, 475-486, 2007.
  30. Park, J. W. et al. Anti-HER2 immunoliposomes for targeted therapy of human tumors. *Cancer Lett.* 118, 153-160. 1997.
  31. Nobs, L., Buchegger, F., Gurny, R. & Allemann, E. Biodegradable Nanoparticles for Direct or Two-Step Tumor Immunotargeting. *Bioconjug. Chem.* 17, 139-145, 2006.
  32. Cheng, W. W. K. & Allen, T. M. Targeted delivery of anti-CD19 liposomal doxorubicin in B-cell lymphoma: A comparison of whole monoclonal antibody, Fab' fragments and single chain Fv. *J. Control. Release*, 126, 50-58, 2008.
  33. Sapra, P. & Allen, T. M. Internalizing antibodies are necessary for improved therapeutic efficacy of antibody-targeted liposomal drugs. *Cancer Res.* 62, 7190-7194, 2002.
  34. Mamot, C., Drummond, D. C., Noble, C. O., Kallab, V., Guo, Z., Hong, K., Kirpotin, D. B. & Park, J. W. Epidermal growth factor receptor-targeted immunoliposomes significantly enhance the efficacy of multiple anticancer drugs in vivo. *Cancer Res.*, 65, 11631-11638, 2005.
  35. Seow, W. Y., Xue, J. M. & Yang, Y. Y. Targeted and intracellular delivery of paclitaxel using multi-functional polymeric micelles. *Biomaterials*, 28, 1730-1740, 2007.
  36. Lee, R. J. & Low, P. S. Folate-mediated tumor cell targeting of liposome-entrapped doxorubicin in vitro. *Biochim. Biophys. Acta*, 1233, 134-144, 1995.
  37. Gabizon, A., Horowitz, A. T., Goren, D., Tzemach, D., Shmeeda, H. & Zalipsky, S. In vivo fate of folate-targeted polyethylene-glycol liposomes in tumor-bearing mice. *Clinical Cancer Res.*, 9, 6551-6559, 2003.
  38. Liao, W. P., DeHaven, J., Shao, J., Chen, J. X., Rojanasakul, Y., Lamm, D. L. & Ma, J. K. H. Liposomal delivery of alpha -interferon to murine bladder tumor cells via transferrin receptor-mediated endocytosis. *Drug Deliv.*, 5, 111-118, 1998.
  39. Sahoo, S. K., Ma, W. & Labhasetwar, V. Efficacy of transferrin-conjugated paclitaxel-loaded nanoparticles in a murine model of prostate cancer. *Int. J. Cancer*, 112, 335-340, 2004.

- 
40. Jain, A. & Jain, S. K. In vitro and cell uptake studies for targeting of ligand anchored nanoparticles for colon tumors. *Eur. J. Pharm. Sci.*, 35, 404-416, 2008.
  41. Obermajer, N., Kocbek, P., Repnik, U., Kuznik, A., Cegnar, M., Kristi, J. & Kos, J. Immunonanoparticles - an effective tool to impair harmful proteolysis in invasive breast tumor cells. *FEBS Journal*, 274, 4416-4427, 2007.
  42. Liang, H. F., Chen, S. C., Chen, M. C., Lee, P. W., Chen, C. T. & Sung, H. W. Paclitaxel-Loaded Poly(g-glutamic acid)-poly(lactide) Nanoparticles as a Targeted Drug Delivery System against Cultured HepG2 Cells. *Bioconjug. Chem.*, 17, 291-299, 2006.
  43. Maruyama, K., Ishida, O., Takizawa, T. & Moribe, K. Possibility of active targeting to tumor tissues with liposomes. *Adv. Drug Deliv. Rev.*, 40, 89-102, 1999.
  44. Elbayoumi, T. A. & Torchilin, V. P. Enhanced cytotoxicity of monoclonal anticancer antibody 2C5-modified doxorubicin-loaded PEGylated liposomes against various tumor cell lines. *Eur. J. Pharm. Sci.*, 32, 159-168, 2007.
  45. Kennel, S. J., Woodward, J. D., Rondinone, A. J., Wall, J., Huang, Y. & Mirzadeh, S. The fate of MAb-targeted Cd125mTe/ZnS nanoparticles in vivo. *Nucl. Med. Biol.*, 35, 501-514, 2008.
  46. Cirstoiu-Hapca, A., Bossy-Nobs, L., Buchegger, F., Gurny, R. & Delie, F. Differential tumor cell targeting of anti-HER2 (Herceptin) and anti-CD20 (Mabthera) coupled nanoparticles. *Int. J. Pharm.*, 331, 190-196, 2007.
  47. Steinhauser, I., Spaenkuch, B., Strebhardt, K. & Langer, K. Trastuzumab-modified nanoparticles: Optimisation of preparation and uptake in cancer cells. *Biomaterials* 27, 4975-4983, 2006.
  48. Wartlick, H., Michaelis, K., Balthasar, S., Strebhardt, K., Kreuter, J., Langer, K., Highly specific HER2-mediated cellular uptake of antibody-modified nanoparticles in tumour cells. *J. Drug Target.* 12, 461-471, 2004.
  49. Park, J. W. et al., Anti-HER2 immunoliposomes: enhanced efficacy attributable to targeted delivery. *Clin. Cancer Res.* 8, 1172-1181, 2002.
  50. Kirpotin, D. B., Drummond, D. C., Shao, Y., Shalaby, M. R., Hong, K., Nielsen, U. B., Marks, J. D., Benz, C. C. & Park, J. W. Antibody Targeting of Long-Circulating

- 
- Lipidic Nanoparticles Does Not Increase Tumor Localization but Does Increase Internalization in Animal Models. *Cancer Res.*, 66, 6732-6740, 2006.
51. Cho, K., Wang, X., Nie, S., Chen, Z. & Shin, D. M. Therapeutic Nanoparticles for Drug Delivery in Cancer. *Clin. Cancer Res.*, 14, 1310-1316, 2008.
  52. Byrne, J. D., Betancourt, T. & Brannon-Peppas, L. Active targeting schemes for nanoparticle systems in cancer therapeutics. *Adv. Drug Deliv. Rev.*, 60, 1615-1626, 2008.
  53. Alexis, F. Rhee J. W., Richie J. P., Moreno A. F., Langer R., Farokhzad O. C. New frontiers in nanotechnology for cancer treatment. *Urol. Oncol. : Semin. Orig. Invest.* 26, 74-85, 2008.
  54. Strebhardt, K. & Ullrich, A. Paul Ehrlich's magic bullet concept: 100 years of progress. *Nat. Rev. Cancer*, 8, 473-480, 2008.
  55. Kohler, G. & Milstein, C. Continuous cultures of fused cells secreting antibody of predefined specificity. *Nature*, 256, 495-497, 1975.
  56. Shawler, D. L., Bartholomew, R. M., Smith, L. M. & Dillman, R. O. Human immune response to multiple injections of murine monoclonal IgG. *J. Immunol.*, 135, 1530-1535, 1985.
  57. Boulianne, G. L., Hozumi, N. & Shulman, M. J. Production of functional chimaeric mouse/human antibody. *Nature*, 312, 643-646, 1984.
  58. Vaughan, T. J., Osbourn, J. K. & Tempest, P. R. Human antibodies by design. *Nat Biotechnol*, 16, 535-539, 1998.
  59. Zhang, Q., Chen, G., Liu, X. & Qian, Q. Monoclonal antibodies as therapeutic agents in oncology and antibody gene therapy. *Cell Res.*, 17, 89-99, 2007.
  60. Yan, L., Hsu, K. & Beckman, R. A. Antibody-based therapy for solid tumors. *Cancer J.*, 14, 178-183, 2008.
  61. Carter, P. J. Potent antibody therapeutics by design. *Nat. Rev. Immunol.*, 6, 343-357, 2006.
  62. Jaracz, S., Kuznetsova, L.V. & Ojima, I. Recent advances in tumor-targeting anticancer drug conjugates. *Bioorg. Med. Chem.* 13, 5043-5054, 2005.
  63. Schrama, D., Reisfeld, R. A. & Becker, J. C. Antibody targeted drugs as cancer therapeutics. *Nat. Rev. Drug Discov.*, 5, 147-159, 2006.
  64. Carter, P. J. & Senter, P. D. Antibody-drug conjugates for cancer therapy. *Cancer J.*, 14, 154-169, 2008.

- 
65. Sapra, P. & Allen, T.M. Ligand-targeted liposomal anticancer drugs. *Prog. Lipid Res.* 42, 439-462, 2003.
  66. Carter, P. Improving the efficacy of antibody-based cancer therapies. *Nat. Rev. Cancer*, 1, 118-129, 2001.
  67. Park, J. W. et al. Tumor targeting using anti-her2 immunoliposomes. *J. Control. Release* 74, 95-113, 2001.
  68. Nobs, L., Buchegger, F., Gurny, R. & Allemann, E. Current methods for attaching targeting ligands to liposomes and nanoparticles. *J. Pharm. Sci.* 93, 1980-1992, 2004.
  69. Kirpotin, D. et al. Sterically stabilized anti-HER2 immunoliposomes: design and targeting to human breast cancer cells in vitro. *Biochemistry* 36, 66-75, 1997.
  70. Slamon, D. J., Godolphin, W., Jones, L. A., Holt, J. A., Wong, S. G., Keith, D. E., Levin, W. J., Stuart, S. G., Udove, J., Ullrich, A. & +.. Studies of the HER-2/neu proto-oncogene in human breast and ovarian cancer. *Science*, 244, 707-712, 1989.
  71. Nahta, R. & Esteva, F. J. Herceptin: mechanisms of action and resistance. *Cancer Lett.* 232, 123-138, 2006.
  72. Sadauskas, E., Wallin, H., Stoltenberg, M., Vogel, U., Doering, P., Larsen, A. & Danscher, G. Kupffer cells are central in the removal of nanoparticles from the organism. *Part. Fibre Toxicol.*, 4, No, 2007.
  73. Yezhelyev, M. V., Gao, X., Xing, Y., Al Hajj, A., Nie, S. & O'Regan, R. M. Emerging use of nanoparticles in diagnosis and treatment of breast cancer. *Lancet Oncol.*, 7, 657-667, 2006.
  74. Hun, X., Zhang, Z. & Tiao, L. Anti-Her-2 monoclonal antibody conjugated polymer fluorescent nanoparticles probe for ovarian cancer imaging. *Anal. Chim. Acta*, 625, 201-206, 2008.
  75. Kawasaki, E. S. & Player, A. Nanotechnology, nanomedicine, and the development of new, effective therapies for cancer. *Nanomedicine*, 1, 101-109, 2005.
  76. Hilgenbrink, A. R. & Low, P. S. Folate receptor-mediated drug targeting: From therapeutics to diagnostics. *J. Pharm. Sci.*, 94, 2135-2146, 2005.
  77. Pan, J. & Feng, S. S. Targeted delivery of paclitaxel using folate-decorated poly(lactide)-vitamin E TPGS nanoparticles. *Biomaterials*, 29, 2663-2672, 2008.
  78. Pan, X. Q., Zheng, X., Shi, G., Wang, H., Ratnam, M. & Lee, R. J. Strategy for the treatment of acute myelogenous leukemia based on folate receptor beta -targeted

- 
- liposomal doxorubicin combined with receptor induction by all-trans-retinoic acid. *Blood*, 100, 594-602, 2002.
79. Pan, X. Q. & Lee, R. J. In vivo antitumor activity of folate receptor-targeted liposomal daunorubicin in a murine leukemia model. *Anticancer Res.*, 25, 343-346, 2005.
80. Qian, Z. M., Li, H., Sun, H. & Ho, K. Targeted drug delivery via the transferrin receptor-mediated endocytosis pathway. *Pharmacol. Rev.*, 54, 561-587, 2002.
81. Beyer, U., Roth, T., Schumacher, P., Maier, G., Unold, A., Frahm, A. W., Fiebig, H. H., Unger, C. & Kratz, F. Synthesis and in vitro efficacy of transferrin conjugates of the anticancer drug chlorambucil. *J. Med. Chem.*, 41, 2701-2708, 1998.
82. Fritzer, M., Szekeres, T., Szuts, V., Jarayam, H. N. & Goldenberg, H. Cytotoxic effects of a doxorubicin-transferrin conjugate in multidrug-resistant KB cells. *Biochem. Pharmacol.*, 51, 489-493, 1996.
83. Bae, Y. H. Drug targeting and tumor heterogeneity. *J. Control. Release*, 133, 2-3, 2009.



---

## **Differential tumor cell targeting of anti-HER2 (Herceptin<sup>®</sup>) and anti-CD20 (Mabthera<sup>®</sup>) coupled nanoparticles**

A. Cirstoiu-Hapca<sup>1</sup>, L. Bossy-Nobs<sup>1</sup>, F. Buchegger<sup>2</sup>, R. Gurny<sup>1</sup> and F. Delie<sup>1</sup>

<sup>1</sup> Department of Pharmaceutics and Biopharmaceutics, School of Pharmaceutical Sciences, University of Geneva, University of Lausanne, 30 Quai Ernest Ansermet, CH-1211 Geneva 4, Switzerland

<sup>2</sup> Division of Nuclear Medicine, University Hospital of Geneva, Switzerland

*Published in the International Journal of Pharmaceutics, 331 (2007) 190-196*

---

Two types of antibody-labeled nanoparticles (mAb-NPs) were prepared with the aim to achieve specific tumor targeting. Anti-HER2 and anti-CD20 monoclonal antibodies (mAb) were used as model ligands. Small poly (DL-lactic acid) nanoparticles (PLA NPs) with a mean size of about 170 nm were prepared by the salting out method. Thereafter, the coating of PLA NPs with mAbs was performed in two steps. First, thiol groups (-SH) were introduced on the surface of PLA-NPs by a two-step carbodiimide reaction. The number of -SH groups on the surface of NPs increased from 150 to 400 mmol-SH/mol PLA when cystamine concentrations of 25 to 1518 mol cystamine/mol PLA were used during the thiolation reaction. In the second step, covalent coupling of antibodies to thiolated NPs (NPs-SH) was obtained via a bifunctional cross-linker, m-maleimidobenzoyl-N-hydroxy-sulfosuccinimide ester (sulfo-MBS). For both mAbs anti-HER2 and anti-CD20, respectively, the number of -SH functions on the NPs had no influence on the amount of mAb coupled to the NPs. Approximately 295 anti-HER2 and 557 anti-CD20 molecules, respectively, were covalently coupled per nanoparticle. The NPs size after the coupling reactions was about 250 nm. The specific interaction between tumor cells and mAb-NPs was determined by confocal microscopy using two cell lines: SKOV-3 human ovarian cancer cells (overexpressing HER2) and Daudi lymphoma cells (overexpressing CD20). The results showed the selective targeting of

---

mAb-NPs to tumor cells overexpressing the specific antigen. While anti-CD20 labeled NPs (anti-CD20 NPs) bound to and remained at the cellular surface, anti-HER2 labeled NPs (anti-HER2 NPs) were efficiently internalized. The mAb-NPs represent a promising approach to improve the efficacy of NPs in active targeting for cancer therapy while the choice of the antibody-target system defines the fate of the mAb-NPs after their binding to the cells.

*Key words: cancer therapy, polymeric nanoparticles, coated nanoparticles, active targeting, monoclonal antibodies, anti-HER2, Herceptin<sup>®</sup>, anti-CD20, Mabthera<sup>®</sup>.*

---

## 1. Introduction

Major drawbacks of conventional chemotherapy are a modest tumor response and dose limiting side effects due to nonspecific biodistribution of drugs. In the last decades significant progress has been made in development of new delivery technologies. Drug carrier systems emerged as promising approaches in anticancer treatment with major advantages: the capacity to improve the therapeutic index of drugs by preferential localization at target sites and lower distribution in healthy tissues, delivery of hydrophobic drugs, high drug loading capacity and controlled release rate <sup>1,2</sup>.

Depending on the nanocarrier formulation, drug targeting concepts can be achieved via either passive or active targeting. Tumors are characterized by pathological angiogenesis, leaky vasculature and poor lymphatic drainage which promote the extravasation and accumulation of macromolecules, a phenomenon known as enhanced permeability and retention (EPR) effect. This phenomenon allows the passive tumor targeting of long-circulating nanocarriers such as nanoparticles or liposomes <sup>1,3,4</sup>.

In a further development, active targeting combines the potential of nanoparticulate systems to carry anticancer drugs with the capacity of the ligand to target specifically malignant cells. More efficient distribution of the drug to tumor tissue, higher efficacy in earlier stages of cancer and higher drug levels in target cells are expected to be reached and maintained for a longer time with this latter approach <sup>5</sup>.

Active targeting can be achieved by covalent attachment to the surface of nanocarrier systems of different target-specific ligands such as antibodies or peptides. Different mAb modified immunoliposomes for specific targeting are described in the literature <sup>6-8</sup>. Polymeric nanoparticles represent an attractive approach for specific targeting especially regarding their

biocompatibility, biodegradability and stability. Polymers such as PLA approved by FDA for medical devices are good candidates for drug delivery applications <sup>9</sup>. Free carboxylic end groups of PLA offer the possibility of surface modification by introduction of sulfhydryl functions which allow the covalent coupling of proteins <sup>10,11</sup>.

Among numerous antigens present on malignant cells, HER2 is an interesting target for therapy. Being a member of the epidermal growth factor (EGF) family of receptor tyrosine kinases, HER2 is overexpressed in a variety of human cancers including lung, breast, and ovarian carcinomas <sup>12</sup>. Anti-HER2 (trastuzumab, Herceptin<sup>®</sup>) is a humanized mAb designed to specifically antagonize the HER-2 function. This monoclonal antibody was approved by the FDA in 1998 for treatment of metastatic breast cancer. Many mechanisms have been proposed to explain the therapeutic effect of Herceptin including internalization and degradation of HER-2, inhibition of angiogenesis and activation of apoptotic signals, but they remain overall controversial <sup>13</sup>.

The chimeric anti-CD20 mAb (rituximab, Mabthera<sup>®</sup>) was approved by the FDA for treatment of non-Hodgkin's B-cell lymphoma in 1997. Its efficacy was also demonstrated in the treatment of rheumatoid arthritis and inflammatory myositis. The mechanism of B-cell depletion and anti-tumor activity of rituximab is still unclear. Its efficacy could be attributed to apoptosis, complement-dependent cytotoxicity (CDC) and antibody-dependent cellular cytotoxicity (ADCC) <sup>14,15</sup>. The specific antigen for rituximab, CD20 is a tetraspan cell surface molecule which is not internalized in response to antibody binding <sup>16,17</sup>. Its restricted expression only in B lymphocytes and absence of expression on bone marrow stem cells represent attractive advantages for targeted therapy. Most efficient rituximab therapy in non Hodgkin B lymphoma is currently achieved by combination with chemotherapy such as in CHOP-Rituximab treatment <sup>18,19</sup>.

In our laboratory two different approaches of active tumor targeting have been previously described: i) direct targeting when PLA NPs were covalently coupled to mAbs and ii) a pretargeting multistep-method which involves an avidin-biotin system <sup>11</sup>. Nobs et al. obtained mAbs modified NPs of around 400 nm. In vivo, these NPs will be preferentially distributed in mononuclear phagocytic system (MPS) rich organs such as liver and spleen and rapidly eliminated after opsonization <sup>1</sup>. Therefore, one of the aims of present work was to decrease the size of NPs in order to have a longer circulation half-live and to increase the chance to reach the target site.

Anti-HER2 (internalizing mAb) and anti-CD20 (non-internalizing mAb) were covalently coupled to the NPs using the direct targeting approach. Assays were also performed to study the influence of different concentrations of -SH groups on the amount of mAbs bound to the NPs. The specific interaction as well as cellular localization of anti-HER2 NPs and anti-CD20 NPs in SKOV-3 and Daudi cells, respectively, were studied by confocal laser scanning microscopy.

## 2. Material and methods

### 2.1 Materials

Poly (DL-lactic acid) (100DL 4A, Mw 57kDa) was provided by Lakeshore Biomaterials, Inc (Birmingham, AL). 1-Ethyl-3-(3-dimethylaminopropyl)-carbodiimide (EDAC), D(+)-Trehalose dihydrate, Phosphate buffer saline (PBS), Poly-L-Lysine solution, 0.1% (w/v) from Sigma (Buchs, Switzerland), m-maleimidobenzoyl-N-hydroxy-sulfosuccinimide ester (sulfo-MBS), Tris (2-carboxyethyl)-phosphine hydrochloride (TCEP) and D-salt dextran plastic columns were supplied by Pierce (Rockford, IL USA), Dioctadecyloxacarbo-cyanine perchlorate (DiO) and Concanavalin A AlexaFluor<sup>®</sup> 594 conjugate were from Molecular Probes (Leiden, The Netherlands). Anti-CD20 (rituximab, Mabthera<sup>®</sup>) and anti-HER2 (trastuzumab, Herceptin<sup>®</sup>) were purchased from Roche (Basle, Switzerland). Poly(vinyl alcohol) (Mowiol 4-88) was purchased from Hoechst (Frankfurt/M, Germany).

### 2.2 Cell lines

The human lymphoma cell line, Daudi and human ovarian carcinoma cells, SKOV-3 (American Type Culture Collection ATCC, Manassas, VA) were grown in RPMI-1640 medium with Glutamax I (Gibco, Grand Island, NY) supplemented with 10% (v/v) fetal calf serum (FCS) (Brunschwig, Basle Switzerland), penicillin (100 units/ml) and streptomycin (100µg/ml) (Gibco, Grand Island, NY) at 37°C in humidified incubator containing 5% CO<sub>2</sub>. For all experiments, before incubation with NPs, SKOV-3 cells, maintained in monolayer, were harvested using TrypLE Express (Gibco, Grand Island, NY), whereas Daudi cells, grown in suspension, were centrifuged. In both cases, the cells were resuspended in fresh complete medium for a concentration of about 1x10<sup>6</sup> cells/ml.

### *2.3 Preparation of PLA NPs*

PLA NPs were prepared by a salting-out process as described previously<sup>20</sup>. Briefly, 10 g of an aqueous solution containing 15% (w/w) poly(vinyl alcohol) (PVAL) and 60% (w/w) magnesium chloride hexahydrate were mixed under vigorous stirring with 4 g of an organic phase containing 18% PLA (w/w) dissolved in acetone. To determine the cellular localization of nanoparticles DiO 0.01% (w/w) was added in the organic phase as fluorescent probe. The NPs were purified by 3 successive centrifugations (26 000xg for 40 min). After preparation and purification, the NPs were lyophilized in presence of trehalose as a lyoprotector.

### *2.4 Thiolation of NPs*

Thiol functions were covalently bound to the PLA NPs by a two-step carbodiimide reaction as described earlier<sup>21</sup>. Briefly, 100 mg PLA NPs were suspended in 5 ml water and reaction was initiated by adding, consecutively 10 ml of a solution of EDAC (24 mg/ml) and 5 ml of cystamine solution at different concentrations: 2; 4; 10; 32; 71; 120 mg/ml (25; 50; 127; 405; 896; 1518 mol cystamine/mol PLA) to vary the -SH concentration on the particle surface. The final suspension was completed with water to 25 ml and stirred under mild conditions during 24h at room temperature. Thereafter, EDAC and non reacted cystamine were removed by 3 successive centrifugations (25 000xg for 30 min). The NPs were re-suspended in purified water. For reduction of disulfide bonds, the NPs were incubated for 3 hours with 1 ml solution of TCEP (6 mg/ml). Finally, the NPs-SH were purified by 3 successive centrifugations (25 000xg for 30 min) and freeze-dried in presence of trehalose (30% w/w). The concentration of -SH functions on the surface of nanoparticles was determined spectrophotometrically at  $\lambda=410$  nm (Hewlett Packard, Model 8453, Germany) using Ellman's reagent<sup>21</sup>. The size of NPs was measured by photon correlation spectroscopy using a Zetasizer 3000 HS (Malvern instruments Ltd, UK).

### *2.5 Activation of mAb and covalent attachment to the thiolated NPs*

The covalent attachment of mAb to the NPs-SH was performed according to a previously described method<sup>11</sup>. mAb were purified by size exclusion chromatography using a D-salt desalting column. 2 mg purified Herceptin<sup>®</sup> or Mabthera<sup>®</sup> were activated in PBS (pH=7.4)

with sulfo-MBS at a molar ratio 1:20 (mAbs:sulfo-MBS) for 1 hour at room temperature. Non-reacted sulfo-MBS was removed by size exclusion chromatography using desalting columns. 500  $\mu$ l activated anti-HER2 or anti-CD20 mAb (1mg/ml) were incubated with 500  $\mu$ l NPs-SH (20 mg/ml) and gently shaken for 60 min at RT. Three batches of NPs-SH have been used with different concentrations of -SH functions: around 200, 300, and 400 mmol-SH/mol PLA. Thereafter, unconjugated mAb were removed by 2 cycles of centrifugation (25 000xg, 10 min). The amount of mAb conjugated to NP was determined indirectly by measuring uncoupled mAb in the supernatant after centrifugation step. A spectrophotometric method ( $\lambda=280$  nm) (Hewlett Packard, Model 8453, Germany) was used assuming an extinction coefficient of  $1.4 \text{ M}^{-1}\text{cm}^{-1}$ . Finally, mAb-NPs were stored in PBS at  $4^{\circ}\text{C}$ . In order to verify the efficacy of mAb-conjugation to NPs, selected experiments were also performed using trace amounts of  $^{125}\text{I}$  radiolabeled rituximab mixed with native antibodies. Antibody radiolabelling was performed using the chloramin T method with minor modifications as described (Schaffland et al., 2004). Briefly, 0.1 ml clinical grade rituximab (1 mg) solution and 100  $\mu$ l freshly prepared chloramine T solution (0.5 mg per 1 ml, in sterile phosphate buffer 0.15 M, pH 7) were reacted with 37 MBq  $\text{Na}^{125}\text{I}$  solutions, previously diluted to 200  $\mu$ l with 0.15 M phosphate buffer pH 7.0, for 5 minutes at room temperature. The solution of labelling antibodies was purified through a 2 ml reversible column (Supelco, Buchs, Switzerland) filled with 1.8 g of anion exchange resin (Dowex 1x8, 100 mesh) at 0.5 ml/min flow. The labelling vial was washed with 2 ml 0.9 % NaCl solution that was also passed through the resin filter. Furthermore, 3 kBq of radio-labelling mAbs (10  $\mu$ l) were added to 2 ml purified rituximab (5mg/ml). The rituximab solution containing a trace amount of  $^{125}\text{I}$ -labelled mAbs was used for coupling reaction. The percentage of rituximab bound to the NPs-SH was determined by direct radioactivity counting of mAb-NPs in comparison with the input radioactivity (100 %). The number of mAbs molecules bound on the surface of a single nanoparticle was calculated using the following equation (Nobs et al., 2004b):

$$n = aN(d/3\pi r^3)$$

with:

$n$ : number of mAbs per nanoparticle

$a$ : mol of mAbs per g PLA

$d$ : density of nanoparticles estimated to be  $1.5 \text{ g/cm}^3$  based on the polymer density

$r$ : mean radius of nanoparticles

$N$ :  $6.022 \times 10^{23}$  (Avogadro Number)

The number of mAb coupled per NP was calculated using an equation mentioned previously<sup>10</sup>. A control was performed using PLA NPs (without -SH groups) to determine the fraction of non-covalently attached mAb on the surface of the NPs.

### *2.6 Cellular localization of anti-HER2 NPs and anti-CD20 NPs*

Cellular distribution experiments were performed using Daudi cells expressing CD20 antigen (negative for HER2) and SKOV-3 cells overexpressing HER2 antigen (negative for CD20). Approximately  $1 \times 10^6$  SKOV-3 or Daudi cells were incubated with 100  $\mu$ l (1mg/ml) suspension of mAbs-NPs, respectively, in fresh culture medium for different times (1 and 6 h) at 37° C. To analyze nonspecific interaction between cells and nanoparticles, controls were performed using unmodified NPs and modified NPs with a non-specific mAb. After incubation the cells were rinsed twice with cold PBS. The cell membranes were stained for 3 min with a solution of Concanavalin A AlexaFlour 594 in PBS (0.05% w/v). After two washing steps with cold PBS the cells were fixed with paraformaldehyde 4% (v/v) for 30 min. The paraformaldehyde was removed by three washings with PBS. The cells were fixed on the slides with poly-L-lysine solution and covered with coverslips. The slides were observed using a confocal laser scanning microscope, LSM 510 META (Zeiss AG, Zurich, Switzerland) equipped with Argon and Helium/Neon lasers. Two channels at 488 and 543 nm laser excitation were chosen. A Zeiss Plan-Apochromat 63x/1.4 oil objective was used. A Z Stack of images was displayed in an orthogonal view using LSM 510 META software.

## **3. Results**

Antibody coupling to NPs was performed in two steps: introduction of -SH groups on the surface of PLA NPs and covalent coupling of antibodies to NPs-SH via the bifunctional crosslinker, sulfo-MBS (Fig.1).

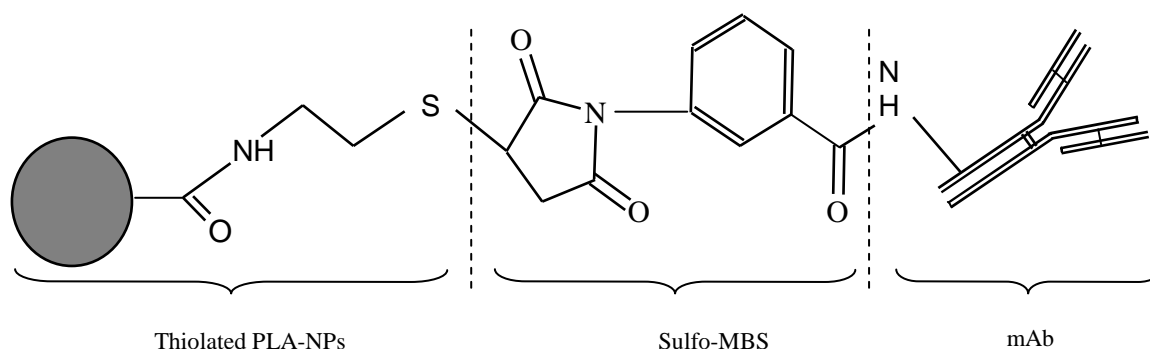


**Figure 1.** Schematic representation of antibody modified nanoparticles (not to scale).

### 3.1 Thiolation of NPs

PLA NPs with free carboxylic functions were prepared by a salting-out method. We selected a high concentration of PVAL (15% w/w) in aqueous solution which allowed obtaining small NPs with a mean size of about  $170\pm 13$  nm.

The influence of cystamine concentration on the amount of -SH introduced on the NPs surface has been studied. With increasing concentrations of cystamine the amount of -SH functions increased and tended, however, to reach saturation at the higher concentrations (Fig.2). The maximum concentration of -SH groups was about 400 mmol-SH/mol PLA. This corresponds to about 25 000 -SH groups per NP. For further experiments three concentrations of cystamine were used: 25, 127, 896 mol cystamine/mol PLA. These concentrations resulted in the introduction of a mean of  $217\pm 30$ ;  $295\pm 27$  and  $385\pm 35$  mmol-SH/mol PLA, respectively, in different experiments.

The nanoparticle size increased from an initial size of  $170\pm 13$  nm to  $202\pm 15$  nm after maximal thiolation.

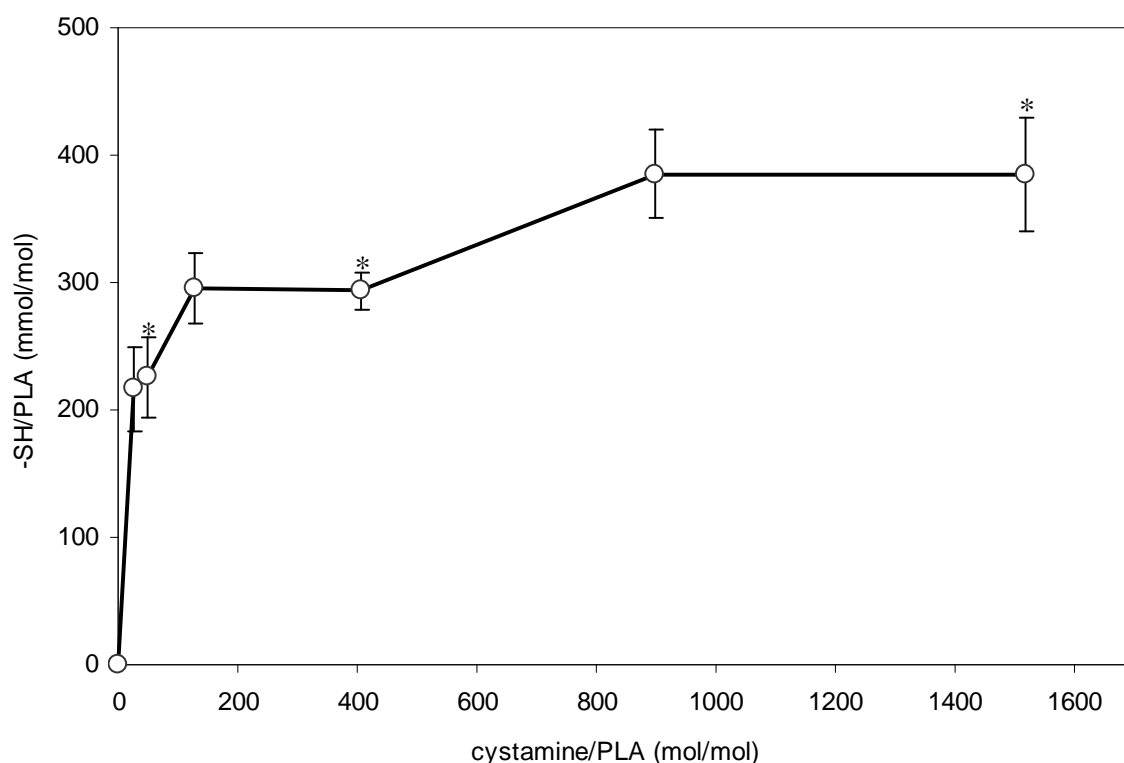


**Figure 2.** Variation of -SH amount on NPs surface in function of cystamine concentration. (O) experimental data; (\*) points used for further experiments. Mean  $\pm$ SD, (n>3).

### 3.2 Covalent coupling of mAb to the NPs-SH

The influence of -SH concentration on the amount of mAb coupled to the NPs was studied using 3 batches of NPs-SH with different concentrations of -SH functions of about 200, 300, 400 mmol-SH/mol PLA. Evaluating constant concentrations of activated mAb with the different batches of NPs-SH, the amount of mAb coupled to the NPs after 1 hour at RT was not influenced by the concentration of -SH functions, both for rituximab and trastuzumab. The control performed with activated anti-CD20 and non-thiolated NPs showed that only a minor quantity of mAb (0.7 mmol anti-CD20/mol PLA) was nonspecifically attached to the NPs.

In order to verify the efficacy of mAb-conjugation to NPs, selected experiments were also performed using trace amounts of radiolabeled antibody mixed with native antibodies. These experiments allowed the calculation of the percentage of mAb coupling by direct radioactivity counting of mAb-NPs in comparison with the input radioactivity (100 %). A

good correlation of results of the optical density measurements, described above, and direct radioactivity counting of mAb-NPs was observed (results not shown).

The amount of mAb conjugated to NPs-SH was in the range of 3 mmol anti-HER2/mg NPs and 5 mmol anti-CD20/mol PLA for the selected condition of incubation of 50  $\mu$ g antibody/mg NPs-SH. These results translate to approximately 295 anti-HER2 and 557 anti-CD20 molecules, respectively, per NP. Antibody coupling efficiency was about 16% and 25% for anti-HER2 and anti-CD20 mAbs, respectively. Figure 3 shows a representative experiment of anti-CD20 coupling.

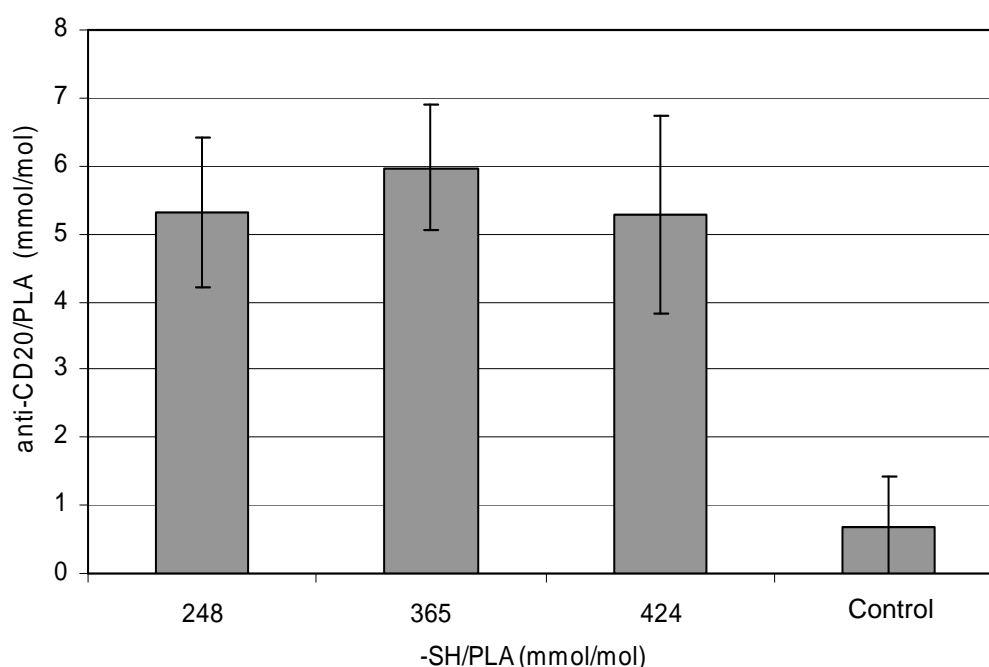


**Figure 3.** Influence of -SH number on the amount of anti-CD20 bound to the NPs.

Control was performed using non-thiolated NPs incubated with activated anti-CD20 mAb.

After antibody coupling the size of both nanoparticle formulations was very similar, about 250 nm (Table 1).

**Table 1.** Physico-chemical characteristics of anti-HER2 and anti-CD20 modified NPs

| Parameter                                | Anti-HER2 NPs | Anti-CD20 NPs |
|--|---------------|---------------|
| Particle size (nm)                       | 264±5         | 256±25        |
| Polydispersity index (P.I.)              | 0.2           | 0.1           |
| Concentration of mAbs<br>(µg mAb/mg NPs) | 8             | 14            |
| Number of antibody/NP                    | 295           | 557           |
| Efficiency of mAb coupling (%)           | 16            | 25            |

P.I.: scale from 0 to 1

### 3.3 Tumor cell interaction with mAb coupled-NPs

The targeting of SKOV-3 and Daudi cells with anti-HER2 NPs and anti-CD20 NPs, respectively, demonstrated for both formulations a strong interaction between cells and NPs modified with the relevant mAb (Fig 4A, E). Control nanoparticles either lacking antibodies or coupled with the non-relevant antibodies showed a very minor non-specific interaction with SKOV-3 (Fig. 4B, C) and Daudi cells (Fig. 4D, F). These results demonstrate the preserved immunoreactivity of the mAb-NPs and the specific interaction of the mAb-NPs with the respective target cells.

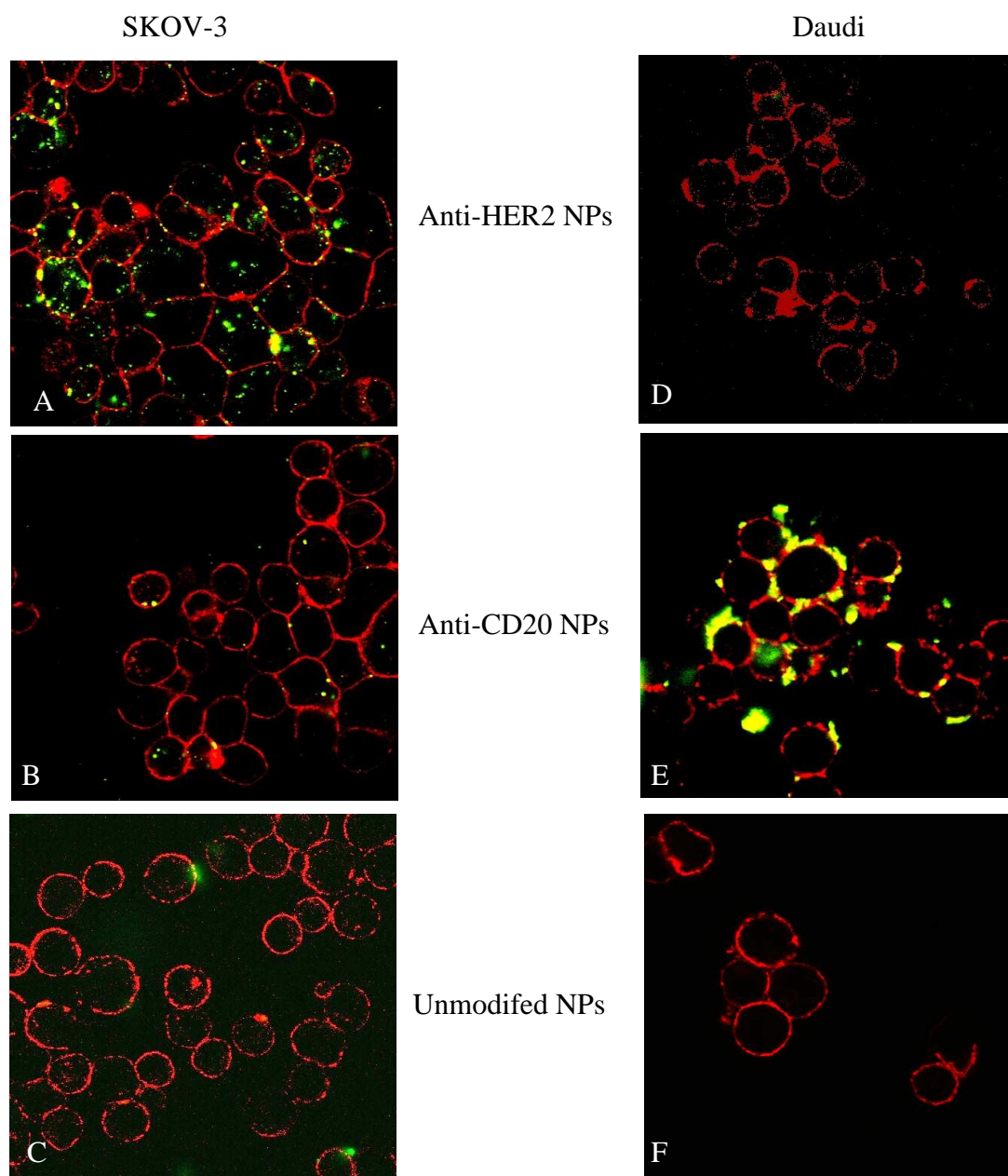


**Figure 4.** Specific interaction of mAb-NPs in SKOV-3 and Daudi cells studied by confocal laser scanning microscopy (objectif: 63x). Cell membranes were stained in red with Concanavalin A AlexaFluor<sup>®</sup> 594 conjugate whereas NPs were stained in green with DiO. The cells were incubated with 1mg/ml mAb labelled NPs or non-conjugated NPs at 37°C for 6 h. (A) and (D) anti-HER2 NPs; (B) and (E) anti-CD20 NPs; (C) and (F) unmodified NPs. Note: in (A) the clear distinction of red membranes and green anti-HER2 NPs, since the latter are internalized and therefore dissociated from the cell membrane while in (E) the binding of anti-CD20 NPs to the cell membrane leads to the superposition of green and red fluorescence and appearance in yellow.

### 3.4 Subcellular localization of mAb coupled-NPs

Confocal microscopy showed two different cellular localizations of mAb-NPs (Fig.5).  $xy$  section views were combined with  $xz/yz$  sections for a better visualization of NPs distribution. In case of SKOV-3 cells the internalization of the anti-HER2 NPs was observed whereas for Daudi cells, the anti-CD20 NPs remained localized on the cellular surface (Fig. 5A, B) after 1h of incubation at 37°C. For anti-HER2 NPs, their intracellular uptake increased after 6 hours of incubation at 37°C compared with 1 hour incubation (data non shown). Extension of the incubation time to 6 hours increased the surface accumulation of anti-CD20 NPs on Daudi cells but still without internalization.

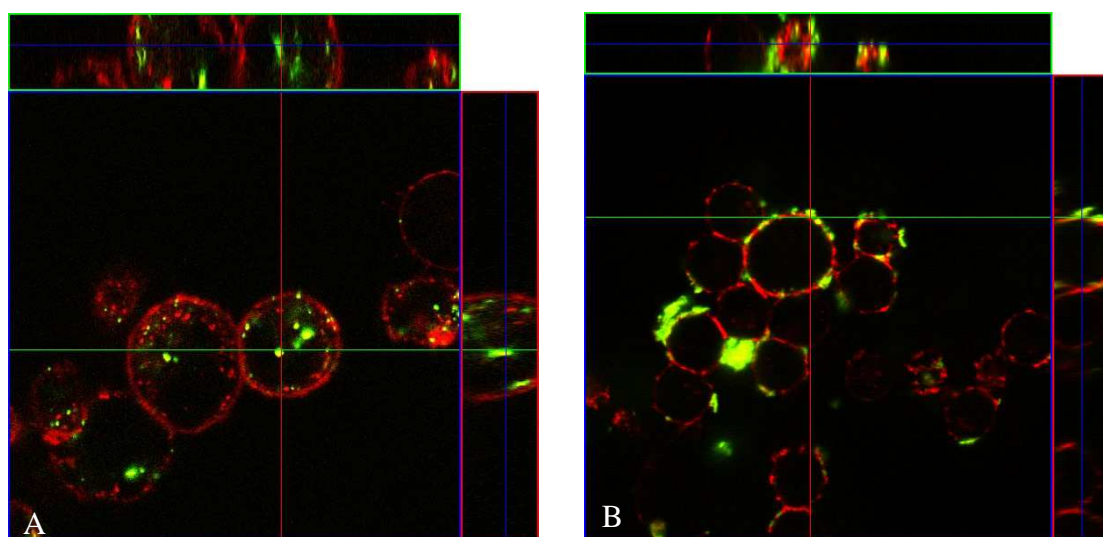


Fig. 5. Orthogonal views of (A) anti-HER2 NPs incubated with SKOV-3 cells and of (B) anti-CD20 NPs incubated with Daudi cells.

## 4. Discussion

Active drug targeting represents a promising approach for treatment of cancer when specific expression of particular target antigens, receptors and biomarkers can be exploited. This condition is fulfilled with the two mAbs used here as shown by multiple clinical studies. For rituximab, the CD20 antigen expression is restricted to normal B cells and B cell lymphoma

while absent of T lymphocytes and bone marrow stem cells. During rituximab treatment, T cell immunity is therefore not affected and repopulation of the normal B cell repertoire after treatment termination remains guaranteed by the preserved stem cells. With respect to trastuzumab, normal cells can express moderate amounts of HER2 target antigen while tumors of certain patients overexpress this antigen. It appears that this difference between healthy tissues and tumors allows the efficient application of this antibody in patients.

The concept of active targeting may be achieved by covalent or non-covalent binding of nanocarrier systems to a tumor recognition moiety which ensures the specific distribution of drug into targeted tissue<sup>22</sup>. Direct conjugation of a drug molecule with a homing moiety is also possible<sup>23</sup> but drug carrier systems have clear advantages such as high drug loading capacity, possibility to control their size and drug activity is not affected by coupling reactions.

Two types of antibody modified nanoparticles, anti-HER2 NPs and anti-CD20 NPs, were prepared in the present work by covalent attachment of the mAb via a thioester linkage with NPs. One of the aims of this study was to develop small NPs. Decreasing the size of NPs might improve their ability to extravasate into target tissues and to avoid phagocytic uptake<sup>1</sup>. Indeed, we managed to obtain antibody coupled nanoparticles of about 250 nm while in previous studies the size of mAb modified nanoparticles were in the range of 340 to 410 nm<sup>11</sup>. Also, we showed that the number of -SH groups on the NPs surface can be modulated using different concentrations of cystamine. However, the -SH concentration at the NPs surface had no influence on the amount of mAb bound. It is possible that steric hindrance of antibodies might limit the number of molecules coupled to the surface of each nanoparticle. The coupling efficiency of antibody could influence cellular interaction of nanocarrier systems. In a previous work, the highest amount of antibody on the NP surface (approximately 2500 mAbs molecules per NPs) showed the lowest cellular binding probably due to an inactivation of antibody<sup>11</sup>. Kirpotin et al. reported that internalization efficacy of anti-HER2 immunoliposomes increased with the increase in surface density of conjugated Fab fragments before reaching a plateau at 15 Fab/liposome<sup>25</sup>. These results suggest that an optimal number of ligands would be necessary to achieve efficient cellular targeting of anti-HER2 nanocarriers. In our study, approximately 295 and 557 molecules of anti-HER2 and anti-CD20 antibodies, respectively, were bound to NPs-SH. Similar results were obtained in other studies using human serum albumin modified NPs, when 429 molecules of trastuzumab were bound per NP<sup>26</sup>.

The two mAbs present different mechanisms of interaction with tumor cells: the CD20 antigen is known not to become internalized upon antibody binding whereas the HER2 antigen is internalized. An efficient internalization of anti-HER2 NPs could indeed be observed in SKOV-3 cells overexpressing HER2 (Fig.4). These results are in line with different other studies that have demonstrated specific binding and internalization of anti-HER2 nanoparticulate drug delivery systems such as immunoliposomes or immunonanoparticles<sup>24,25</sup>.

Also, therapeutic efficiency of anti-HER2 immunoliposomes-doxorubicine was shown in a tumor xenograft model<sup>27</sup>.

In contrast to anti-HER2 NPs, the anti-CD20 NPs were not internalized. Despite the fact that multiple antibodies per NP can react with cells, internalization could not be observed with the anti-CD20 NPs even after prolonged incubation. The proposed mechanism of interaction between Daudi and anti-CD20 NPs is a cell surface clustering.

Non-internalizing NPs remain of interest as anti-tumor drug carriers for at least 2 reasons: first, the drug released on the cell surface can be taken up by passive diffusion or another mechanism via endocytic pathways including clathrin-coated pits, caveole membrane invaginations, phagocytosis and pinocytosis phenomena<sup>5, 28</sup>. Secondly, the observation of direct induction of apoptosis by crosslinked anti-CD20 antibodies<sup>29</sup> might provide additional efficacy to anti-CD20 NPs by the fact that the multiple antibodies per NP might represent a new efficient method of crosslinking.

## 5. Conclusion

The efficiency of mAb modified NPs in specific tumor cell targeting was demonstrated *in vitro*. Furthermore, confocal microscopy showed the different cellular localization of NPs depending on the type of antibody-antigen interaction that was involved. These two model situations will allow evaluating in a next step the efficiency of the mAb-NPs as carrier of cytostatic drugs. Finally, different *in vivo* tumor models are available for these two mAb-NPs conjugates that will allow testing of their efficiency in specific tumor targeting.

---

**Reference List**

1. Brigger, I., Dubernet, C. & Couvreur, P. Nanoparticles in cancer therapy and diagnosis. *Adv. Drug Deliv. Rev.* 54, 631-651, 2002.
2. Panyam, J. & Labhasetwar, V. Biodegradable nanoparticles for drug and gene delivery to cells and tissue. *Adv. Drug Deliv. Rev.* 55, 329-347, 2003.
3. Maeda, H. The enhanced permeability and retention (EPR) effect in tumor vasculature: The key role of tumor-selective macromolecular drug targeting. *Adv. Enzyme Regul.* 41, 189-207, 2001.
4. Duncan, R. Polymer conjugates for tumor targeting and intracytoplasmic delivery. The EPR effect as a common gateway? *Pharm. Sci. Technol. Today* 2, 441-449, 1999.
5. Koo, O. M., Rubinstein, I. & Onyuksel, H. Role of nanotechnology in targeted drug delivery and imaging: A concise review. *Nanomed.* 1, 193-212, 2005.
6. Sapra, P. & Allen, T. M. Ligand-targeted liposomal anticancer drugs. *Prog. Lipid Res.* 42, 439-462, 2003.
7. Park, J. W. et al. Anti-HER2 immunoliposomes for targeted therapy of human tumors. *Cancer Lett.* 118, 153-160, 1997.
8. Lukyanov, A. N., Elbayoumi, T. A., Chakilam, A. R. & Torchilin, V. P. Tumor-targeted liposomes: doxorubicin-loaded long-circulating liposomes modified with anti-cancer antibody. *J. Control. Release* 100, 135-144, 2004.
9. Ignatius, A. A. & Claes, L. E. In vitro biocompatibility of bioresorbable polymers: poly(L,DL-lactide) and poly(L-lactide-coglycolide). *Biomaterials* 17, 831-839, 1996.
10. Nobs, L., Buchegger, F., Gurny, R. & Allemann, E. Poly(lactic acid) nanoparticles labeled with biologically active Neutravidin for active targeting. *Eur. J. Pharm. Biopharm.* 58, 483-490, 2004.

- 
11. Nobs, L., Buchegger, F., Gurny, R. & Allemann, E. Biodegradable Nanoparticles for Direct or Two-Step Tumor Immunotargeting. *Bioconjug. Chem.* 17, 139-145, 2006.
  12. Harries, M. & Smith, I. The development and clinical use of trastuzumab (Herceptin). *Endocr. Relat. Cancer* 9, 75-85, 2002.
  13. Nahta, R. & Esteva, F. J. Herceptin: mechanisms of action and resistance. *Cancer Lett.* 232, 123-138, 2006.
  14. Hiddemann, W., Buske, C., Dreyling, M., Weigert, O., Lenz, G., Forstpointner, R., Nickenig, C., Unterhalt, M. Treatment strategies in follicular lymphomas: current status and future perspectives. *J. Clin. Oncol.* 23, 6394-6399, 2005.
  15. Harris, M. Monoclonal antibodies as therapeutic agents for cancer. *Lancet Oncol.* 5, 292-302, 2004.
  16. Eisenberg, R. & Looney, R. J. The therapeutic potential of anti-CD20. *Clin. Immunol.* 117, 207-213, 2005.
  17. Boye, J., Elter, T. & Engert, A. An overview of the current clinical use of the anti-CD20 monoclonal antibody rituximab. *ESMO* 14, 520-535, 2003.
  18. Czuczman, M. S., Weaver, R., Alkuzweny, B., Berlfein, J. & Grillo-Lopez, A. J. Prolonged clinical and molecular remission in patients with low-grade or follicular non-Hodgkin's lymphoma treated with rituximab plus CHOP chemotherapy: 9-year follow-up. *J. Clin. Oncol.* 22, 4711-4716, 2004.
  19. Hiddemann, W., Kneba, M., Dreyling, M., Schmitz, N., Lengfelder, E., Schmits, R., Reiser, M., Metzner, B., Harder, H., Hegewisch-Becker, S., Fischer, T., Kropff, M., Reis, H. E., Freund, M., Wormann, B., Fuchs, R., Planker, M., Schimke, J., Eimermacher, H., Trumper, L., Aldaoud, A., Parwaresch, R., Unterhalt, M., Frontline therapy with rituximab added to the combination of cyclophosphamide, doxorubicin, vincristine, and prednisone (CHOP) significantly improves the outcome for patients with advanced-stage follicular lymphoma compared with therapy with CHOP alone: Results of a prospective randomized study of the German Low-Grade Lymphoma Study Group. *Blood* 106, 3725-3732, 2005.

- 
20. De Jaeghere, F., Allemann, E., Feijen, J., Kissel, T., Doelker, E., Gurny, R. Freeze-drying and lyopreservation of diblock and triblock poly(lactic acid)-poly(ethylene oxide) (PLA-PEO) copolymer nanoparticles. *Pharm. Dev. Technol.* 5, 473-483, 2000.
  21. Nobs, L., Buchegger, F., Gurny, R. & Allemann, E. Surface modification of poly(lactic acid) nanoparticles by covalent attachment of thiol groups by means of three methods. *Int. J. Pharm.* 250, 327-337, 2003.
  22. Nobs, L., Buchegger, F., Gurny, R. & Allemann, E. Current methods for attaching targeting ligands to liposomes and nanoparticles. *J. Pharm. Sci.* 93, 1980-1992, 2004.
  23. Jaracz, S., Kuznetsova, L. V. & Ojima, I. Recent advances in tumor-targeting anticancer drug conjugates. *Bioorg. Med. Chem.* 13, 5043-5054, 2005.
  24. Wartlick, H., Michaelis, K., Balthasar, S., Strebhardt, K., Kreuter, J., Langer, K. Highly specific HER2-mediated cellular uptake of antibody-modified nanoparticles in tumour cells. *J. Drug. Target.* 12, 461-471, 2004.
  25. Kirpotin, D., Park, J. W., Hong, K., Zalipsky, S., Li, W. L., Carter, P., Benz, C. C., Papahadjopoulos, D. Sterically stabilized anti-HER2 immunoliposomes: design and targeting to human breast cancer cells in vitro. *Biochemistry* 36, 66-75, 1997.
  26. Steinhauser, I., Spaenkuch, B., Strebhardt, K. & Langer, K. Trastuzumab-modified nanoparticles: Optimisation of preparation and uptake in cancer cells. *Biomaterials* 27, 4975-4983, 2006.
  27. Park, J. W., Hong, K., Kirpotin, D. B., Colbern, G., Shalaby, R., Baselga, J., Shao, Y., Nielsen, U. B., Marks, J. D., Moore, D., Papahadjopoulos, D., Benz, C. C., 2002. Anti-HER2 immunoliposomes: enhanced efficacy attributable to targeted delivery. *Clin. Cancer Res.* 8, 1172-1181, 2002.
  28. Rejman, J., Oberle, V., Zuhorn, I. S. & Hoekstra, D. Size-dependent internalization of particles via the pathways of clathrin- and caveolae-mediated endocytosis. *Biochem. J.* 377, 159-169, 2004.
  29. Shan, D., Ledbetter, J. A. & Press, O. W. Apoptosis of malignant human B cells by ligation of CD20 with monoclonal antibodies. *Blood* 91, 1644-1652, 1998.



---

**Nanomedicines for active targeting:  
Physico-chemical characterization of paclitaxel-loaded anti-HER2  
immunonanoparticles and *in vitro* functional studies on target cells**

A. Cirstoiu-Hapca<sup>a</sup>, F. Buchegger<sup>b</sup>, L. Bossy<sup>a\*</sup>, M. Kosinski<sup>c</sup>, R. Gurny<sup>a</sup>, F. Delie<sup>a</sup>

<sup>a</sup> School of Pharmaceutical Sciences, University of Geneva, University of Lausanne, Quai Ernest Ansermet 30, CH-1211 Geneva 4, Switzerland

<sup>b</sup> Division of Nuclear Medicine, University Hospital of Geneva, Switzerland

<sup>c</sup> Nuclear Medicine, University Hospital of Lausanne, Switzerland

\* Current address: TRB Chemedica International SA, Geneva, Switzerland

*Published in European Journal of Pharmaceutical Sciences 38 (2009) 230-237*

---

Paclitaxel (Tx)-loaded anti-HER2 immunonanoparticles (NPs-Tx-HER) were prepared by the covalent coupling of humanized monoclonal anti-HER2 antibodies (trastuzumab, Herceptin<sup>®</sup>) to Tx-loaded poly (DL-lactic acid) nanoparticles (NPs-Tx) for the active targeting of tumor cells that overexpress HER2 receptors. Paclitaxel (Tx)-loaded anti-HER2 immunonanoparticles (NPs-Tx-HER) were prepared by the covalent coupling of humanized monoclonal anti-HER2 antibodies (trastuzumab, Herceptin<sup>®</sup>) to Tx-loaded poly (DL-lactic acid) nanoparticles (NPs-Tx) for the active targeting of tumor cells that overexpress HER2 receptors. The physico-chemical properties of NPs-Tx-HER were compared to unloaded immunonanoparticles (NPs-HER) to assess the influence of the drug on anti-HER2 coupling to the NP surface. The immunoreactivity of sulfo-MBS activated anti-HER2 mAbs and the *in vitro* efficacy of NPs-Tx-HER were tested on SKOV-3 ovarian cancer cells that overexpress HER2 antigens. Tx-loaded nanoparticles (NPs-Tx) obtained by a salting-out method had a size of  $171 \pm 22$  nm (P.I. = 0.1) and an encapsulation efficiency of about  $78 \pm 10\%$ , which corresponded to a drug loading of  $7.8 \pm 0.8\%$  (w/w). NPs-Tx were then thiolated and conjugated to activated anti-HER2 mAbs to obtain immunonanoparticles of  $237 \pm 43$  nm

---

(P.I. = 0.2). The influence of the activation step on the immunoreactivity of the mAbs was tested on SKOV-3 cells using  $^{125}\text{I}$ -radiolabeled mAbs, and the activity of the anti-HER2 mAbs was minimally affected after sulfo-MBS functionalization. Approximately 270 molecules of anti-HER2 mAbs were bound per nanoparticle. NPs-Tx-HER exhibited a zeta potential of  $0.2 \pm 0.1$  mV. The physico-chemical properties of the Tx-loaded immunonanoparticles were very similar to unloaded immunonanoparticles, suggesting that the encapsulation of the drug did not influence the coupling of the mAbs to the NPs. No drug loss was observed during the preparation process. DSC analysis showed that encapsulated Tx is in an amorphous or disordered crystalline phase. These results suggest that Tx is entrapped in the polymeric matrix and not adsorbed to the surface of the NPs. *In vitro* studies on SKOV-3 ovarian cancer cells demonstrated the greater cytotoxic effect of NPs-Tx-HER compared to other Tx formulations. The results showed that at 1 ng Tx/ml, the viability of cells incubated with drugencapsulated in NP-Tx-HER was lower ( $77.32 \pm 5.48\%$ ) than the viability of cells incubated in NPs-Tx ( $97.4 \pm 12\%$ ), immunonanoparticles coated with Mabthera<sup>®</sup>, as irrelevant mAb, (NPs-Tx-RIT) ( $93.8 \pm 12\%$ ) or free drug ( $92.3 \pm 9.3\%$ )

**Keywords:** Immunonanoparticle, nanomedicine, active targeting, ovarian cancer, paclitaxel, monoclonal antibody, anti-HER2, Herceptin<sup>®</sup>, SKOV-3

---

## 1. Introduction

The benefits of traditional chemotherapy are limited by the toxicity associated with anticancer drugs in healthy tissues. The common features of cancer and healthy cells make it difficult to achieve pharmacoselectivity of drugs at the target site. For example, hematopoietic cells, the gastrointestinal tract mucosa or hair follicle cells with a high proliferation rate are severely affected during treatment. Hence, over the past decades, efforts have been focused on the development of nanomedicines such as nanoparticles (NPs), liposomes, micelles or dendrimers for the specific delivery of anticancer drugs to tumor tissues <sup>1</sup>. The physicochemical characteristics of nanocarriers, such as composition, particle size, surface charge and the presence of ligands on their surface, will dictate their biodistribution, pharmacokinetics <sup>2</sup>. These nanomedicines allow the sustained release of the drug, the administration of liposoluble molecules and an improvement in the stability of fragile therapeutic agents <sup>3,4</sup>. Moreover, due to the pathophysiological characteristics of tumors, a

preferential accumulation of encapsulated drug at desired sites can be obtained either by passive or active targeting. On one hand, the enhanced permeability and retention effect (EPR effect), which characterizes malignant tissues, allows the passive accumulation of encapsulated drugs to tumor sites<sup>5</sup>. On the other hand, cancer cells often overexpress specific proteins, such as growth factor receptors related to the high proliferation rate and angiogenesis process<sup>6</sup>; or transferrin and folate receptors related to the increased need for nutrients<sup>7,8</sup>. These typical tumor bio-markers can be exploited to achieve active targeting by the specific recognition of a ligand. This approach represents a very promising strategy to further increase the selective delivery of anticancer agent to target sites. Indeed, recognition moieties such as complete or fragmented monoclonal antibodies (mAbs), glycoproteins and peptides that specifically bind to receptors or antigens may be associated with drug delivery systems<sup>9</sup>. Further to the development of antibody therapies and the significant improvement of cancer treatment using mAbs alone or in combination with chemotherapeutics or radiotherapy<sup>10,11</sup>, active immunonanotargeting has aroused the interest of researchers<sup>12-15</sup>. Some mAb ligands, such as Herceptin<sup>®</sup> or Mabthera<sup>®</sup>, are used in clinics as therapeutic agents. Therefore, a synergistic or additive effect between an entrapped drug and mAbs could be considered<sup>13</sup>. For a successful targeting strategy, the target antigens must be specifically and stably expressed in tumor cells and not present or expressed at very low levels in host cells. On the other hand, the lack of immunogenicity, a long half-life and a specific interaction with the relevant antigen is required for mAbs used as a ligand<sup>9</sup>. The internalization of the receptor after its interaction with the specific ligand is a very interesting feature, as it implies the possibility of delivering a drug directly into cancer cells.

We have previously developed polymeric immunonanoparticles for specific tumor targeting using anti-HER2 and anti-CD20 mAbs as ligands<sup>16,17</sup>. Anti-HER2-coated immunonanoparticles containing Tx, as a drug model, were selected to further demonstrate the *in vitro* and *in vivo* efficacy of the NPs.

Tx is one of the most efficient agents against a wide spectrum of cancers, such as ovarian, breast, lung, bladder, head and neck cancer. Tx induces cell division arrest at the G2 mitotic phase by tubulin polymerization and the stabilization of microtubules. It also inhibits angiogenesis, cell migration and collagenase production<sup>18,19</sup>. However, Tx suffers from a poor solubility in water and a low therapeutic index that is associated with serious side effects. The Cremophor EL (polyethoxylated castor oil):dehydrated ethanol 50:50 (v/v) used as vehicle in Taxol<sup>®</sup> is often associated with severe adverse effects such as allergic reactions,

nephrotoxicity and neurotoxicity, as well as physical instability and incompatibility with the materials used for its infusion<sup>20</sup>. To circumvent these limitations, several carrier systems for Tx delivery have been investigated, and Tx-conjugated albumin NPs (Abraxane<sup>®</sup>) were approved in 2005 by the FDA for the treatment of metastatic breast cancer<sup>21</sup>. Opaxio<sup>™</sup> (formerly known as Xyotax<sup>™</sup>), an ester-linked poly-(L)-glutamic acid-Tx conjugate, has also been tested in phase III clinical trials against non-small-cell lung cancer<sup>22,23</sup>. The active targeting of encapsulated Tx has been explored using transferrin, galactosamine, anti-HER2 or fragments of mAbs (anti-HER2 scFv F5) as moieties for selective treatment against prostate, breast or liver tumors<sup>12,15,24-27</sup>.

Among tumor bio-markers, the HER2 membrane receptor is one of the most promising targets for immunotherapy. The surface accessibility, the high level of expression in certain primary and metastatic tumors and the internalization of these antigens via receptor-mediated endocytosis<sup>28</sup> promotes preferential intracellular accumulation of drug nanocarriers<sup>29</sup>. The overexpression of HER2 antigens (*c-erbB-2*, *neu*) in 20-30% of breast and ovarian cancers is correlated with a high occurrence of metastasis and angiogenesis processes, as well as with a poor prognosis<sup>30</sup>. Herceptin<sup>®</sup>, a humanized mAb designed to specifically antagonize HER2 function, was approved in 1998 for metastatic breast cancer overexpressing HER2 antigens<sup>31</sup>. Clinical trials demonstrated an improvement of the median survival rate to approximately 25 months after Herceptin<sup>®</sup> treatment combined with chemotherapy, compared to only 13 months in the case of Herceptin<sup>®</sup> used as a single agent<sup>10,32</sup>. Therefore, the development of immunocarriers or drug-immunoconjugates based on the additive effects of Herceptin<sup>®</sup> and Tx represents very encouraging approaches to improve cancer treatment. Unlike drug-immunoconjugates, immunonanoparticles offer the possibility of delivering a large payload of drug to the target site, while the encapsulation process avoids the production of a new chemical entity (NCE) during the coupling reactions<sup>1</sup>.

The aim of the present work was to prepare and characterize Tx-loaded immunonanoparticles coated with anti-HER2 mAbs. The immunoreactivity of the sulfo-MBS activated anti-HER2 mAbs and the cytotoxicity of NPs-Tx-HER compared to the other Tx formulations was assessed *in vitro*.

## 2. Material and methods

### 2.1 Materials

Tx was obtained from Cfm Oskar Tropitzsch (Marktredwitz, Germany). Poly (DL-lactic acid) (100DL 4A, Mw 57kDa) was provided by Lakeshore Biomaterials, Inc (Birmingham, USA). Anti-HER2 (trastuzumab, Herceptin<sup>®</sup>) and Anti-CD20 (rituximab, Mabthera<sup>®</sup>) were purchased from Roche (Basle, Switzerland). 1-Ethyl-3-(3-dimethylaminopropyl)-carbodiimide (EDAC), D(+)-trehalose dehydrate and phosphate buffer saline (PBS) were from Sigma (Buchs, Switzerland). Dimethylsulfoxide (DMSO) was obtained from Acros (Geel, Belgium), while m-maleimidobenzoyl-N-hydroxy-sulfosuccinimide ester (sulfo-MBS) and Tris (2-carboxyethyl)-phosphine hydrochloride (TCEP) were supplied by Pierce (Rockford, IL, USA). Poly (vinyl alcohol) Mowiol 4-88 was obtained from Hoechst (Frankfurt/M, Germany). Magnesium chloride hexahydrate was obtained from Fluka (Buchs, Switzerland). Amicon Ultra-4 (Ultracel-100k) centrifugal filter devices were provided by Millipore (Ireland).

### 2.2 Tx-loaded immunonanoparticle preparation

#### 2.2.1 Preparation of Tx-loaded NPs (NP-Tx)

NPs containing Tx were prepared by a salting-out method, as previously described<sup>33</sup> with a slight modification to improve the drug encapsulation efficiency rate. Briefly, 24 mg of Tx dissolved in 0.5 g acetone was added to a solution of 240 mg poly (DL-lactic acid) (PLA) in 1 g acetone (drug to polymer ratio = 1:10). The organic phase was mixed under vigorous stirring (2000 rpm) for 15 min at 45°C with 3.5 g of aqueous phase containing 15% (w/w) poly (vinyl alcohol) (PVAL) and 60% (w/w) magnesium chloride hexahydrate. The miscibility of the two phases was prevented by the high concentration of salt. Then, 20 ml of pure water was added to the NP suspension, and the stirring was maintained for 10 min. NPs were recovered by centrifugation at 50000xg for 30 min (Optima<sup>®</sup> XL-100K, rotor 70.1 Ti Centrifuge, Beckman Coulter Inc., Fullerton, CA, USA) and were washed twice with pure water to remove unencapsulated drug, PVAL and magnesium salt. After preparation and

purification, NPs were lyophilized (Edwards, Modulyo, Oberwil, Switzerland) for 2 days in the presence of trehalose (30 % w/w) as a lyoprotector before storage at 4°C until use.

### *2.2.2 Coating of NPs-Tx surface with mAbs*

NPs-Tx-HER were prepared by a two step process involving the thiolation of free carboxyl groups on the NP surface, followed by the covalent attachment of mAbs to thiolated NPs via a sulfo-MBS cross-linker.

#### *2.2.2.1 Thiolation of NPs-Tx*

Thiol functions (-SH) were covalently bound to the NPs-Tx by a two-step carbodiimide reaction, as described previously<sup>33</sup>. Briefly, 100 mg of NPs-Tx were suspended in 5 ml water, and the reaction was initiated by consecutively adding 10 ml of a solution of EDAC (24 mg/ml) and 5 ml of a cystamine solution (71 mg/ml corresponding to 896 mol cystamine/mol PLA). The final suspension was completed with water to 25 ml and stirred under mild conditions for 24 h at room temperature. Thereafter, EDAC and non-reacted cystamine were removed by two successive centrifugations (50000xg for 20 min). NPs were then re-suspended in purified water and incubated for 3 h with 1 ml of an aqueous solution of TCEP (6 mg/ml) to reduce disulfide bonds. Finally, thiolated Tx-loaded NPs (NPs-Tx-SH) were purified by two successive centrifugations (50000xg for 15 min) and freeze-dried in presence of trehalose (30% w/w). The concentration of the -SH functions on the surface of NPs was determined spectrophotometrically at  $\lambda=410$  nm (Hewlett Packard, Model 8453, Germany) using Ellman's reagent.

#### *2.2.2.2. Activation of mAb and covalent binding to NPs-Tx-SH*

The covalent binding of mAbs to the NPs-Tx-SH was performed according to a previously described method<sup>16</sup>. Briefly, 1 ml of clinical grade anti-HER2 (Herceptin<sup>®</sup>) solution was purified by centrifugation at 4000xg for 15 min (Centaur 2 MSE) using Amicon Ultra-4 centrifugal filter devices. Two milligrams of purified mAbs were activated in PBS (pH=7.4) with sulfo-MBS at a molar ratio 1/20 (mAbs/sulfo-MBS) for 45 min at room temperature. Non-reacted sulfo-MBS was removed by centrifugation (4000xg for 15 min) using Amicon Ultra-4

centrifugal filter devices. Five hundred microliters of activated anti-HER2 (1 mg/ml) was reacted for 1, 6 or 12 h with gentle shaking at room temperature with 500  $\mu$ l NPs-Tx-SH (20 mg/ml). Unconjugated mAbs were removed by 2 cycles of centrifugation (48000xg for 10 min) using a Beckman Avanti<sup>TM</sup> 30 centrifuge (rotor 1202; Beckman Coulter Inc., Fullerton, CA, USA). Finally, NPs-Tx-HER were stored in PBS at 4°C and used within a week after preparation. The amount of mAb conjugated to NPs was determined indirectly by measuring uncoupled mAb in the supernatant after a centrifugation step. A spectrophotometric method ( $\lambda=280$  nm) (Hewlett Packard, Model 8453, Germany) was used by assuming an extinction coefficient of  $1.4 \text{ M}^{-1}\text{cm}^{-1}$ . The number of mAbs coupled per NP was calculated as previously published<sup>17</sup>.

NPs-Tx-RIT were obtained in the same manner and used as a negative control in further experiments.

## 2.3 Characterization of NPs

### 2.3.1 Size and morphology

The size and morphology of NPs were analyzed by photon correlation spectroscopy (PCS) using a Zetasizer 3000 HS (Malvern instruments Ltd, United Kingdom). Scanning electron microscopy (SEM) was performed on gold-coated freeze-dried samples (Balzers SCD 004 Sputter Coater) with a JEOL JSM-6400 microscope (JEOL, Tokyo, Japan) at an accelerating voltage of 10 or 15 kV.

### 2.3.2 DSC analysis

The physical state of the Tx encapsulated into the polymeric NPs was studied by differential scanning calorimetric (DSC) thermogram analysis (DSC Seiko, 220C LabPlus, Swizerland). About 6 mg of NPs-Tx, unloaded NPs and free Tx were sealed separately in aluminum pans. The samples were heated at 10°C/min in the 20 to 300°C range, cooled at 20°C with pure dry nitrogen and then reheated at 100°C. The instrument was calibrated using indium.

### 2.3.3 *Surface charge*

Zeta potential measurements of NP suspensions were performed in a  $10^{-3}$  M NaCl solution using the electrophoretic mode of Zetasizer 3000 HS.

### 2.3.4 *Encapsulation efficiency and drug loading*

Three milligrams of NPs-Tx were dispersed in 1 mL of acetone and sonicated for 5 min. The solution was centrifuged at  $7200\times g$  for 5 min (Beckman Avanti<sup>TM</sup> 30 centrifuge, rotor 1202). Tx content in the supernatant was measured by reverse-phase HPLC with UV detection. The HPLC system consisted of a Waters 600 Controller separation module fitted with a Waters 2487 Dual  $\lambda$  absorbance detector, a Waters 717 Plus Autosampler and a NUCLEOSIL C18 column (4.6mm x 125cm, 5  $\mu$ m; Macherey-Nagel, Switzerland). The mobile phase (acetonitrile/water = 50/50) was delivered at a flow rate of 1 ml/min, the injection volume was 20  $\mu$ l, and the drug was detected at 227 nm. A standard plot for Tx (0.08-0.50 mg/ml) dissolved in acetone was prepared under identical conditions. The encapsulation efficiency (%) was calculated as the percentage of drug entrapped into the NPs with respect to the initial amount of drug added in the formulation. The drug loading was expressed as the amount of drug encapsulated in 100 mg NPs. The amount of Tx in NPs-Tx-SH and NPs-Tx-HER was evaluated under the same conditions in order to determine the drug loss during coupling reactions.

## 2.4 **Cell culture**

The SKOV-3 line of human ovarian carcinoma cells is known to overexpress HER2-specific antigens (American Type Culture Collection ATCC, Manassas, VA). Cells were grown in RPMI-1640 medium with Glutamax I (Gibco Invitrogen, Grand Island, USA) supplemented with 10% (v/v) fetal calf serum (FCS) (Brunschwig, Basle Switzerland), penicillin (100 units/ml) and streptomycin (100  $\mu$ g/ml) (Gibco Invitrogen, Grand Island, USA) at 37°C in a humidified incubator containing 5% CO<sub>2</sub>. SKOV-3 cells were maintained as a monolayer, and the cells were harvested using TrypLE Express (Gibco Invitrogen, Grand Island, USA) and resuspended in fresh complete medium before performing experiments.

## 2.5 Immunoreactivity of sulfo-MBS activated anti-HER2 mAbs

The immunoreactivity of anti-HER2 mAbs after functionalization with sulfo-MBS was compared to the non-activated mAbs on SKOV-3 cells using  $^{125}\text{I}$  radiolabeled antibodies. Antibody radiolabeling was performed using the chloramine T method with minor modifications<sup>34</sup>. Briefly, 0.25 ml of clinical grade Herceptin (5 mg) and 100  $\mu\text{l}$  of freshly prepared chloramine T solutions (0.5 mg per 1 ml, in sterile 0.15 M phosphate buffer, pH 7) were reacted for 5 min at room temperature with 20 MBq  $\text{Na}^{125}\text{I}$  that was previously diluted to 200  $\mu\text{l}$  with 0.15 M phosphate buffer pH 7.0. The solution of labeled antibodies was purified through 2 ml reversible columns (Supelco, Buchs, Switzerland) filled with 1.8 g of anion exchange resin (Dowex 1 x 8, 100 mesh) at a flow rate of 0.5 ml/min. The labeling vial was washed with 2 ml of a 0.9% NaCl solution. One milligram of radiolabeled anti-HER2 mAbs was activated with sulfo-MBS and purified as described in 2.2.2.2.

SKOV-3 cells were harvested from exponential phase cultures, washed and counted. The immunoreactivity of activated and non-activated anti-HER2 mAbs was measured using three dilutions of cells:  $1 \times 10^6$ ,  $3 \times 10^6$  and  $1 \times 10^7$ /ml. Twenty-five nanograms of activated or non-activated anti-HER2 mAbs diluted in 100  $\mu\text{l}$  of phosphate buffered saline (0.15 mol/l NaCl and 0.01 mol/l phosphate buffer, pH 7) containing 2% fetal calf serum were added to the cells and incubated at  $0^\circ\text{C}$  for 2h under mild agitation. The incubation at low temperature prevents the internalization of antibodies, which can induce the de-halogenation of the radiolabeled mAbs and the subsequent loss of radioactivity. Thereafter, cells were washed three times with 3 mL of PBS and centrifuged to remove unbound mAbs. Nonspecific binding was generally less than 1% and was assessed by competition with 100  $\mu\text{g}$  of unlabeled antibody and subtracted when specific binding was determined. Two paired binding assays were performed with a total of five samples per number of cells. Results from the two tests overlapped and were pooled. The nonparametric paired two-sample Wilcoxon signed rank test was used for the statistical comparison of results.

Furthermore, the possible formation of aggregates during the antibody activation process was detected by using an HPLC size chromatography technique and spectrophotometry. Analytic size chromatography of activated and non-activated Herceptin<sup>®</sup> was performed on a BioSep-sec-S3000 column (300 x 7.8 mm, Phenomenex) in a physiologic NaCl solution (0.15 M) using a Varian ProStar HPLC, Model 220. The optical density of non-radiolabeled samples was read at 280 nm, while sets of analyses were performed on two different

preparations of radiolabeled non-activated and activated Herceptin<sup>®</sup> measured with a Raytest (GABY) radiation detector.

## 2.6 *In vitro* cytostatic assay

*In vitro* cytotoxicity of the following Tx formulations was tested on SKOV-3 cells using the MTT test: NPs-Tx-HER, NPs-Tx, NPs-Tx-RIT and free Tx. Unconjugated and conjugated unloaded NPs (NPs and NPs-HER) were tested to determine the effects of polymer and ligand on cell viability.

SKOV-3 cells were seeded in 96-well plates at a density of 20 000 cells/well and incubated for 24 h to allow cellular adhesion and recovery of normal cycle. Cell culture medium was then replaced by 200  $\mu$ l of the formulations. For free drug, a stock solution of Tx was prepared in ethanol (5 mg/mL), and suitable concentrations were obtained by dilution of the initial stock solution in culture medium. The ethanol concentration in the medium was lower than 0.1 %, at which level it has no effect on cell proliferation. The suspensions of NPs were diluted in culture medium at equivalent Tx concentrations ranging from 0.001 to 0.1  $\mu$ g/ml, corresponding to approximately 0.0013-0.13  $\mu$ g/ml NPs. After 5 h of incubation, the supernatants were removed, and the cells were washed with HBSS (Gibco Invitrogen, Grand Island, USA) and incubated with 200  $\mu$ l of normal culture medium for 4 days. Then, the cells were washed twice with HBSS, and 50  $\mu$ l/well of a 0.1% (m/v) MTT solution was added and incubated for 3 h at 37°C. Two hundred microliters of DMSO was added to dissolve the precipitant, and the plates were analyzed after 1 h using a microplate reader (Model 550, Bio-RAD, Hercules, USA) at  $\lambda = 595$  nm. Cell viability was calculated by comparing the samples to cells incubated with normal culture medium as 100% survival rate.

## 2.7 Statistical analysis

Two statistical analyses were applied for MTT test results. In the first analysis, the data set was split according to the different treatments and each treatment was analyzed separately using one-way ANOVA and Dunnet's posthoc comparison test against the control (concentration 0), to determine a threshold in the concentration level for which the treatments would generate a cytotoxic effect significantly different from the control. In the second approach, to determine a possible difference between treatments at the same concentration, NPs, NPs-

---

HER treatments were removed from the dataset and a Scheffe multiple comparison test was applied to the remaining four treatments each at five different concentration levels.

### 3. Results and discussion

Immunonanoparticles represent a very interesting concept for cancer treatment, and they may improve the therapeutic index of a drug by preferential accumulation at target sites and lower distribution in healthy tissues. However, the properties of mAbs used as ligands to achieve active targeting could be altered during immunonanoparticle preparation. Thus, it is essential to determine the influence of chemical reactions on the immunoreactivity of mAbs and to obtain a good knowledge of the physico-chemical characteristics of immunonanoparticles.

This study is dedicated to the preparation of Tx-loaded NPs coated with anti-HER2 mAbs and their characterization in terms of size and size distribution, surface charge, number of thiol groups, number of anti-HER2 molecules bound per NP, drug loading and encapsulation efficiency. The effect of mAb activation on the immunoreactivity was evaluated on SKOV-3 cells. The cytotoxicity of different Tx formulations was also tested on these cells.

#### 3.1 Characterization of Tx-loaded NPs

The characteristics of the NPs used in this study are summarized in Table 1. Tx was successfully encapsulated in the polymeric NPs by using the salting out method. The method was modified in order to improve the encapsulation of Tx. Indeed, when using the original method as previously described<sup>33</sup>, Tx precipitated in the outer aqueous phase, and typical needle crystals were seen under microscope (data not shown). The desolvation of Tx may occur during the dilution step when water is added to the emulsion to induce particle formation. Thus, the first preparation step was performed at 45°C to favor acetone evaporation before solvent dilution with the prevention of Tx escape from the organic phase before matrix formation. Furthermore, maintaining a high concentration of salt in the external phase during particle preparation promotes a better entrapment of the drug into the matrix<sup>35</sup>. This modification of the initial process avoids the formation of Tx needles, allowing the encapsulation efficiency to increase considerably.

**Table 1.** Physico-chemical properties of unloaded and Tx loaded anti-HER2 immunonanoparticles

|                                 | <b>n</b> | <b>Unloaded NPs</b> | <b>Paclitaxel-loaded NPs</b> |
|---------------------------------|----------|---------------------|------------------------------|
| <b>NPs size (nm) (P.I)</b>      | 6        | 170 ± 13 (0.1)      | 171 ± 22 (0.1)               |
| <b>NPs-SH size (nm) (P.I.)</b>  | 6        | 202 ± 15 (0.1)      | 208 ± 13 (0.15)              |
| <b>NPs-HER size (nm) (P.I.)</b> | 6        | 264 ± 5 (0.2)       | 237 ± 43 (0.2)               |
| <b>-SH groups (number) / NP</b> | 3        | 375 ± 31            | 384 ± 14                     |
| <b>mmol -SH/mol PLA</b>         | 3        | 25 253 ± 2207       | 24 421 ± 1061                |
| <b>anti-HER2 (number) / NP</b>  | 5        | 289 ± 46            | 248 ± 58                     |
| <b>Zeta potential (mV)</b>      | 3        | -5.4 ± 1.6          | -1.3 ± 0.4                   |

P.I.: Polydispersity index scale from 0 to 1

In the literature, encapsulation efficiency rates ranging from 0.13 to 97% were reported for Tx depending on the polymers, the drug/polymer ratio, the organic solvents, the surfactants or the methods of preparation<sup>20,35-41</sup>. A high drug encapsulation efficiency correlates with a reduced loss of drug during the preparation process, and a high drug loading promotes the delivery to the target site of a greater quantity of drug for a minimal quantity of the polymer. However, it was demonstrated that an increase in the drug/polymer ratio induces a decrease in drug loading efficiency<sup>40</sup>. A drug/polymer ratio of 1:10 represents a good compromise between drug loading content and drug loading efficiency<sup>27</sup>. In our study, a Tx/PLA ratio of 1/10 allowed us to obtain an encapsulation efficiency of drug of  $78 \pm 10\%$ , with a drug loading of  $7.8 \pm 0.8\%$  (w/w).

The NPs-Tx-HER were prepared by covalent coupling of mAbs to the NPs-Tx using a two step reaction. The covalent binding between NPs and ligand is expected to provide good stability and a long circulation half-life for the immunonanoparticles, thereby allowing them to reach and interact with target cells<sup>42</sup>. The thiolation of the NPs-Tx allowed us to obtain a concentration of -SH groups of approximately 400 mmol-SH/mol PLA, which corresponds to about 25000 -SH groups per NP. Taking in consideration that the number of conjugated mAbs on the surface of NPs could influence the cellular interaction of nanocarrier systems, we have studied the influence of the reaction time on the amount of mAb coupled to the NPs-Tx-SH. In previous work, the highest amount of antibody on the NP surface (approximately 2500 mAb molecules per NP) induced the lowest cellular binding, which was likely due to a partial

inactivation of antibodies. However, at 1000 mAbs/NP, a good cellular response was observed<sup>16</sup>. Kirpotin et al. reported that cellular internalization of anti-HER2 immunoliposomes was higher when the surface density of conjugated Fab fragments increased and reached a plateau at 15 Fab/liposome<sup>43</sup>. These results indicate that an optimal number of ligands would be necessary to achieve efficient cellular targeting of anti-HER2 nanocarriers. The data presented in Table 2 show that, at a constant concentration of activated mAb, the amount of mAb coupled to the NPs increased from  $324 \pm 107$  mAbs/NP after 1 h to  $497 \pm 100$  mAbs/NP after 6 h and to  $617 \pm 118$  mAbs/NP after 12 h of reaction time. However, an increase in size was also observed with aggregate formation after 12 h of incubation, which was likely due to a secondary cross-reaction between antibody molecules in the presence of residual sulfo-MBS cross-linker. To avoid the presence of aggregates, which are highly undesirable for parenteral applications, one hour incubation time was selected for the preparation of immunonanoparticles.

The size of the NPs is a very important parameter because it influences drug release kinetics, drug biodistribution and drug clearance from the organism. Nanocarrier systems smaller than 250 nm can significantly accumulate in tumor tissues due to the EPR effect and avoid rapid clearance by the reticulo-endothelial system (RES)<sup>44</sup>. We have prepared NPs-Tx with a mean hydrodynamic diameter of 171 nm and a polydispersity index (P.I.) of 0.1, suggesting a narrow distribution of particle size. The uniform distribution and spherical shape of NPs-Tx and NPs-Tx-HER were confirmed by electron microscopy (Fig. 1). The mean size of the NPs-Tx determined by SEM was slightly smaller ( $132 \pm 21$  nm) than the hydrodynamic diameter ( $171 \pm 22$  nm) measured by PCS. This difference is explained in the literature by the hydration and presence of PVAL on the surface of the NPs.

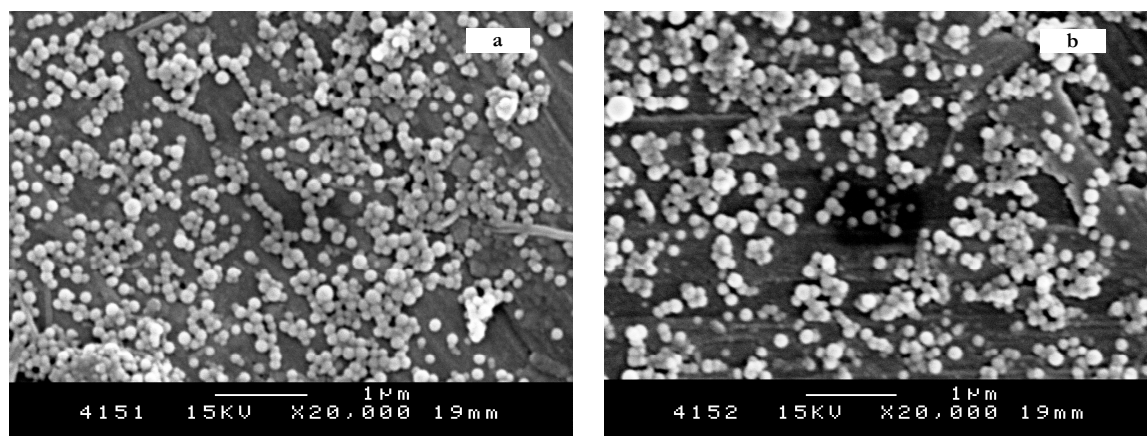


**Figure 1.** SEM images of NPs-Tx (a) and NPs-Tx-HER (b)

The conjugation reactions induced an increase in the NP hydrodynamic diameter. The PCS analysis demonstrated that the size of NPs-SH was about 210 nm, whereas the size increased to about 250 nm after the covalent attachment of mAbs to the NPs-SH (Table 1). However, the measurements by SEM showed that the NPs-Tx-HER have a similar size ( $148 \pm 28$  nm) compared to the NPs-Tx ( $132 \pm 21$  nm). A slight aggregation of smaller NPs, which can occur during the preparation due to multiple steps of centrifugation and the freeze drying process, could explain the larger size measured by PCS<sup>38</sup>.

The surface charge of NPs influences the stability of the suspension due to the presence of electrostatic forces and determines the interaction of the NPs with cells that are usually negatively charged<sup>46</sup>. In our case, the unloaded and Tx-loaded NPs exhibited a slightly negative zeta potential (Table 1), which can be explained by the presence of PVAL at the surface of the NPs<sup>47</sup>. After the coupling of anti-HER2 mAbs to the surface of the NPs-Tx, the value of the zeta potential was  $0.2 \pm 0.1$  mV, suggesting that the encapsulation of the drug and conjugation of mAbs to the NPs does not significantly influence the surface charge.

DSC analysis was performed to determine the physical state of entrapped Tx and the thermal behavior of the polymer after drug encapsulation. Tx loaded in the polymeric matrix did not show the characteristic endothermic melting peak determined for pure Tx at about 223°C. This result indicated that, after the encapsulation process, Tx is in an amorphous or disordered-crystalline phase<sup>38</sup>. The glass transition of PLA polymer is shifted from 40°C to 54°C after drug encapsulation, indicating that Tx acts as an impurity and changes the melting temperature (data not shown).

The data presented in Table 1 show that the properties of unloaded and Tx-loaded NPs are very similar, suggesting that the presence of drug during the process does not influence the coupling of antibodies to the surface of NPs. Also, the encapsulation of drug does not induce an increase in size compared to the unloaded NPs. The concentration of Tx, which was determined after each step of the NPs preparation, was  $7.8 \pm 0.8\%$ ,  $7.6 \pm 0.8\%$  and  $7.7 \pm 0.8\%$  in NP-Tx, NPs-Tx-SH and NPs-Tx-HER, respectively, indicating that no drug loss occurred during the coupling reactions. These results suggest that Tx is entrapped in the polymeric matrix and not adsorbed on the surface of the NPs.

### 3.2 Immunoreactivity of sulfo-MBS functionalized anti-HER2 mAbs

An essential condition for optimal tumor targeting is the preservation of antibody immunoreactivity and receptor specificity after coupling to the NPs. Structural modifications or an aggregation process can occur during the conjugation, and changes in biological activity of mAbs may be observed<sup>48</sup>. The preservation of the anti-HER2 mAb activity after coupling to the NPs was already qualitatively demonstrated in our previous studies by confocal microscopy and FACSCAN analysis, when anti-HER2 immunonanoparticles presented a strong and specific interaction with SKOV-3 cells<sup>16,17</sup>.

In the present study, the immunoreactivity of anti-HER2 mAbs activated with sulfo-MBS was quantitatively measured on SKOV-3 cells using I<sup>125</sup> radiolabeled mAbs. Only a minor difference was observed in specific binding between native and activated anti-HER2 mAbs (Fig. 2;  $p < 0.05$  in the paired 2-sample Wilcoxon signed rank T test, two-tailed P value). This result indicates that the variable region of the mAbs that is responsible for binding antigen was minimally affected (less than 2% difference in binding capacity) by activation with sulfo-MBS. Moreover, the purity of non-activated and sulfo-MBS-activated radiolabeled Herceptin<sup>®</sup> was tested twice by HPLC size chromatography. Both solutions contained a major symmetric peak of antibody (elution time 7.7 min) and a small percentage of aggregates of (< 2%) in the repeated spectrophotometric analysis after activation ( $\lambda = 280$  nm; Fig. 3).

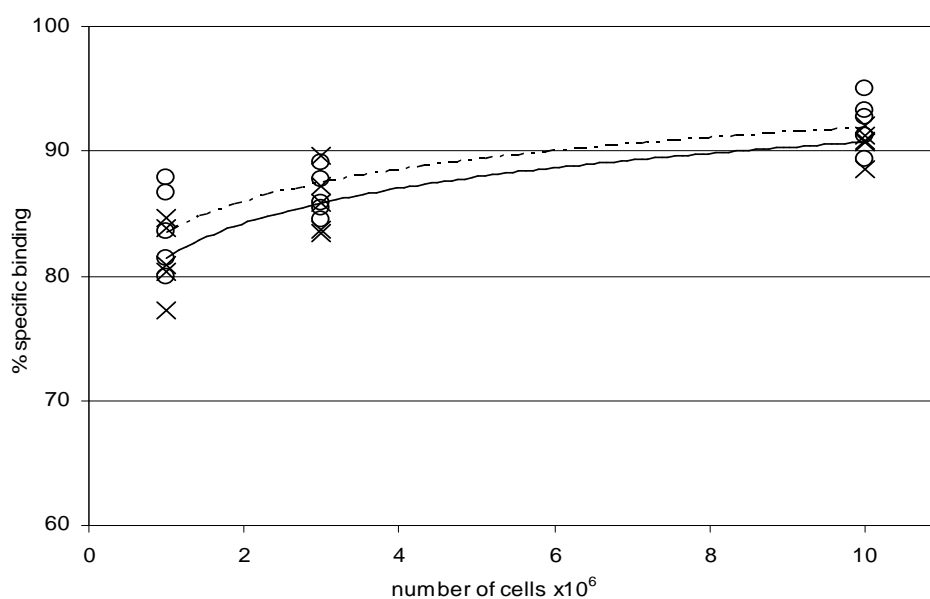


**Figure 2.** Comparison of specific binding of non-activated (O) and sulfo-MBS activated (X) radiolabeled anti-HER2 mAb to SKOV-3 cells as measured on different numbers of live cells (n=5).

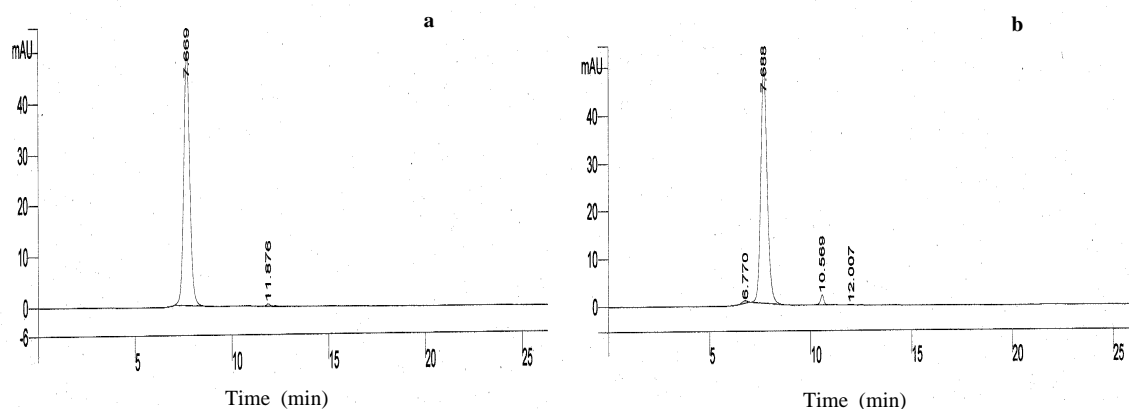


**Figure 3.** Representative HPLC analysis of non-activated (a) and sulfo-MBS (b) activated anti-HER2 mAbs as measured by optical density (280 nm). Numbers on the peaks indicate retention time. After activation, the small peak eluting at 6.77 minutes corresponds to aggregates and represents 0.8 % protein in this case. The small peak eluting at 10.6 minutes (indicating a molecular weight < 10 kDa) was not visible after radioiodination.

### 3.3 *In vitro* cytostatic assay

The *in vitro* cytostatic activity of NPs-Tx-HER, NPs-Tx, NPs-Tx-RIT and free Tx on SKOV-3 cells was assessed by using the MTT test. Unloaded NPs and NPs-HER were also tested to determine the effects of polymer and ligand on cell viability. The statistical analysis showed that unloaded NPs and NPs-HER do not influence cell viability at different Tx concentrations ( $p = 0.460$ ). Thus, the cytotoxic effect is due only to the presence of encapsulated drug for the other formulations. As seen in Fig. 4, the difference in cytotoxicity of the Tx formulations appeared only for the lowest concentrations of Tx (1-10 ng/ml). For the high concentrations (50 and 100 ng Tx/ml), the Tx released after 5 h of incubation seems to be sufficient to kill the cells in the same manner, independent of the drug formulations.

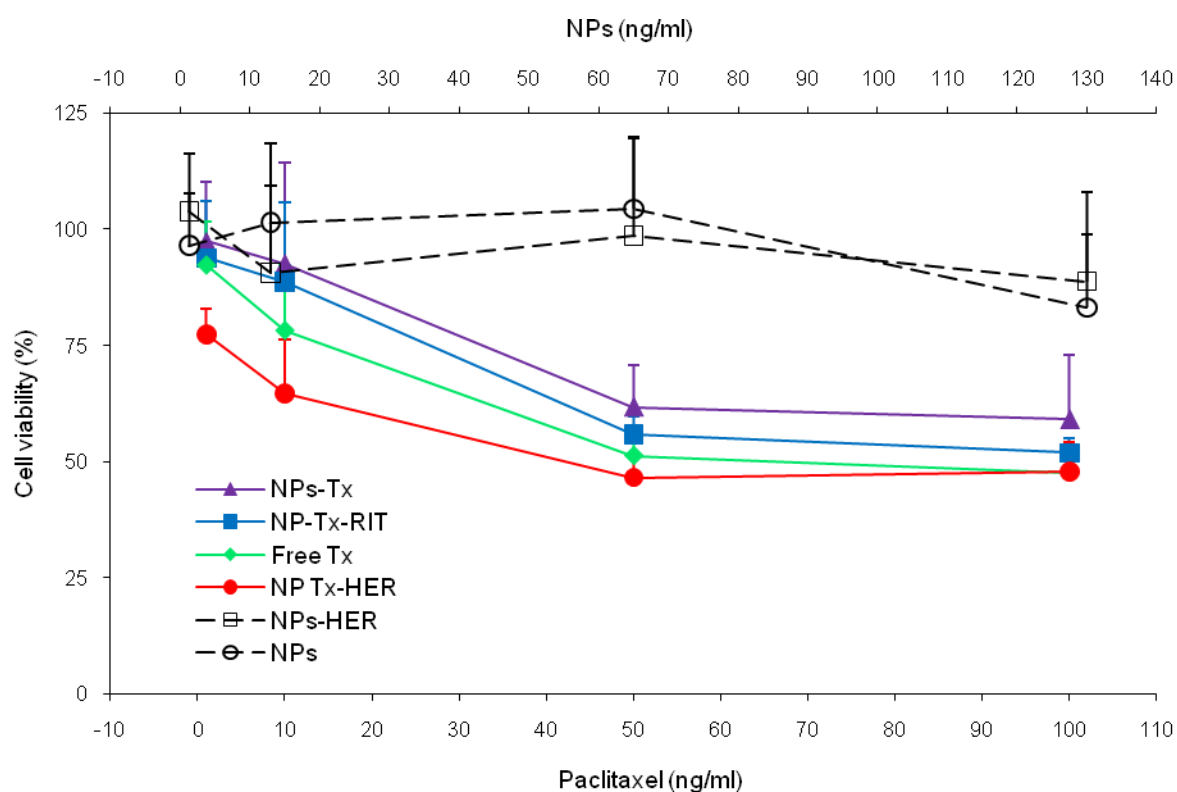


**Figure 4.** Cytotoxicity of Tx formulations on SKOV-3 cells overexpressing HER2. Different concentrations of Tx ranging from 1 to 100 ng/ml either as solution (free Tx) or encapsulated in NPs (NPs-Tx) or immunonanoparticles (NPs-Tx-HER or NPs-Tx-RIT) were tested. Unloaded NPs and NPs-HER were used as controls. The cells were incubated with the formulations for 5h. The growth inhibition was measured 5 days later by a MTT test. Cell viability was calculated taking cells incubated with culture medium as the 100% survival rate.

Dunnet's test pointed out that NP-Tx-HER was the only treatment exhibiting significant differences in the mean value of cytotoxicity at the lowest concentration (1 ng/ml). For Free Tx the threshold was observed at 10 ng/ml, while for both NPs-Tx and NP-Tx-RIT it was determined at 50 ng/ml. Scheffe multiple comparison test showed that NP-Tx-HER was significantly different from NP-Tx-RIT and NPs-Tx but not from free Tx, while Free-Tx was not significantly different from either NP-Tx-RIT or NPs-Tx.

The lower cytotoxicity of the NPs-Tx and Tx-loaded NPs coated with an irrelevant mAb (NPs-Tx-RIT) compared to free Tx is explained by the easier interaction of the Tx solution with the cells compared to the encapsulated drug which may be susceptible to matrix effects. The lower cytotoxicity of the NPs-Tx and Tx-loaded NPs coated with an irrelevant mAb (NPs-Tx-RIT) compared to free Tx is explained by the easier interaction of the Tx solution with the cells compared to the encapsulated drug which may be susceptible to matrix effects.

---

The greater efficiency of the immunonanoparticles can be explained by their specific interaction with and internalization into the SKOV-3 cells after 5 h of incubation, while NPs-Tx showed only a slight non-specific cell interaction<sup>17</sup>. Under our experimental conditions, no cytostatic effect greater than 50% was observed, which is likely related to the short incubation time. Indeed, other studies showed that increasing the incubation time induced a decrease in cell viability<sup>12,45</sup>.

#### **4. Conclusions**

In this study, we have successfully prepared and characterized NPs-Tx-HER for the specific targeting of tumors that overexpress HER2 antigens. The preservation of anti-HER2 immunoreactivity after activation with sulfo-MBS, an important requirement to achieve an efficient specific targeting, was demonstrated on SKOV-3 cells. Furthermore, *in vitro* results demonstrated a higher antiproliferative effect of immunonanoparticles at low concentrations of Tx compared to the other formulations, suggesting the possibility of increasing the therapeutic index of drugs by using immunonanoparticles.

#### **Acknowledgements**

The authors express their gratitude to Corinne Paschoud-Graber from the Division of Nuclear Medicine, Centre Hospitalier Universitaire Vaudois, for her help in the binding assays of radiolabeled antibodies to SKOV-3 cells.

---

### Reference List

1. Cho, K., Wang, X., Nie, S., Chen, Z. & Shin, D. M. Therapeutic Nanoparticles for Drug Delivery in Cancer. *Clin. Cancer Res.*, 14, 1310-1316, 2008.
2. Panyam, J. & Labhasetwar, V. Biodegradable nanoparticles for drug and gene delivery to cells and tissue. *Adv. Drug Deliv. Rev.* 55, 329-347, 2003.
3. Brannon-Peppas, L. & Blanchette, J. O. Nanoparticle and targeted systems for cancer therapy. *Adv. Drug Deliv. Rev.*, 56, 1649-1659, 2004.
4. Koo, O. M., Rubinstein, I. & Onyuksel, H. Role of nanotechnology in targeted drug delivery and imaging: A concise review. *Nanomed.* 1, 193-212, 2005.
5. Maeda, H., Wu, J., Sawa, T., Matsumura, Y. & Hori, K. Tumor vascular permeability and the EPR effect in macromolecular therapeutics. A review. *J. Control. Release*, 65, 271-284, 2000.
6. Moghimi, S. M., Hunter, A. C. & Murray, J. C. Long-circulating and target-specific nanoparticles: theory to practice. *Pharmacol. Rev.*, 53, 283-318, 2001.
7. Abou-Jawde, R., Choueiri, T., Alemany, C. & Mekhail, T. An overview of targeted treatments in cancer. *Clin. Ther.*, 25, 2121-2137, 2003.
8. Gatter, K. C., Brown, G., Trowbridge, I. S., Woolston, R. E. & Mason, D. Y. Transferrin receptors in human tissues: their distribution and possible clinical relevance. *J. Clin. Pathol.*, 36, 539-545, 1983.
9. Marcucci, F. & Lefoulon, F. Active targeting with particulate drug carriers in tumor therapy: fundamentals and recent progress. *Drug Discov. Today*, 9, 219-228, 2004.
10. Yan, L., Hsu, K. & Beckman, R. A. Antibody-based therapy for solid tumors. *Cancer J.*, 14, 178-183, 2008.
11. Carter, P. J. Potent antibody therapeutics by design. *Nat. Rev. Immunol.*, 6, 343-357, 2006.

- 
12. Sun, B., Ranganathan, B. & Feng, S. S. Multifunctional poly(lactide-co-glycolide)/montmorillonite (PLGA/MMT) nanoparticles decorated by Trastuzumab for targeted chemotherapy of breast cancer. *Biomaterials*, 29, 475-486, 2007.
  13. Sapra, P. & Allen, T. M. Ligand-targeted liposomal anticancer drugs. *Prog. Lipid Res.* 42, 439-462, 2003.
  14. Carter, P. Improving the efficacy of antibody-based cancer therapies. *Nat. Rev. Cancer*, 1, 118-129, 2001.
  15. Park, J. W. et al. Tumor targeting using anti-her2 immunoliposomes. *J. Control. Release* 74, 95-113, 2001.
  16. Nobs, L., Buchegger, F., Gurny, R. & Allemann, E. Biodegradable Nanoparticles for Direct or Two-Step Tumor Immunotargeting. *Bioconjug. Chem.* 17, 139-145, 2006.
  17. Cirstoiu-Hapca, A., Bossy-Nobs, L., Buchegger, F., Gurny, R. & Delie, F. Differential tumor cell targeting of anti-HER2 (Herceptin) and anti-CD20 (Mabthera) coupled nanoparticles. *Int. J. Pharm.*, 331, 190-196, 2007.
  18. Singla, A. K., Garg, A. & Aggarwal, D. Paclitaxel and its formulations. *Int. J. Pharm.*, 235, 179-192, 2002.
  19. Kuh, H. J., Jang, S. H., Wientjes, M. G. & Au, J. L. S. Computational model of intracellular pharmacokinetics of paclitaxel. *J. Pharmacol. Exp. Ther.*, 293, 761-770, 2000.
  20. Mitra, A. & Lin, S. Effect of surfactant on fabrication and characterization of paclitaxel-loaded polybutylcyanoacrylate nanoparticulate delivery systems. *J. Pharm. Pharmacol.*, 55, 895-902, 2003.
  21. Hawkins, M. J., Soon-Shiong, P. & Desai, N. Protein nanoparticles as drug carriers in clinical medicine. *Adv. Drug Deliv. Rev.*, 60, 876-885, 2008.
  22. Chipman, S. D., Oldham, F. B., Pezzoni, G. & Singer, J. W. Biological and clinical characterization of paclitaxel poliglumex (PPX, CT-2103), a macromolecular polymer-drug conjugate. *Int. J. Nanomedicine*, 1, 375-383, 2006.

- 
23. Paz-Ares, L. Phase III trial comparing paclitaxel poliglumex vs docetaxel in the second-line treatment of non-small-cell lung cancer. *Br. J. Cancer*, 98, 1608-1613, 2008.
  24. Xu, Z., Gu, W., Huang, J., Hong, S., Zhou, Z., Yang, Y., Yan, Z. & Li, Y. In vitro and in vivo evaluation of actively targetable nanoparticles for paclitaxel delivery. *Int. J. Pharm.*, 288, 361-368, 2005.
  25. Sahoo, S. K. & Labhasetwar, V. Enhanced Antiproliferative Activity of Transferrin-Conjugated Paclitaxel-Loaded Nanoparticles Is Mediated via Sustained Intracellular Drug Retention. *Molecular Pharmaceutics, Mol. Pharm.*, 2, 373-383, 2005
  26. Steinhauser, I., Spaenkuch, B., Strebhardt, K. & Langer, K. Trastuzumab-modified nanoparticles: Optimisation of preparation and uptake in cancer cells. *Biomaterials* 27, 4975-4983, 2006.
  27. Liang, H. F., Chen, C. T., Chen, S. C., Kulkarni, A. R., Chiu, Y. L., Chen, M. C. & Sung, H. W. Paclitaxel-loaded poly(g-glutamic acid)-poly(lactide) nanoparticles as a targeted drug delivery system for the treatment of liver cancer. *Biomaterials*, 27, 2051-2059, 2006.
  28. Nahta, R. & Esteva, F. J. Herceptin: mechanisms of action and resistance. *Cancer Lett.* 232, 123-138, 2006.
  29. Kirpotin, D. B., Drummond, D. C., Shao, Y., Shalaby, M. R., Hong, K., Nielsen, U. B., Marks, J. D., Benz, C. C. & Park, J. W. Antibody Targeting of Long-Circulating Lipidic Nanoparticles Does Not Increase Tumor Localization but Does Increase Internalization in Animal Models. *Cancer Res.*, 66, 6732-6740, 2006.
  30. Slamon, D. J., Godolphin, W., Jones, L. A., Holt, J. A., Wong, S. G., Keith, D. E., Levin, W. J., Stuart, S. G., Udove, J., Ullrich, A. & +. Studies of the HER-2/neu proto-oncogene in human breast and ovarian cancer. *Science*, 244, 707-712, 1989.
  31. Harries, M. & Smith, I. The development and clinical use of trastuzumab (Herceptin). *Endocr. Relat. Cancer* 9, 75-85, 2002.
  32. Slamon, D. J., Leyland-Jones, B., Shak, S., Fuchs, H., Paton, V., Bajamonde, A., Fleming, T., Eiermann, W., Wolter, J., Pegram, M., Baselga, J. & Norton, L. Use of

- 
- chemotherapy plus a monoclonal antibody against HER2 for metastatic breast cancer that overexpresses HER2. *N. Engl. J. Med.*, 344, 783-792, 2001.
33. Nobs, L., Buchegger, F., Gurny, R. & Allemann, E. Surface modification of poly(lactic acid) nanoparticles by covalent attachment of thiol groups by means of three methods. *Int. J. Pharm.* 250, 327-337, 2003.
  34. Schaffland, A. O. et al. <sup>131</sup>I-rituximab: relationship between immunoreactivity and specific activity. *J. Nucl. Med.* 45, 1784-1790, 2004.
  35. Fonseca, C., Simoes, S. & Gaspar, R. Paclitaxel-loaded PLGA nanoparticles: preparation, physicochemical characterization and in vitro anti-tumoral activity. *J. Control. Release*, 83, 273-286, 2002.
  36. Sahoo, S. K., Ma, W. & Labhasetwar, V. Efficacy of transferrin-conjugated paclitaxel-loaded nanoparticles in a murine model of prostate cancer. *Int. J. Cancer*, 112, 335-340, 2004.
  37. Koziara, J. M., Lockman, P. R., Allen, D. D. & Mumper, R. J. Paclitaxel nanoparticles for the potential treatment of brain tumors. *J. Control. Release*, 99, 259-269, 2004.
  38. Mu, L. & Feng, S. S. PLGA/TPGS Nanoparticles for Controlled Release of Paclitaxel: Effects of the Emulsifier and Drug Loading Ratio. *Pharm. Res.*, 20, 1864-1872, 2003.
  39. Mu, L. & Feng, S. S. A novel controlled release formulation for the anticancer drug paclitaxel (Taxol): PLGA nanoparticles containing vitamin E TPGS. *J. Control. Release*, 86, 33-48, 2003.
  40. Potineni, A., Lynn, D. M., Langer, R. & Amiji, M. M. Poly(ethylene oxide)-modified poly(b-amino ester) nanoparticles as a pH-sensitive biodegradable system for paclitaxel delivery. *J. Control. Release*, 86, 223-234, 2003.
  41. Debotton, N., Parnes, M., Kadouche, J. & Benita, S. Overcoming the formulation obstacles towards targeted chemotherapy: In vitro and in vivo evaluation of cytotoxic drug loaded immunonanoparticles. *J. Control. Release*, 127, 219-230, 2008.

- 
42. Nobs, L., Buchegger, F., Gurny, R. & Allemann, E. Current methods for attaching targeting ligands to liposomes and nanoparticles. *J. Pharm. Sci.* 93, 1980-1992, 2004.
  43. Kirpotin, D., Park, J. W., Hong, K., Zalipsky, S., Li, W. L., Carter, P., Benz, C. C., Papahadjopoulos, D. Sterically stabilized anti-HER2 immunoliposomes: design and targeting to human breast cancer cells in vitro. *Biochemistry* 36, 66-75, 1997.
  44. Brigger, I., Dubernet, C. & Couvreur, P. Nanoparticles in cancer therapy and diagnosis. *Adv. Drug Deliv. Rev.* 54, 631-651, 2002.
  45. Sahoo, S. K. & Labhasetwar, V. Enhanced Antiproliferative Activity of Transferrin-Conjugated Paclitaxel-Loaded Nanoparticles Is Mediated via Sustained Intracellular Drug Retention. *Mol. Pharm.*, 2, 373-383, 2005.
  46. Dong, Y. & Feng, S. S. Methoxy poly(ethylene glycol)-poly(lactide) (MPEG-PLA) nanoparticles for controlled delivery of anticancer drugs. *Biomaterials*, 25, 2843-2849, 2004.
  47. Sahoo, S. K., Panyam, J., Prabha, S. & Labhasetwar, V. Residual polyvinyl alcohol associated with poly (D,L-lactide-co-glycolide) nanoparticles affects their physical properties and cellular uptake. *J. Control. Release*, 82, 105-114, 2002.
  48. Yokoyama, M. Drug targeting with nano-sized carrier systems. *J. Artif. Organs*, 8, 77-84, 2005.



---

**Benefit of anti-HER2-coated paclitaxel-loaded immunonanoparticles in the  
treatment of disseminated ovarian cancer:  
Therapeutic efficacy and biodistribution in mice**

A. Cirstoiu-Hapca<sup>a</sup>, F. Buchegger<sup>b,c</sup>, N. Lange<sup>a</sup>, L. Bossy<sup>a\*</sup>, R. Gurny<sup>a</sup>, F. Delie<sup>a</sup>

<sup>a</sup> School of Pharmaceutical Sciences, University of Geneva, University of Lausanne, 30 Quai Ernest Ansermet, CH-1211 Geneva 4, Switzerland

<sup>b</sup> Division of Nuclear Medicine, University Hospital of Geneva, Switzerland

<sup>c</sup> Nuclear Medicine, University Hospital of Lausanne, Switzerland

\* Current address: TRB Chemedica International SA, Geneva, Switzerland

*Accepted for publication in Journal of Controlled Release (2010)*

---

The benefit of anti-HER2 paclitaxel (Tx)-loaded polymeric immunonanoparticles consisting of paclitaxel (Tx)-loaded nanoparticles coated with anti-HER2 monoclonal antibodies (Herceptin<sup>®</sup>, trastuzumab), in cancer treatment was assessed in a disseminated xenograft ovarian cancer model induced by intraperitoneal inoculation of SKOV-3 cells overexpressing HER2 antigens. The study was focused on the evaluation of therapeutic efficacy and biodistribution of NPs-Tx-HER compared to other Tx formulations. The therapeutic efficacy was determined by two methods: bioluminescence imaging and survival rate. The treatment regimen consisted in an initial dose of 20 mg/kg Tx administered as 10 mg/kg intravenously (IV) and 10 mg/kg intraperitoneally (IP), followed by five alternative IP and IV injections of 10 mg/kg Tx every 3 days. The bioluminescence study has clearly shown the superior anti-tumor activity of NPs-Tx-HER compared to free Tx. As a confirmation of these results, a significantly longer survival of mice was observed for NPs-Tx-HER treatment compared to free Tx, Tx-loaded nanoparticles coated with an irrelevant mAb (Mabthera<sup>®</sup>, rituximab) or Herceptin<sup>®</sup> alone, indicating the potential of immuno-nanoparticles in cancer treatment. The biodistribution pattern of Tx was assessed on healthy and tumor bearing mice after IV or IP

administration. An equivalent biodistribution profile was observed in healthy mice for Tx encapsulated either in uncoated nanoparticles (NPs-Tx) or in NPs-Tx-HER. No significant difference in Tx biodistribution was observed after IV or IP injection, except for a lower accumulation in the lungs when NPs were administered by IP. Encapsulated Tx accumulated in the organs of reticulo-endothelial system (RES) such as liver and spleen, whereas free Tx had a non-specific distribution in all tested organs. Compared to free Tx, the single dose injection (IV or IP) of encapsulated Tx in mice bearing tumors induced a higher tumor accumulation. However, no difference in overall tumor accumulation between NPs-Tx-HER and NPs-Tx was observed.

In conclusion, encapsulation of Tx into NPs-Tx-HER immuno-nanoparticles resulted in an improved efficacy of drug in the treatment of disseminated ovarian cancer overexpressing HER2 receptors

**Keywords:** *immunonanoparticles, active targeting, paclitaxel, Herceptin<sup>®</sup>, ovarian cancer, bioluminescence imaging, biodistribution.*

---

## 1. Introduction

Ovarian cancer is the most lethal form of all gynecological malignancies<sup>1,2</sup>. The lethality is closely related to the lack of specific symptoms which leads to a late detection of the disease. As a result, more than 70% of patients present intraperitoneal metastasis at the time of diagnosis<sup>3</sup>. Following initial surgery, the combination of platinum (cisplatin and carboplatin) plus taxanes (paclitaxel and docetaxel) represents the standard treatment in advanced ovarian cancer<sup>4,5</sup>. Despite a high initial response, the patients often relapse within a median time of less than 2 years<sup>6,7</sup>. The current chemotherapy is associated with serious side effects such as neutropenia and neurotoxicity due to the non-specific biodistribution and low therapeutic index of anticancer agents<sup>8</sup>. New drug formulations and targeting approaches have been developed to better control the biodistribution of drugs and to improve the therapeutic efficacy<sup>9</sup>. Another strategy is based on intraperitoneal administration of drugs<sup>10,11</sup>.

Drug delivery systems including nanoparticles, liposomes, micelles or dendrimers have been widely investigated to develop safer and more effective formulations in cancer treatment. These nanomedicines allow to overcome solubility problems of different drug molecules<sup>12-14</sup>. Furthermore, the encapsulated drug will be selectively distributed at target site via so called

EPR effect<sup>15</sup>. This approach, taking advantage of the characteristic features of tumor vasculature and lymphatic drainage, is designated as passive targeting<sup>16</sup>. PEG-ylated liposomal doxorubicine, Caelyx<sup>®</sup>, approved by FDA in 1999, is used in the second line of treatment for advanced ovarian cancer<sup>17</sup>. Paclitaxel-conjugated albumin nanoparticles (Abraxane<sup>®</sup>), approved in 2005 by the FDA for the treatment of metastatic breast cancer<sup>18</sup> is in phase II clinical trials for the treatment of ovarian cancer<sup>19</sup>.

The specific delivery at target site of nanomedicines can be further improved by active targeting using surface functionalization with ligands such as antibodies or peptides that recognize and bind specifically to biomarkers overexpressed on cancer cells<sup>20-22</sup>. Among targeting moieties, monoclonal antibodies have been extensively employed for the development of targeted nanocarriers called immuno-nanocarriers. The improvement of drug selectivity, the capacity to deliver high payloads of drug to target sites, the protection of drugs from enzymatic degradation and the possibility to use the same carrier system to encapsulate different drugs without the need of covalent conjugation for each drug molecule illustrate some advantages of immuno-nanocarriers<sup>23,24</sup>.

The molecular specificities of ovarian cancer cells may be exploited to achieve active tumor targeting. HER2 (Neu/ErbB-2), one of the members of the epidermal growth factor receptors stably and highly expressed in 20 to 30% of ovarian cancer patients, is a good candidate for active targeting using immuno-nanoparticles<sup>25</sup>. HER2 is a trans-membrane receptor that is easily accessible to antibody-based therapies<sup>26</sup>. The ability of these receptors to be internalized via receptor-mediated endocytosis is clearly an advantage when active targeting is considered. Indeed, this feature promotes preferential intracellular accumulation of anti-HER2 coated immuno-nanocarriers containing an anticancer agent<sup>27</sup>.

The IP administration of chemotherapeutic agents in the treatment of advanced ovarian cancer is a rational strategy based on anatomic and pharmacokinetic considerations, allowing to expose tumors confined into the peritoneal cavity to higher drug concentrations for a longer period of time<sup>28,29</sup>. IP injection was shown to induce the accumulation of paclitaxel (Tx) in the peritoneal cavity 1000-fold higher than IV application and an extended survival of patients<sup>30</sup>. However, due to the limited penetration of anticancer drugs from the tumor surface, IP chemotherapy is effective only in micrometastasis or tumors smaller than 0.5 cm in diameter<sup>31</sup>. Therefore, combined IV and IP treatment has been tested to reach tumors of larger size and micrometastasis spread in the peritoneal cavity<sup>32</sup>.

According to the literature, after IV injection the drug or nanocarriers accumulate in tumors via three processes: (i) distribution through vascular compartment, (ii) transport across microvessel walls and (iii) diffusion through interstitial space of the tumor<sup>33</sup>. For IP therapy, the molecules reach tumors mainly through the tumor interstitium, and, in a minor quantity, after recirculation, via the capillary blood vessels adjacent to the peritoneum and the systemic circulation<sup>31</sup>. In addition, the carrier systems are also drained through the local lymphatic ducts<sup>34</sup>.

Tx is characterized by a high hydrophobicity that limits aqueous formulation for parenteral delivery<sup>35</sup>. Encapsulation process represents an interesting approach for alternative dosage forms avoiding the use of Cremophor EL as vehicle which is responsible for serious side effects<sup>36</sup>. In an effort to better target ovarian cancer disseminated in the peritoneal cavity, immuno-nanoparticles containing paclitaxel and coated with anti-HER2 mAbs (NPs-Tx-HER) were developed. Our previous study demonstrated the *in vitro* specific interaction and internalization of anti-HER2-coated immuno-nanoparticles in SKOV-3 cells overexpressing HER2 receptors<sup>37</sup>. Also, the preparation and physico-chemical characterization of NPs-Tx-HER have been described in an earlier paper<sup>38</sup>. In the present work, we have evaluated the advantages of NPs-Tx-HER in the treatment of disseminated ovarian tumors after a combined IV/IP administration. The study was performed in a xenograft cancer model induced by IP inoculation of SKOV-3 cells in severe combined immunodeficient (SCID) mice.

## 2. Material and methods

### 2.1 Materials

Tx was obtained from Cfm Oskar Tropitzsch (Marktredwitz, Germany). Poly (DL-lactic acid) (100DL 4A, Mw 57kDa) was provided by Lakeshore Biomaterials, Inc (Birmingham, USA). Anti-HER2 (trastuzumab, Herceptin<sup>®</sup>) and Anti-CD20 (rituximab, Mabthera<sup>®</sup>) from Roche (Basle, Switzerland) were kindly provided by the Department of Oncology and Unit of Oncogynecology, University Hospital of Geneva, Switzerland. Isoflurane was obtained from Halocarbon (River Edge, NJ, USA).

## 2.2 Preparation of Tx loaded immuno-nanoparticles

The Tx-loaded immuno-nanoparticles were prepared according to the protocol previously described<sup>38</sup>. Briefly, Tx was encapsulated in the polymeric poly (DL-lactic acid) NPs using a salting out method. NPs-Tx were then thiolated and conjugated to sulfo-MBS activated anti-HER2 or anti-CD20 mAbs to obtain NPs-Tx-HER or NPs-Tx-RIT, respectively.

### 2.2.1 Preparation of Tx-loaded NPs (NP-Tx)

Briefly, 24 mg of Tx dissolved in 0.5 g acetone was added to a solution of 240 mg poly (DL-lactic acid) (PLA) in 1 g acetone (drug to polymer ratio = 1:10). The organic phase was mixed under vigorous stirring with 3.5 g of aqueous phase containing 15% (w/w) poly (vinyl alcohol) (PVAL) and 60% (w/w) magnesium chloride hexahydrate. Then, 20 ml of pure water was added to the NP suspension, and the stirring was maintained for 10 min. NPs were recovered by centrifugation, washed twice with pure water and lyophilized in the presence of trehalose (30 % w/w) before storage at 4°C until use.

### 2.2.2 Thiolation of NPs-Tx

Thiol functions (-SH) were covalently bound to the NPs-Tx by a two-step carbodiimide reaction. Briefly, 100 mg of NPs-Tx were suspended in 5 ml water, and the reaction was initiated by consecutively adding 10 ml of a solution of EDAC (24 mg/ml) and 5 ml of a cystamine solution (71 mg/ml). The final suspension was completed with water to 25 ml and stirred under mild conditions for 24 h at room temperature. Thereafter, EDAC and non-reacted cystamine were removed by two successive centrifugations (50000xg for 20 min). NPs were then re-suspended in purified water and incubated for 3 h with 1 ml of an aqueous solution of TCEP (6 mg/ml) to reduce disulfide bonds. Finally, thiolated Tx-loaded NPs (NPs-Tx-SH) were purified by two successive centrifugations and freeze-dried in presence of trehalose (30% w/w).

### 2.2.3 Activation of mAb and covalent binding to NPs-Tx-SH

To perform the covalent binding of mAbs to the NPs-Tx-SH, 1 ml of clinical grade anti-HER2 or anti-CD20 solution was purified by centrifugation using Amicon Ultra-4 centrifugal filter devices. Two milligrams of purified mAbs were activated in PBS (pH=7.4) with sulfo-MBS at a molar ratio 1/20 for 45 min at room temperature. Five hundred microliters of activated anti-HER2 (1mg/ml) was reacted for 1 h under gentle shaking at room temperature with 500 µl

NPs-Tx-SH (20 mg/ml). Unconjugated mAbs were removed by 2 cycles of centrifugation. Finally, NPs-Tx-HER and NPs-Tx-RIT were stored in PBS at 4°C.

### 2.3 Tumor cell lines

Human ovarian carcinoma cells, SKOV-3, known to overexpress HER2 specific antigens, (American Type Culture Collection ATCC, Manassas, VA) were grown in RPMI-1640 medium with Glutamax I (Gibco, Grand Island, NY, USA) supplemented with 10% (v/v) foetal calf serum (FCS) (Brunschwig, Basle, Switzerland), penicillin (100 units/ml) and streptomycin (100 µg/ml) (Gibco) at 37°C in a humidified incubator containing 5% CO<sub>2</sub>. SKOV3-luc-D3 cell line, a generous gift from Caliper LifeSciences (Alameda, CA, USA), were cultured in McCoy's 5a medium supplemented with 10% (v/v) fetal calf serum (FCS) (Brunschwig) in the conditions mentioned above. The cells were maintained as a monolayer and, for experiments, were harvested using TrypLE Express (Gibco, Grand Island, NY, USA) and resuspended in fresh complete medium.

### 2.4 Animals

Females BALB/cOlaHsd mice (females, 5-6 weeks, 17-22g) and C.B-17/IcrHan<sup>TM</sup>-Hsd-*Prkdc*<sup>scid</sup> mice, (females, 5-7 weeks old, 18-20g) were supplied by Harlan Laboratories (Horst, The Netherlands). All experimental procedures on animals were performed in compliance with the Swiss Federal Law on the Protection of the Animals, according to a protocol approved by the local and Swiss authorities. The animals were acclimatized at 22 ± 2°C in a light cycled room for a week before experiments. Water and food were freely available to the animals. The SCID mice were maintained under specific pathogen free status with *ad libitum* access to sterile food and acidified water.

### 2.5 Ovarian xenograft cancer model

The ovarian cancer was induced by intraperitoneal inoculation of 5x10<sup>6</sup> SKOV-3 cells (ATCC, American Type Culture Collection, Manassas, VA) in 200 µl complete medium into SCID mice. Luminescent SKOV-3-luc-D3 cells transfected with luciferase were used for the bioluminescence imaging (BLI).

## 2.6 Evaluation of antitumor activity

Therapeutic efficacy of Tx formulations was determined in the animal model mentioned above using survival rate and bioluminescence imaging.

### 2.6.1 Bioluminescence imaging (BLI)

This method is based on the enzymatic generation of visible light by living organisms after interaction between luciferase, encoded in the transfected cancer cells as a bioluminescent reporter, and luciferin, as substrate, administered few minutes prior to analysis<sup>39</sup>.

At day zero, nine SCID mice were inoculated IP with SKOV3-luc-D3 cells and randomly divided into three groups of three animals. The control group was left untreated. At day five, treated groups received either NPs-Tx-HER suspended in PBS or free Tx solubilized in 100  $\mu$ l PEG 400/ethanol/water = 30/20/50 mixture, according to the following schedule: an initial dose of 20 mg/kg Tx administered 10 mg/kg IV via the tail vein and 10 mg/kg IP, followed by five alternative IP and IV injections of 10 mg/kg Tx every 3 days as shown in Fig. 1a.

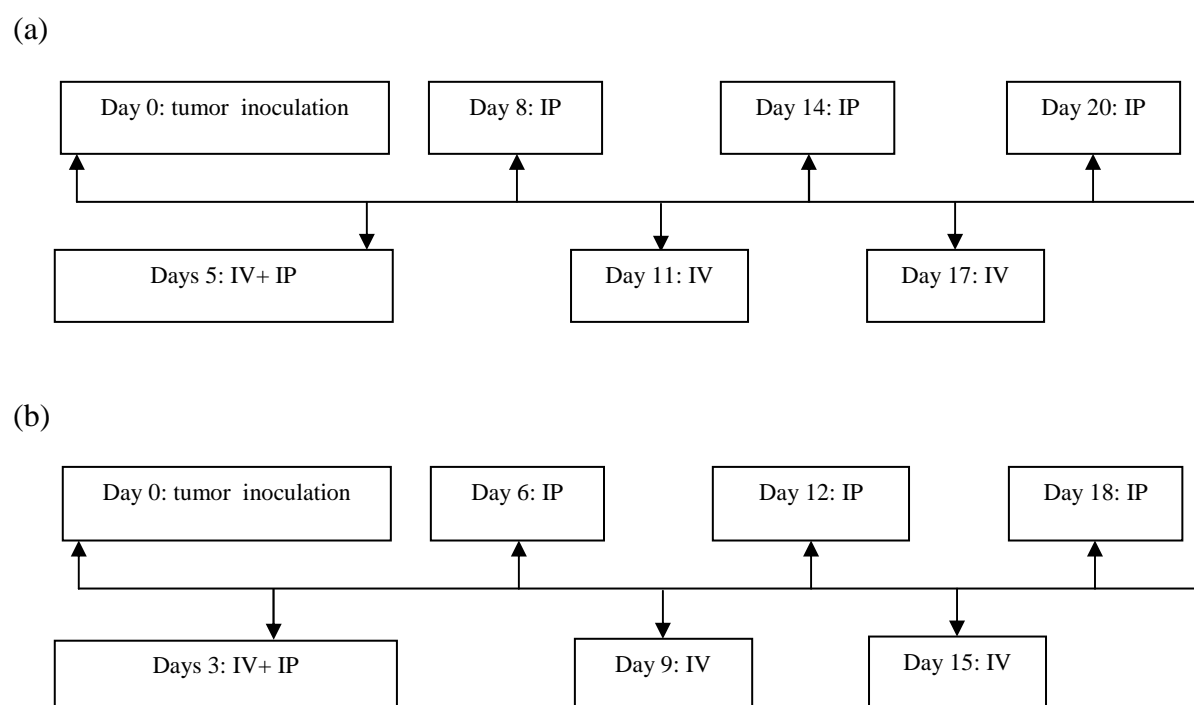


**Figure 1.** Treatment schedule for tumor bearing animals consisting in an initial dose of 20 mg/kg Tx administered as 10 mg/kg IV via tail vein and 10 mg/kg IP, followed by five alternative IP and IV injections of 10 mg/kg Tx every three days: (a) treatment initiated on day five; (b) treatment initiated on day three. Treated groups received either NPs-Tx-HER or free Tx.

The bioluminescent signal associated to the tumor was monitored weekly from day four until the sacrifice of animals. BLI was performed with an IVIS<sup>®</sup> 200 Imaging System (Xenogen Caliper Life Sciences, CA, USA) equipped with a highly sensitive, cooled CCD camera. Image processing was carried out using Living Image<sup>®</sup> software (Caliper Life Sciences, CA, USA). For analysis, mice were pre-anaesthetized with isoflurane (2-3% v/v) and were administered IP with the substrate D-Luciferin (150 mg/kg) in DPBS (15 mg/ml). After waiting for three minutes for proper distribution of luciferin, the mice were placed in IVIS<sup>®</sup> 200 chamber and imaged ventrally under isoflurane anesthesia (1-2% v/v). Imaging exposure time ranged from five to ten seconds depending on tumor luminescence, and, generally, three animals were imaged at a time. A series of ten images at one minute intervals was taken to control the stability of the signal during analysis and there was no difference in the intensity of the bioluminescence signal. Regions of interest (ROIs) from the displayed images covering the peritoneal cavity including the tumours were quantified as photons/s using Living Image<sup>®</sup> software. Background bioluminescence was about  $7 \times 10^4$  photons/s. The tumor bioluminescence measured for each mouse on day four was considered as 100%. For each time point, the bioluminescence value has been calculated according to the following equation:

$$\% \text{ bioluminescence} = (B_n/B_0) * 100$$

where  $B_n$  is the bioluminescence measured at a given time point, and  $B_0$  is the initial bioluminescence measured on day four. The data were analyzed by the Generalized Estimation Equations (GEEs) method for Gamma data with log-link function to test if the two treatments had a significantly different effect. Consequently, the treatment variable was introduced into the model as a factor term (with the two levels NPs-Tx-HER and free Tx) and day variable as a covariate. SPSS v.16 statistical package (NCSS, Utah, USA) was used for the analysis.

### 2.6.2 Survival rate

After tumor inoculation (day zero) the mice were randomly separated in five groups, each consisting of three animals that received different treatments. Group A: NPs-Tx-HER, group B: NPs-Tx-RIT, group C: free Tx, group D: Herceptin<sup>®</sup> alone, and group E: untreated mice used as controls. The treatments were started either on day five or three (Fig. 1a and b) and consisted in the same dosing protocol as in the BLI study: an initial dose of 20 mg/kg Tx

administered as 10 mg/kg IV via the tail vein and 10 mg/kg IP, followed by five alternative IP and IV injections of 10mg/kg Tx every three days. The antitumor efficacy of Tx formulations was evaluated using survival rates and body weight. Mice that presented inactivity, hunched position, spiky hair, or 20% weight loss or gain, were euthanized. Survival rates were expressed using the Kaplan-Meier curves and their comparison was performed by the Logrank Test (GraphPad Prism Software, version 4.00, San Diego, CA, USA).

## 2.7 Biodistribution studies

### 2.7.1 Biodistribution in healthy mice

The biodistribution of Tx was analysed after IV or IP injections of a single dose of Tx (20 mg/kg) either in solution or encapsulated in NPs-Tx-HER and NPs-Tx. The BALB/cOlaHsd mice were randomly assigned to six groups, according to the route of administration and drug formulation.

- Groups 1 and 2 received IV through the tail vein or IP, respectively, free Tx dissolved in 100 µl of PEG 400/ethanol/water = 30/20/50 mixture.
- Groups 3 and 4 received IV or IP, respectively, a single dose of 5 mg NPs-Tx-HER equivalent to a 20 mg/kg Tx resuspended in 100 µl of PBS solution.
- Groups 5 and 6 received IV or IP, respectively, a single dose 5 mg NPs-Tx equivalent to a 20 mg/kg Tx in a volume of 100 µl of PBS solution.

The animals in groups 1, 3 and 5, were sacrificed at 1, 4, 12 and 24h after IV administration, whereas for groups 2, 4 and 6 receiving IP injections, the mice were sacrificed at 4, 12, 24 and 48h (n = 4 or 5 mice/time point). The blood samples, collected by cardiac puncture, and the organs (heart, lungs, spleen, liver and kidneys) were harvested and stored at -20°C until Tx analysis. Tx was extracted from tissues using acetonitrile. Typically, 10 ml of solvent was added to the sample and homogenized for three minutes at 2000 rpm using a Potter Elvehjem tissue grinder attached to a stirring machine (Eurostar-digital, IKA-Werke, Germany). More than 90% of Tx was extracted from tissue samples containing a known amount of Tx. After centrifugation at 9500 rpm for five minutes, (Beckman Avanti<sup>TM</sup> 30 centrifuge, rotor F1010, Beckman Coulter Inc., Fullerton, CA, USA), the supernatant was separated and evaporated under nitrogen at room temperature. The residue was reconstituted in 200 µl of acetonitrile and centrifuged at 9500 rpm for five minutes. One hundred fifty microliters of the clear upper layer was transferred to autosampler vials containing limited-volume inserts (200 µl). Tx

concentration was measured by reverse-phase HPLC with UV detection ( $\lambda = 227$  nm). The HPLC system consisted of a Waters 600 Controller separation module fitted with a Waters 2487 Dual  $\lambda$  absorbance detector, a Waters 717 Plus Autosampler and a NUCLEOSIL C18 column, 4.6mm x 125cm, 5  $\mu$ m, (Macherey-Nagel, Switzerland). The mobile phase (acetonitrile/water = 50/50) was delivered at a flow rate of 1ml/min and a volume of 20  $\mu$ l was injected. A standard curve for Tx (0.0073-0.50 mg/ml) was prepared under identical conditions.

### *2.7.2 Biodistribution in SCID mice bearing tumors*

SCID mice were inoculated IP with  $5 \times 10^6$  of SKOV-3 cells. Eleven days after tumor inoculation the mice were given IV or IP 10 mg/kg of free Tx, encapsulated in NPs-Tx or NPs-Tx-HER. Twenty four hours after administration, the samples of blood, organs (heart, lungs, spleen, liver and kidneys) and tumors were harvested and stored at  $-20^\circ\text{C}$  until Tx analysis. The drug extraction and the analytical procedures were the same as described above.

## **3. Results and discussion**

### *3.1 Characterization of NPs-Tx-HER*

Tx was successfully encapsulated in poly (DL-lactic acid) NPs with an encapsulation efficacy of  $78 \pm 10\%$  and a drug loading of  $7.8 \pm 0.8\%$  (w/w). After covalent coupling of anti-HER2 mAbs on the NPs-Tx surface, the size of NPs-Tx-HER was  $237 \pm 43$  nm. About 250 molecules of mAbs were bound per nanoparticle<sup>38</sup>.

### *3.2 Therapeutic efficacy of NPs-Tx-HER*

The therapeutic efficacy of Tx formulations was evaluated in a IP disseminated xenograft ovarian cancer model using survival rate and bioluminescence imaging methods. The IP model was selected due to the resemblance with the clinical physio-pathological features of ovarian cancer by the presence of intraperitoneal dissemination and ascites<sup>40</sup>.

#### *3.2.1 Bioluminescence imaging*

In a first stage, the therapeutic efficacy of NPs-Tx-HER and free Tx was compared using bioluminescence imaging (BLI), a sensitive and non-invasive method successfully used to monitor tumor progression in living animals<sup>41,42</sup>. The advantages of this technique include the

---

visualisation and quantification of disseminated ovarian tumors without need of animal sacrifice at each time point of analysis<sup>43</sup>.

For the untreated group, the imaging data (Fig. 2a) showed a high and relatively stable bioluminescent signal during the first two weeks followed by an increase in signal until the animals were sacrificed. This initial stability of signal is probably due to the reorganization of the tumors when some of the inoculated cells are destroyed and the others start to progress. The mice died or were euthanized three weeks post-inoculation when their behaviour indicated serious signs of disease. Due to the early death of the control mice as a consequence of rapid growth of tumors, this group was not included in the statistical analysis.

The treatment with free Tx or NPs-Tx-HER was started on day five and continued every three days until day 20. Images presented in Fig. 2b show that in the group receiving free Tx the bioluminescent signal decreased in one mouse and remains relatively stable in two others, one week after the end of the treatment. As shown in Fig. 2c, the NPs-Tx-HER demonstrated a higher efficacy by the disappearance of the signal in two mice and a significant decrease in the third one. However, 50 days after the end of the treatment, the tumors started to grow again in all treated mice. This suggests that the tumors were not totally eradicated despite of the visual disappearance of bioluminescent signal.



The quantitative analysis of tumor signal demonstrated a significantly higher efficacy of NPs-Tx-HER than free Tx ( $p < 0.005$ ). While free Tx treatment resulted in a relatively constant bioluminescence over 70 days without any significant change in the slope from zero ( $p = 0.22$ ), NPs-Tx-HER treatment gave a significantly lower bioluminescence ( $p < 0.005$ ), indicative of significantly decreased tumor size (Fig. 3).

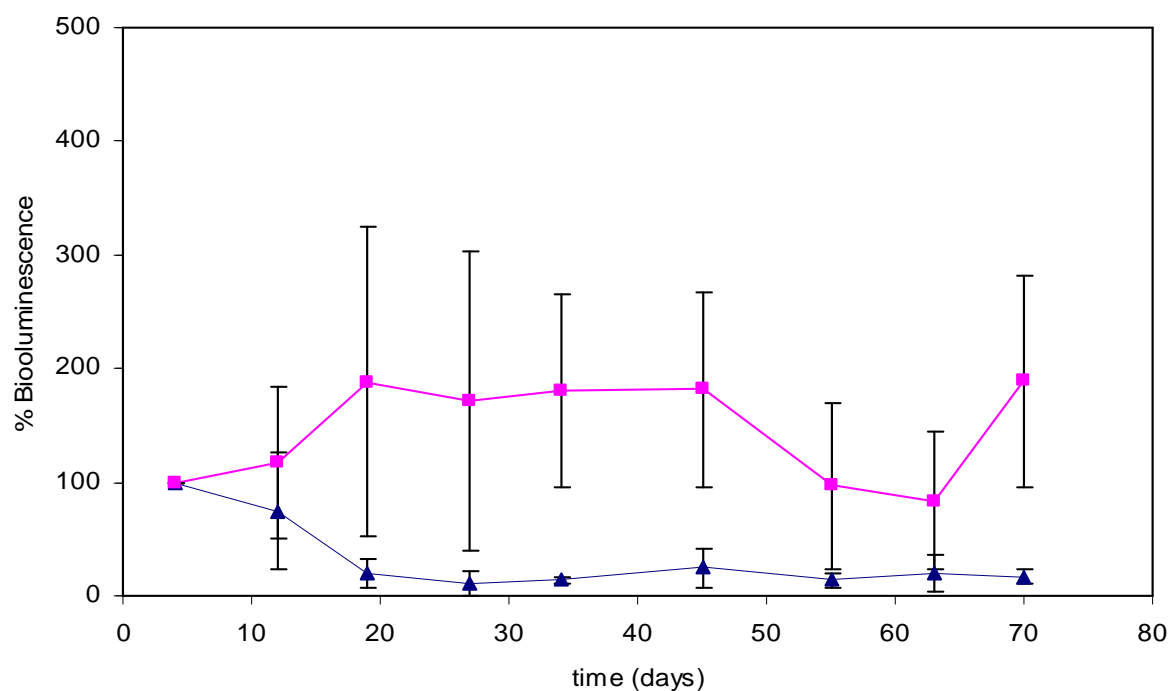


**Figure 3.** Evaluation of tumor progression in mice receiving NPs-Tx-HER (▲) and free Tx (■). Measurement of tumor bioluminescent surface using Living Image<sup>®</sup> software. The Generalized Estimation Equations (GEEs) demonstrated a significantly higher efficacy of NPs-Tx-HER compared to free Tx ( $p < 0.005$ ). ( $n = 3$ )

The BLI showed the superior therapeutic efficacy of NPs-Tx-HER compared to the free drug thus, demonstrating the advantage of active targeting in the treatment of tumors overexpressing specific antigens.

### 3.2.2 Survival rate

In the second stage, the therapeutic efficacy of NPs-Tx-HER compared to NPs-Tx-RIT, free Tx and Herceptin<sup>®</sup> alone was evaluated using Kaplan-Meier survival curves.

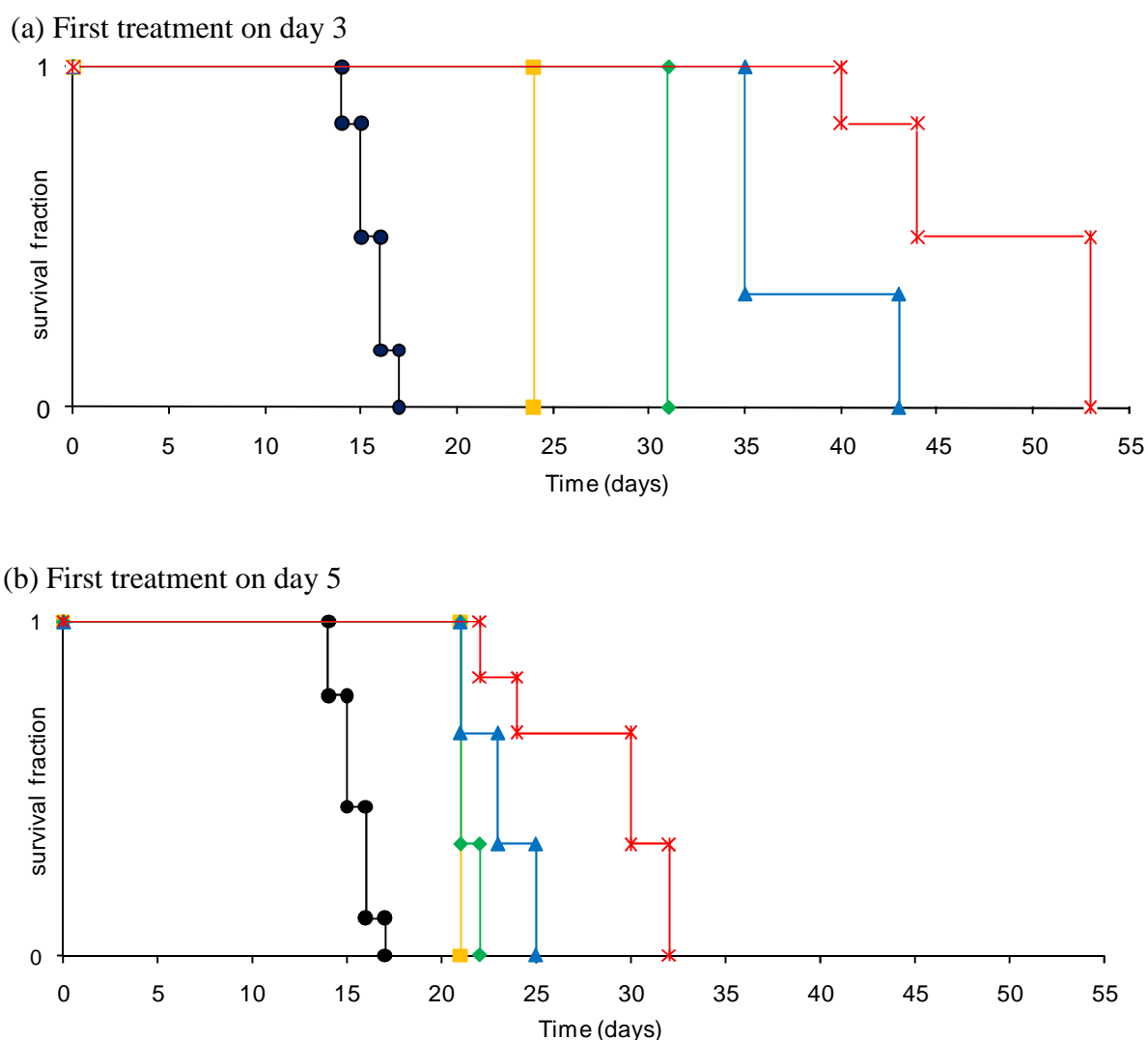


**Figure 4.** Therapeutic efficacy of Tx formulations on survival rate (Kaplan-Meier curves). Untreated mice were used as control (●). The treatments were initiated either on day five (a) or three (b) after tumor inoculation. The animals received IV/IP multiple dose of Herceptin<sup>®</sup> (■), free Tx (◆), NPs-Tx-RIT (▲), or NPs-Tx-HER (\*). Significant improvement of survival have been observed when treatments were started on day three compared to day five ( $p < 0.0001$ ). (n= 3-6)

When the treatment was initiated on day five (Fig. 4a), the median survival rate of untreated mice used as control was about 15 days. A slight increase of survival to about 20 days was observed for the groups treated with Herceptin<sup>®</sup> alone (1mg/kg), administered in a dose corresponding to the amount bound to NP-Tx-HER (approximately 8  $\mu\text{g}$  Herceptin/mg NPs) and representing about 20% of therapeutic dose used in clinics. Similar results were obtained for free Tx. The immuno-nanoparticles coated with an irrelevant antibody, NPs-Tx-RIT, showed a greater therapeutic effect than free Tx most likely due to the passive targeting

mechanism. NPs-Tx-HER exhibited the highest therapeutic effect. As observed in our previous *in vitro* studies on SKOV-3 cells overexpressing HER2, this might be the result of the specific interaction and internalization of anti-HER2 immuno-nanoparticles via receptor-mediated endocytosis<sup>37</sup>.

However, therapeutic efficacy of treatments was not significantly different from each other and the mice did not totally recover. Strategies such as increase of dose, prolongation of treatment, or earlier initiation of treatment can be used to improve the therapeutic effect. We have chosen to initiate the treatment on day three after cell inoculation, using the same schedule of treatment.

When treatment was initiated on day three (Fig. 4b), the Herceptin<sup>®</sup> alone increased the survival to about 25 days. Unlike treatment started in day five, free Tx showed a higher efficiency than Herceptin<sup>®</sup>. A higher efficacy of NPs-Tx-RIT compared to free Tx was observed, and the highest therapeutic effect was obtained using NPs-Tx-HER treatment.

A higher survival of animals was observed when treatments were initiated on day three compared to day five. Moreover, at day three, the therapeutic efficacy of Tx formulations was significantly different. These indicate that the efficacy of the treatments depends on its onset.

However, no complete recovery was observed in any treated mice. The necropsy of treated mice at the end of experiments showed the presence of tumors especially under the liver which likely are difficult to reach, which is in line with the results of BLI studies. This is related to the high volume of the tumor when the treatment starts and also to the difficulty to deliver an efficient dose of drug at tumor site despite of combination of IP and IV injection. An increase in Tx dose and/or prolongation of treatment period might allow a complete eradication of tumors.

We have observed that in bioluminescence study the mice inoculated with luminescent SKOV-3-luc-D3 lived longer than those in survival study that received native SKOV-3 cells. As described by the provider, SKOV3-luc-D3 tumors appear less aggressive than native cells explaining the longer survival of mice inoculated with these cells.

The imaging data and survival studies clearly showed the higher antitumor activity of Tx when administered as nanoparticles. The decrease of tumor signal and superior survival rate are highly and significantly improved when NPs are coated with anti-HER2 mAbs as targeting agent. This effect may be related to a more selective distribution of drug but also to a higher intracellular accumulation of Tx<sup>27</sup>.

---

### *3.3 Biodistribution studies*

#### *3.3.1 Biodistribution in healthy mice*

The biodistribution of Tx formulated as NPs-Tx-HER, NPs-Tx and free Tx in healthy mice was analyzed at different time points after injection of a single dose (20 mg Tx/kg) administered either IV or IP (Fig. 5). No Tx was detected in the plasma samples. Tissue concentrations were higher when Tx was administered as nanoparticles compared to free Tx with a preferential distribution in RES organs such as the liver and spleen as a consequence of the uptake of NPs by phagocytic cells<sup>24</sup>.

Even though a lower accumulation in lungs was observed when NPs were given IP compared to IV, biodistributions of NPs-Tx-HER and NPs-Tx are not significantly different. This data strongly suggests that the coating of NPs does not cause their aggregation in which case modifications in the biodistribution and the pharmacokinetics such as rapid uptake and clearance of immuno-nanoparticles by RES system would have been observed. The presence of Tx after IP injection of nanoparticles with a similar profile as after IV injection suggests that IP is an interesting route for administration of nanocarriers for cancer treatment. Furthermore, the different pattern observed when particles were administered IP compared to free Tx suggest that the resorption may have occurred as particles and not the product of drug release from the solid phase. No substantial accumulation of encapsulated Tx was observed in the heart or the kidneys.

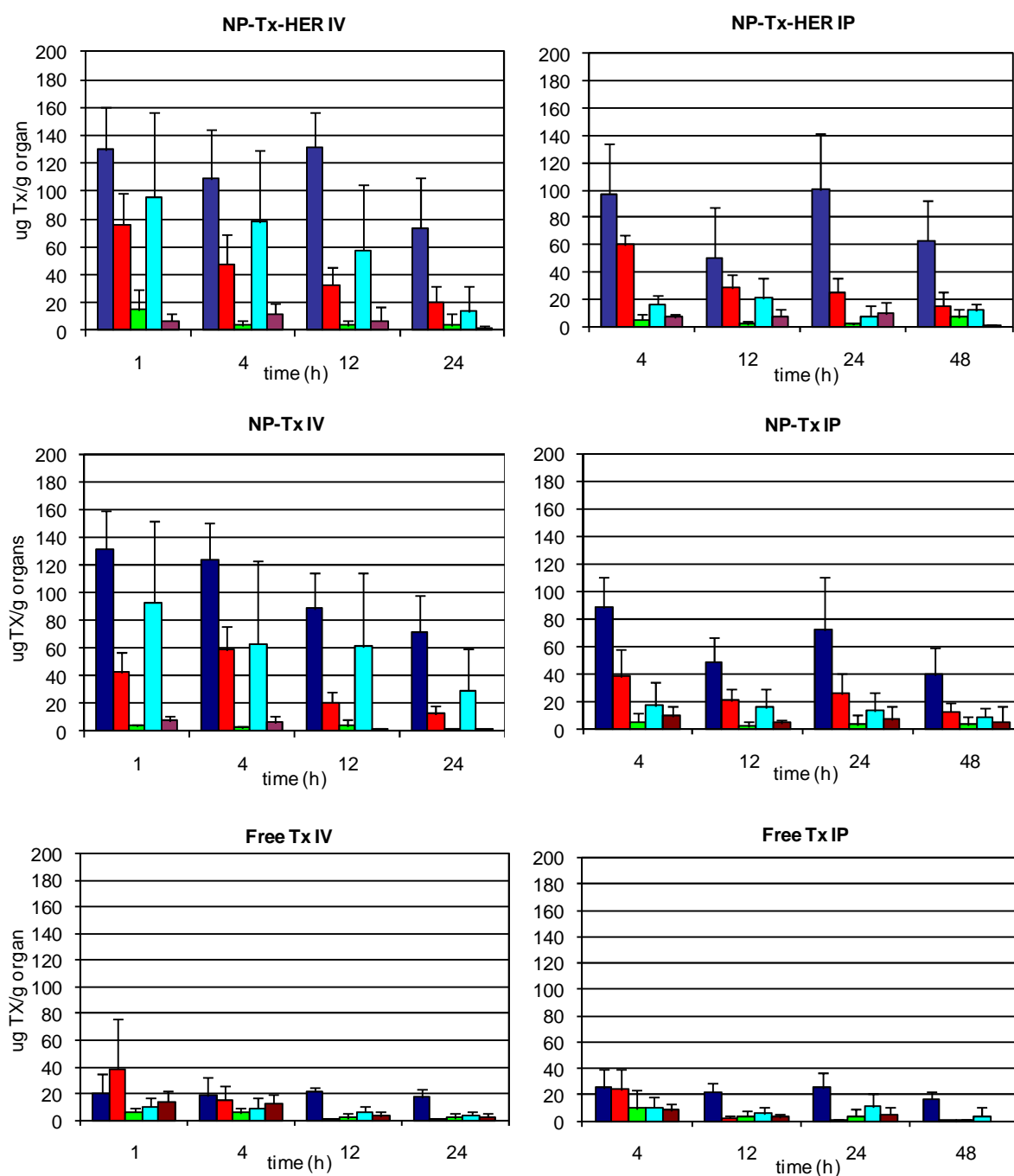


**Figure 5.** Biodistribution of NPs-Tx-HER, NP-Tx and free Tx in healthy BALB/c mice after a single dose of 20 mg Tx/kg administrated IV (left column ) or IP (right column).

Analyzed organs: spleen (■), liver (■), heart (■), lungs (■), kidneys (■).

### 3.3.2 Biodistribution in mice bearing tumors

The biodistribution was assessed at a one time point, namely, 24h after either IV or IP administration of different Tx formulations. As in healthy mice, the similar tissue distribution pattern of encapsulated Tx was observed after IV or IP administration and the Tx was not detected in the blood samples.

For IV injection a selective distribution in spleen of encapsulated Tx either in NPs-Tx-HER or NPs-Tx was observed compared to the non-specific tissue distribution of free Tx (Fig. 6a).

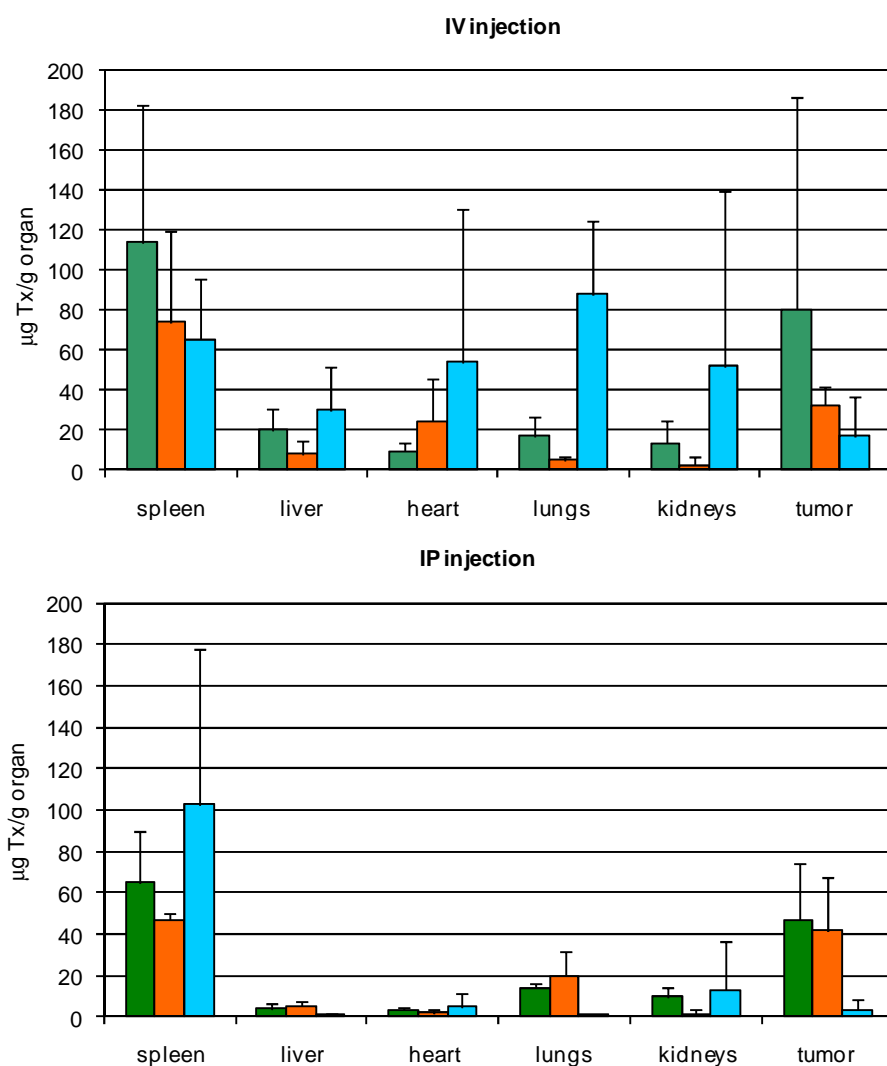


**Figure 6.** Biodistribution of Tx, 10 mg Tx/kg, 24h after a single IV (a) or IP (b) dose of NPs-Tx-HER (■), NPs-Tx (■) and free Tx (■) in mice bearing tumors. (n=3)

A higher drug accumulation in tumors was determined for encapsulated Tx compared to free Tx. Moreover, the NPs-Tx-HER showed a higher tumor accumulation than NPs-Tx. However, the difference is not statistically different due to the important variance related to the small number of animals per group.

After IP administration, Tx formulations demonstrated the same distribution profile in all tested organs (Fig. 6b). However, the tumor concentration of encapsulated Tx was 10-fold higher compared to the free Tx.

The selective tumor accumulation at similar levels of encapsulated Tx after IP or IV injection validates our strategy to combine local and systemic administration in order to better reach the tumors disseminated in the peritoneal cavity.

#### **4. Conclusions**

The combined product, associating paclitaxel encapsulated into the polymeric nanoparticles to circumvent solubility hurdle, with the surface coating, using anti-HER2 mAbs as a recognition ligand for ovarian cancer cells, resulted in a significant improvement of anticancer activity on a disseminated xenograft ovarian cancer model. This effect, assessed by two independent methods, bioluminescence and survival rate, reflects an increased biodistribution at the target site combined with a preferential internalization of the paclitaxel due to the presence of antibodies at the particle surface.

Higher tumor accumulation of encapsulated paclitaxel compared to the drug in solution was observed after IV or IP administration. Therefore, the association of regional and systemic applications is particularly interesting when the development of peritoneal micrometastasis is concerned such as for ovarian cancer. However, additional pharmacokinetic and toxicity studies are required to better understand the fate of immuno-nanoparticles and their possible adverse effects.

BLI used for tumor detection proved to be a very efficient non-invasive method to monitor tumor evolution in the disseminated ovarian cancer model and also to evaluate the pre-clinical efficacy of novel therapeutics without the need to sacrifice the animals.

To our knowledge, this is the first study demonstrating the efficacy of combined IV and IP treatment using immuno-nanoparticles.

**Acknowledgements**

The authors express their gratitude to Dr. Xavier Montet and Kerstin Grosdemange from Departement de physiologie cellulaire et metabolisme, Centre Medical Universitaire Genève, for the help in bioluminescence imaging, and to Dr. Simona Hapca from SIMBIOS Centre, University of Abertay Dundee, United Kingdom, for statistical analysis.

## Reference List

1. A. Jemal, R. Siegel, E. Ward, Y. Hao, J. Xu, T. Murray, and M. J. Thun, Cancer statistics, 2008, *CA Cancer J. Clin.* 58 (2) (2008) 71-96.
2. J. Ferlay, P. Autier, M. Boniol, M. Heanue, M. Colombet, and P. Boyle, Estimates of the cancer incidence and mortality in Europe in 2006, *Ann. Oncol.* 18 (3) (2007) 581-592.
3. S. A. Cannistra, Cancer of the ovary, *N. Engl. J. Med.* 351 (24) (2004) 2519-2529.
4. T. Safra, J. Menczer, R. M. Bernstein, S. Shpigel, D. Matcejevsky, M. J. Inbar, A. Golan, D. Grisaru, and T. Levy, Combined weekly carboplatin and paclitaxel as primary treatment of advanced epithelial ovarian carcinoma, *Gynecol. Oncol.* 114 (2) (2009) 215-218.
5. J. Pfisterer, A. du Bois, U. Wagner, J. Quaas, J. U. Blohmer, D. Wallwiener, and F. Hilpert, Docetaxel and carboplatin as first-line chemotherapy in patients with advanced gynecological tumors. A phase I/II trial of the Arbeitsgemeinschaft Gynakologische Onkologie (AGO-OVAR) Ovarian Cancer Study Group, *Gynecol. Oncol.* 92 (3) (2004) 949-956.
6. R. F. Ozols, B. N. Bundy, B. E. Greer, J. M. Fowler, D. Clarke-Pearson, R. A. Burger, R. S. Mannel, K. de Geest, E. M. Hartenbach, and R. Baergen, Phase III trial of carboplatin and paclitaxel compared with cisplatin and paclitaxel in patients with optimally resected stage III ovarian cancer: a Gynecologic Oncology Group Study, *J. Clin. Oncol.* 21 (17) (2003) 3194-3200.
7. F. M. Muggia, P. S. Braly, M. F. Brady, G. Sutton, T. H. Niemann, S. L. Lentz, R. D. Alvarez, P. R. Kucera, and J. M. Small, Phase III randomized study of cisplatin versus paclitaxel versus cisplatin and paclitaxel in patients with suboptimal stage III or IV ovarian cancer: a gynecologic oncology group study, *J. Clin. Oncol.* 18 (1) 106-115.
8. W. P. McGuire and M. Markman, Primary ovarian cancer chemotherapy: current standards of care, *Br. J. Cancer* 89 (3) (2003) S3-S8.
9. A. du Bois, and J. Pfisterer, Future options for first-line therapy of advanced ovarian cancer, *Int. J. Gynecol. Cancer* (15) (2005) 42-50.
10. E. de Bree, H. Rosing, J. Michalakis, J. Romanos, K. Relakis, P. A. Theodoropoulos, J. H. Beijnen, V. Georgoulas, and D. D. Tsiftsis, Intraperitoneal chemotherapy with taxanes for ovarian cancer with peritoneal dissemination, *Eur. J. Surg. Oncol.* 32 (6) (2006) 666-670.
11. M. Markman, Intraperitoneal antineoplastic drug delivery: rationale and results, *Lancet Oncol.* 4 (5) (2003) 277-283.
12. I. Brigger, C. Dubernet, and P. Couvreur, Nanoparticles in cancer therapy and diagnosis, *Adv. Drug Deliv. Rev.* 54 (5) (2002) 631-651.

13. K. Cho, X. Wang, S. Nie, Z. Chen, and D. M. Shin, Therapeutic Nanoparticles for Drug Delivery in Cancer, *Clin. Cancer Res.* 14 (5) (2008) 1310-1316.
14. B. Haley and E. Frenkel, Nanoparticles for drug delivery in cancer treatment, *Urol. Oncol.: Semin. Orig. Invest.* 26 (1) (2008) 57-64.
15. H. Maeda, J. Wu, T. Sawa, Y. Matsumura, and K. Hori, Tumor vascular permeability and the EPR effect in macromolecular therapeutics. A review, *J. Control. Release* 65 (1-2) (2000) 271-284.
16. M. Yokoyama, Drug targeting with nano-sized carrier systems, *J. Artif. Organs* 8 (2) (2005) 77-84.
17. A. N. Gordon, and J. Butler, Chemotherapeutic management of advanced ovarian cancer, *Semin. Oncol. Nursing* 19 (3) (2003) 3-18.
18. M. J. Hawkins, P. Soon-Shiong, and N. Desai, Protein nanoparticles as drug carriers in clinical medicine, *Adv. Drug Deliv. Rev.* 60 (8) (2008) 876-885.
19. M. G. Teneriello, P. C. Tseng, M. Crozier, C. Encarnacion, K. Hancock, M. J. Messing, K. A. Boehm, A. Williams, and L. Asmar, Phase II evaluation of nanoparticle albumin - bound paclitaxel in platinum-sensitive patients with recurrent ovarian, peritoneal, or fallopian tube cancer, *J. Clin. Oncol.* 27 (9) (2009) 1426-1431.
20. T. M. Allen, Ligand-targeted therapeutics in anticancer therapy, *Nat. Rev. Cancer* 2 (10) (2002) 750-763.
21. F. Marcucci and F. Lefoulon, Active targeting with particulate drug carriers in tumor therapy: fundamentals and recent progress, *Drug Discov. Today* 9 (5) (2004) 219-228.
22. J. D. Byrne, T. Betancourt, and L. Brannon-Peppas, Active targeting schemes for nanoparticle systems in cancer therapeutics, *Adv. Drug Delivery Rev.* 60 (15) (2008) 1615-1626.
23. P. Sapra and T. M. Allen, Ligand-targeted liposomal anticancer drugs, *Prog. Lipid Res.* 42 (5) (2003) 439-462.
24. S. M. Moghimi, A. C. Hunter, and J. C. Murray, Long-circulating and target-specific nanoparticles: theory to practice, *Pharmacol. Rev.* 53 (2) (2001) 283-318.
25. C. J. Sunderland, M. Steiert, J. E. Talmadge, A. M. Derfus, and S. E. Barry, Targeted nanoparticles for detecting and treating cancer, *Drug Dev. Res.* 67 (1) (2006) 70-93.
26. R. Nahta and F. J. Esteva, Herceptin: mechanisms of action and resistance, *Cancer Lett.* 232 (2) (2006) 123-138.
27. D. B. Kirpotin, D. C. Drummond, Y. Shao, M. R. Shalaby, K. Hong, U. B. Nielsen, J. D. Marks, C. C. Benz, and J. W. Park, Antibody targeting of long-circulating lipidic nanoparticles does not increase tumor localization but does increase internalization in animal models, *Cancer Res.* 66 (13) (2006) 6732-6740.

28. D. K. Armstrong, B. Bundy, L. Wenzel, H. Q. Huang, R. Baergen, S. Lele, L. J. Copeland, J. L. Walker, and R. A. Burger, Intraperitoneal cisplatin and paclitaxel in ovarian cancer, *N. Engl. J. Med.* 354 (1) (2006) 34-43.
29. M. Markman, Intraperitoneal drug delivery of antineoplastics, *Drugs* 61 (8) (2001) 1057-1065.
30. M. Markman, E. Rowinsky, T. Hakes, B. Reichman, W. Jones, J. L. Lewis, Jr., S. Rubin, J. Curtin, R. Barakat, and M. Phillips, Phase I trial of intraperitoneal taxol: a Gynecologic Oncology Group study, *J. Clin. Oncol.* 10 (9) (1992) 1485-1491.
31. K. Fujiwara, D. Armstrong, M. Morgan, and M. Markman, Principles and practice of intraperitoneal chemotherapy for ovarian cancer, *Int. J. Gynecol. Cancer* 17 (1) (2007) 1-20.
32. M. L. Rothenberg, P. Y. Liu, P. S. Braly, S. P. Wilczynski, E. V. Hannigan, S. Wadler, G. Stuart, C. Jiang, M. Markman, D. S. Alberts, and A. A. Garcia, Combined intraperitoneal and intravenous chemotherapy for women with optimally debulked ovarian cancer: results from an intergroup phase II trial, *Women's Oncol. Rev.* 3 (2) (2003) 149-150.
33. J. L. S. Au, S. H. Jang, J. Zheng, C. T. Chen, S. Song, L. Hu, and M. G. Wientjes, Determinants of drug delivery and transport to solid tumors, *J. Control. Release* 74 (1-3) (2001) 31-46.
34. H. Lu, B. Li, Y. Kang, W. Jiang, Q. Huang, Q. Chen, L. Li, and C. Xu, Paclitaxel nanoparticle inhibits growth of ovarian cancer xenografts and enhances lymphatic targeting, *Cancer Chemother.* 59 (2) (2007) 175-181.
35. A. K. Singla, A. Garg, and D. Aggarwal, Paclitaxel and its formulations, *Int. J. Pharm.* 235 (1-2) (2002) 179-192.
36. C. Fonseca, S. Simoes, and R. Gaspar, Paclitaxel-loaded PLGA nanoparticles: preparation, physicochemical characterization and in vitro anti-tumoral activity, *J. Control. Release* 83 (2) (2002) 273-286.
37. A. Cirstoiu-Hapca, L. Bossy-Nobs, F. Buchegger, R. Gurny, and F. Delie, Differential tumor cell targeting of anti-HER2 (Herceptin) and anti-CD20 (Mabthera) coupled nanoparticles, *Int. J. Pharm.* 331 (2) (2007) 190-196.
38. A. Cirstoiu-Hapca, F. Buchegger, L. Bossy, M. Kosinski, R. Gurny, and F. Delie, Nanomedicines for active targeting: Physico-chemical characterization of paclitaxel-loaded anti-HER2 immunonanoparticles and in vitro functional studies on target cells, *Eur. J. Pharm. Sci.* 38 (3) (2009) 230-237.
39. M. Edinger, Y. Cao, Y. S. Hornig, D. E. Jenkins, M. R. Verneris, M. H. Bachmann, R. S. Negrin, and C. H. Contag, Advancing animal models of neoplasia through in vivo bioluminescence imaging, *Eur. J. Cancer* 38 (16) (2002) 2128-2136.
40. K. Garson, T. J. Shaw, K. V. Clark, D. S. Yao, and B. C. Vanderhyden, Models of ovarian cancer - Are we there yet?, *Mol. Cell. Endocrinol.* 239 (1-2) (2005) 15-26.

- 
41. D. E. Jenkins, Y. Oei, Y. S. Hornig, S. F. Yu, J. Dusich, T. Purchio, and P. R. Contag, Bioluminescent imaging (BLI) to improve and refine traditional murine models of tumor growth and metastasis, *Clin. Exp. Metastasis* 20 (8) (2003) 733-744.
  42. D. E. Jenkins, S. Yu, Y. S. Hornig, T. Purchio, and P. R. Contag, In vivo monitoring of tumor relapse and metastasis using bioluminescent PC-3M-luc-C6 cells in murine models of human prostate cancer, *Clin. Exp. Metastasis* 20 (8) (2003) 745-756.
  43. V. Vassileva, E. H. Moriyama, R. De Souza, J. Grant, C. J. Allen, B. C. Wilson, and M. Piquette-Miller, Efficacy assessment of sustained intraperitoneal paclitaxel therapy in a murine model of ovarian cancer using bioluminescent imaging, *Br. J. Cancer* 99 (12) (2008) 2037-2043.



---

## Conclusions and perspectives

The main objective of this work was the preparation and evaluation of anti-HER2 polymeric immunonanoparticles loaded with an anticancer agent, paclitaxel (Taxol<sup>®</sup>), for active targeting of disseminated ovarian tumors overexpressing HER2 receptors.

In a preliminary study, two types of unloaded immunonanoparticles (PLA-NPs) were prepared by covalent attachment of anti-CD20 (rituximab, Mabthera<sup>®</sup>) or anti-HER2 (trastuzumab, Herceptin<sup>®</sup>) mAbs to the PLA-NPs via sulfo-MBS cross-linker. The choice of mAbs used as ligands was based on their capacity to be internalized (anti-HER2) or not (anti-CD20) after interaction with the specific receptor. Taking into account the critical role of NPs size in their ability to extravasate into target tissues and avoiding phagocytic uptake<sup>1</sup>, we have managed to obtain immunonanoparticles of about 250 nm. The proof of concept of the specific tumor targeting and cellular localization of immunonanoparticles have been demonstrated *in vitro* by confocal microscopy on an ovarian cancer cell line (SKOV-3) overexpressing HER2 receptors, and Daudi cells overexpressing CD20 receptors. While immunonanoparticles coated with anti-CD20 mAbs bound to and remained on the cellular surface, those coated with anti-HER2 were efficiently internalized via receptor mediated endocytosis. The internalization capacity is a decisive factor in the selection of targeting ligands, as it implies the possibility of delivering a drug directly into the cancer cells.

The next step focused on the development, the physico-chemical characterization and the *in vitro* studies of the effect of anti-HER2 paclitaxel-loaded immunonanoparticles (NPs-Tx-HER) on target cells.

Despite its high potential against a wide spectrum of cancers such as ovarian, breast, lung, bladder, head and neck cancer, paclitaxel (Tx) is poorly soluble in water and has a low therapeutic index, which is associated with serious side effects. Its encapsulation in nanocarrier systems allows to circumvent these limitations and to improve the therapeutic efficiency<sup>2,3</sup>.

The developed salting out method resulted in efficient Tx encapsulation in PLA-NPs of  $78 \pm 10\%$ , corresponding to a drug loading of  $7.8 \pm 0.8\%$  (w/w). Comparable physico-chemical features of unloaded and Tx-loaded immunonanoparticles demonstrated

that coupling of mAbs to the NP surface was not influenced by the presence of the drug. Moreover, no drug loss was observed during coupling reactions. The preservation of mAb immunoreactivity after activation with sulfo-MBS, an important requirement to achieve an efficient active targeting, was demonstrated on SKOV-3 cells. The higher anti-proliferative effect of immunonanoparticles at low concentrations of Tx compared to the other formulations such as free Tx or Tx-loaded immunonanoparticles with an irrelevant mAb, anti-CD20, (NPs-Tx-RIT), indicated the possibility of increasing the therapeutic index of Tx by using active targeting.

Finally, the therapeutic efficiency and the biodistribution of NPs-Tx-HER were determined in an IP xenograft model of ovarian cancer in SCID mice. The IP model was chosen due to its pathophysiological similarity to ovarian cancer, such as intraperitoneal dissemination of metastases and the presence of ascites. Bioluminescence imaging and survival rate analysis demonstrated an improved efficiency of NPs-Tx-HER compared to other formulations such as free Tx or NPs-Tx-RIT. In the biodistribution studies, similar concentrations of encapsulated Tx were found in tumors, after both IV or IP injections. The combined or alternative IV/IP administration seems, at this stage of our work, a good strategy to improve the treatment of tumors and micrometastasis in ovarian cancer.

In this study we have demonstrated the possibility of improving the anticancer drug efficacy by active targeting using immunonanoparticles. The proof of concept was assessed using anti-HER2 paclitaxel-loaded immunonanoparticles directed against ovarian cancer overexpressing HER2 receptors in a disseminated IP xenograft model in SCID mice. To our knowledge, this is the first study demonstrating the antitumor efficiency of combined IV and IP treatment using immunonanoparticles.

New perspectives could be envisaged to improve the formulation of NPs-Tx-HER and their therapeutic efficiency in ovarian cancer treatment. In this way, the PEG-ylated polymers may be used to obtain a longer circulation time of immunonanoparticles and the entire mAb could be replaced with fragments to reduce the immunogenic risk. Pharmacokinetic and toxicological studies could be designed to better understand the fate of eventual toxic effects of immunonanoparticles in the organism. Moreover, a total recovery of mice bearing tumors

could be attempted by increasing the administered dose of drug and/or prolonging the treatment period.

The possibilities of encapsulating various drugs and attaching other mAbs on the NPs-PLA surface allow the design of a wide variety of immunonanoparticles for personalized and tailored cancer treatments.

---

**Reference list**

1. Gaumet, M., Vargas, A., Gurny, R. & Delie, F. Nanoparticles for drug delivery: The need for precision in reporting particle size parameters. *Eur. J. Pharm. Biopharm.*, 69, 1-9, 2008.
2. Desai, N. P., Trieu, V., Hwang, L. Y., Wu, R., Soon-Shiong, P. & Gradishar, W. J. Improved effectiveness of nanoparticle albumin-bound (nab) paclitaxel versus polysorbate-based docetaxel in multiple xenografts as a function of HER2 and SPARC status. *Anti-Cancer Drugs*, 19, 899-909, 2008.
3. Teneriello, M. G., Tseng, P. C., Crozier, M., Encarnacion, C., Hancock, K., Messing, M. J., Boehm, K. A., Williams, A. & Asmar, L. Phase II evaluation of nanoparticle albumin - bound paclitaxel in platinum-sensitive patients with recurrent ovarian, peritoneal, or fallopian tube cancer. *J. Clin. Oncol.*, 27, 1426-1431, 2009.



## Résumé

Le cancer est une des plus importante cause de mortalité dans le monde. Malgré leur efficacité reconnue, le succès des traitements chimiothérapeutiques du cancer reste encore limité par les multiples effets secondaires qui leur sont associés. Ces effets secondaires sont en partie liés à un manque de spécificité dans la biodistribution des agents cytotoxiques. De ce fait, leur activité cytotoxique s'exerce autant sur les tissus sains que sur les cellules malignes. Ces effets secondaires sont donc plus souvent rencontrés avec les tissus à taux de renouvellement élevés engendrant des troubles tels que myélosuppression, neuropathie périphérique, trouble cardiaque, effet thrombotique sévère, manifestation gastro-intestinale, alopecie, etc. De plus, en raison de leur élimination rapide, l'administration de doses élevées de médicaments est souvent nécessaire pour avoir une efficacité thérapeutique.

Le ciblage actif des tumeurs suscite beaucoup d'intérêt en vue d'obtenir une biodistribution plus favorable des principes actifs chimiotoxiques. Cette approche prend en compte la surexpression de certaines molécules à la surface des cellules tumorales. En général, les cellules sont caractérisées par l'expression à leur surface de protéines telles que des récepteurs, des enzymes ou des transporteurs. Les cellules tumorales se distinguent des tissus sains par l'expression ou la surexpression de protéines spécifiques qui peuvent être utilisées comme cibles pour différents ligands <sup>1</sup>. L'utilisation de ligands spécifiques permettant de reconnaître des récepteurs de surface des cellules cancéreuses est une approche thérapeutique prometteuse qui a vu son développement couronné de succès en particulier dans le cas des anticorps monoclonaux tel que l'Erbix<sup>®</sup> (cetuximab), l'Avastin<sup>®</sup> (bevacizumab), le Gleevec<sup>®</sup> (imatinib), ou encore l'Herceptin<sup>®</sup> (trastuzumab) ou le Mabthera<sup>®</sup> (rituximab) <sup>2</sup>. Pour favoriser la biodistribution d'un principe actif anticancéreux au sein de la tumeur, il est possible de cibler sélectivement ces cellules en développant une approche où le principe actif est associé à un ou plusieurs anticorps capables d'identifier l'antigène à la surface de cellules. Le principe actif est alors dirigé spécifiquement vers sa cible, la distribution vers les tissus sains est réduite et l'efficacité thérapeutique améliorée <sup>3</sup>.

Par ailleurs, une alternative pour diminuer les effets indésirables et améliorer l'efficacité des médicaments anticancéreux est l'utilisation de vecteurs comme les nanoparticules polymériques. Les nanoparticules sont les particules submicroniques faites d'une matrice

polymère dans laquelle le principe actif est soit adsorbé à la surface ou dispersé à l'intérieur de la matrice <sup>4</sup>. Cette stratégie permet, d'une part, d'apporter une solution à la formulation de molécules peu solubles en milieu aqueux tout en offrant l'opportunité de fournir un système réservoir libérant la molécule active selon une cinétique contrôlée. En outre, les nanoparticules polymériques bénéficient d'une biodistribution préférentielle au niveau tumoral encore appelé ciblage passif. En effet, la présence de fenestrations au niveau de la vascularisation tumorale et le drainage lymphatique restreint qui caractérise les tissus tumoraux, phénomène connu sous le nom de "enhanced permeation and retention effect (EPR)" favorise la rétention de particules de diamètre entre 200 et 700 nm au sein des tumeurs <sup>5</sup>.

Le développement d'immunonanoparticules chargées en anticancéreux et dont la surface est recouverte d'anticorps spécifiques d'une tumeur donnée permet de combiner les potentialités de ciblage passif par l'emploi de particules de faible diamètre et celui de la reconnaissance anticorps/antigène.

L'objectif principal de ce travail de thèse a été de développer et d'évaluer l'efficacité d'un nouveau traitement du cancer ovarien par ciblage actif de la tumeur, en utilisant des immunonanoparticules polymériques biodégradables chargées en anticancéreux.

Le cancer de l'ovaire est, de tous les cancers gynécologiques, celui qui présente le taux de mortalité le plus élevé. Le traitement standard consiste en une laparotomie initiale pour enlever la masse tumorale souvent accompagnée de multiples micrométastases envahissant la cavité abdominale suivie d'une chimiothérapie. La difficulté d'éradiquer ces métastases entraîne la mort dans plus de 50% des cas. Les immunonanoparticules permettant un meilleur ciblage de la tumeur primaire et des micrométastases grâce à la reconnaissance antigène/anticorps représentent une approche prometteuse pour améliorer le traitement.

Dans un premier temps, des études préliminaires ont permis de mettre au point deux types d'immunonanoparticules à base d'acide poly(lactique) fonctionnalisées avec différents anticorps monoclonaux: Herceptin<sup>®</sup> (trastuzumab, anti-HER2) internalisé après l'interaction avec le récepteur spécifique et Mabthera<sup>®</sup> (rituximab, anti-CD20) non-internalisé. La taille des particules étant un paramètre crucial dans le mécanisme de capture par les macrophages et la biodistribution <sup>5</sup>, nous avons pu obtenir des immunonanoparticules d'environ 250 nm

censées éviter leur élimination rapide de l'organisme tout en favorisant l'accumulation dans le tissu tumoral.

La fixation spécifique et la localisation cellulaire des immunonanoparticules ayant à leur surface des anticorps spécifiques, anti-HER2 ou anti-CD20, ont été démontrées *in vitro* par microscopie confocale sur les cellules SKOV3 (exprimant des antigènes HER2) et Daudi (exprimant des antigènes CD20). L'internalisation des immunonanoparticules fonctionnalisées avec anti-HER2 a été mise en évidence, alors que celles fonctionnalisées avec le anti-CD20 restent à la surface des cellules. L'internalisation est un facteur décisif dans la sélection des cibles tumorales et leurs ligands spécifiques grâce à la capacité de distribution intracellulaire du médicament encapsulé.

Dans une deuxième étape nous avons mis au point et caractérisé des immunonanoparticules chargées en paclitaxel (Tx) et recouvertes des anticorps monoclonaux anti-HER2 (NPs-Tx-HER). Le paclitaxel (Taxol<sup>®</sup>) est un médicament anticancéreux dont l'efficacité thérapeutique est démontrée dans le traitement de plusieurs types de cancers, comme le cancer de l'ovaire, du sein, du poumon ou le sarcome de Kaposi. Malgré les propriétés antitumorales, son utilisation en clinique reste limitée à cause d'une biodistribution non spécifique et ses nombreux effets secondaires en partie liés au véhicule utilisé pour améliorer sa solubilité. Ainsi l'encapsulation du Tx dans les immunonanoparticules permettrait de le transporter plus efficacement jusqu'aux cellules cancéreuses tout en diminuant les effets secondaires et en évitant l'administration de solvants et co-solvants souvent responsables d'intolérances.

Un taux d'encapsulation de  $78 \pm 10\%$  a pu être obtenu par la méthode dite de « salting out ». La présence de Tx dans les NPs n'a pas eu d'influence sur les réactions de couplage des anticorps, démontrée par les caractéristiques physico-chimiques similaires des nanoparticules chargées et non chargées en principe actif. Aucun relargage du Tx pendant les réactions de couplage n'a pas été observé. Les études *in vitro* sur les cellules SKOV-3 ont démontré la préservation de l'immunoreactivité d'anticorps après l'activation avec le sulfo-MBS, condition nécessaire pour accomplir le ciblage actif. L'efficacité supérieure des NPs-Tx-HER comparée au Tx libre et aux NPs chargées en Tx sans anticorps à la surface ou recouvertes d'un anticorps non spécifique, anti-CD20, (NPs-Tx-RIT) a pu être mise en évidence.

Ces résultats encourageants ont permis de continuer dans une étape finale et la plus importante du projet, l'évaluation *in vivo* de l'efficacité des NPs-Tx-HER dans un modèle

---

intraperitoneal de cancer ovarien chez les souris SCID. Ce modèle a été choisi en raison de sa ressemblance avec la physiopathologie clinique du cancer ovarien qui implique le développement des micrométastases confinées à la cavité péritonéale et la présence d'ascite. La meilleure efficacité thérapeutique des NPs-Tx-HER comparée aux Tx libre ou NPs-Tx-RIT a été démontrée par l'augmentation de la survie. L'imagerie par bioluminescence nous a permis de mettre en évidence une diminution plus importante de la taille des tumeurs ou, voir leur disparition suite au traitement avec NPs-Tx-HER comparé au médicament libre. L'accumulation tumorale spécifique du Tx encapsulé après l'administration intraveineuse ou intrapéritonéale représente un avantage certain dans le traitement du cancer ovarien. L'administration concomitante ou alternative IV/IP semble, à ce stade de notre travail, une stratégie d'améliorer le traitement des tumeurs et micrométastases du cancer ovarien.

Cette étude nous a permis de démontrer la remarquable efficacité des NPs-Tx-HER dans le ciblage actif des tumeurs ovariennes surexprimant des récepteurs HER2. A notre connaissance il s'agit de la première étude montrant l'activité antitumorale des immunonanoparticules à l'aide d'un traitement combiné intraveineux (IV) et intraperitoneal (IP).

Des nouvelles perspectives pourraient être envisagées en vue d'améliorer la formulation des nanoparticules anti-HER2 chargées en paclitaxel et leur effet thérapeutique. Dans ce sens l'utilisation des polymères PEG-ylés permettraient d'obtenir un temps de circulation plus long, ou, pour minimaliser le risque des réactions immunologiques, les anticorps monoclonaux pourraient être remplacés avec leurs fragments. Des études de pharmacocinétique et toxicologie seront très utiles pour mieux comprendre le sort de ces immunonanoparticules dans l'organisme. Concernant l'efficacité thérapeutique, l'administration des doses du Tx plus fortes et/ou un traitement plus long pourrait être tenter pour obtenir une rémission totale des tumeurs chez les souris.

La stratégie d'encapsuler différentes molécules actives dans les nanoparticules et d'utiliser d'autres anticorps monoclonaux comme ligands ouvre des perspectives particulièrement intéressantes pour créer des traitements adaptés et personnalisés aux différents types de cancer.

**Reference List**

1. Byrne, J. D., Betancourt, T. & Brannon-Peppas, L. Active targeting schemes for nanoparticle systems in cancer therapeutics. *Adv. Drug Deliv. Rev.* 60, 1615-1626, 2008.
2. Reichert, J. M. Monoclonal antibodies as innovative therapeutics. *Curr. Pharm. Biotechnol.* 9, 423-430, 2008.
3. Jaracz, S., Kuznetsova, L. V. & Ojima, I. Recent advances in tumor-targeting anticancer drug conjugates. *Bioorg. Med. Chem.* 13, 5043-5054, 2005.
4. Allemann, E., Gurny, R. & Doelker, E. Drug-loaded nanoparticles. Preparation methods and drug targeting issues. *Eur. J. Pharm. Biopharm.* 39, 173-191, 1993.
5. Brigger, I., Dubernet, C. & Couvreur, P. Nanoparticles in cancer therapy and diagnosis. *Adv. Drug Deliv. Rev.* 54, 631-651, 2002.



---

### List of abbreviations

|               |  |
|---------------|--|
| ADCC          | antibody-dependent cellular cytotoxicity                                 |
| anti-HER2 NPs | modified NPs with anti-HER2 monoclonal antibody                          |
| anti-CD20 NPs | modified NPs with anti-CD20 monoclonal antibody                          |
| BLI           | bioluminescence imaging  |
| CDC           | complement-dependent cytotoxicity  |
| CHOP          | combination of cyclophosphamide, doxorubicin, vincristine and prednisone |
| DSC           | differential scanning calorimetric analysis                              |
| EDAC          | 1-Ethyl-3-(3-dimethylaminopropyl)-carbodiimide                           |
| EPR effect    | enhanced permeability and retention effect                               |
| FDA           | United States Food and Drug Administration                               |
| FR            | Folate receptor  |
| IP            | intraperitoneal  |
| IV            | intravenous  |
| mAb           | monoclonal antibody  |
| MPS           | mononuclear phagocytic system  |
| NCE           | new chemical entity  |
| NP            | nanoparticle   |
| NPs-SH        | thiolated nanoparticles  |
| NPs-Tx        | paclitaxel-loaded poly (DL-lactic acid)                                  |
| NPs-HER       | anti-HER2 immunonanoparticles  |
| NPs-Tx-SH     | thiolated paclitaxel loaded NPs  |
| NPs-Tx-HER    | Paclitaxel-loaded anti-HER2 immunonanoparticles                          |
| NPs-Tx-RIT    | Paclitaxel-loaded anti-CD-20 immunonanoparticles                         |
| PCS           | photon correlation spectroscopy  |
| PEG           | poly ethylene glycol   |
| PLA           | Poly (DL-lactic acid)  |
| PLA-NPs       | Poly (DL-lactic acid) nanoparticles                                      |
| P.I.          | Polydispersity index   |
| PBS           | phosphate buffer saline  |

---

|           |   |
|-----------|---|
| PVAL      | poly (vinyl alcohol)                                    |
| RES       | reticulo-endothelial system                             |
| SCID mice | sever combined immunodeficient mice                     |
| SELEX     | systemic evolution of ligands by exponential enrichment |
| SEM       | scanning electron microscopy                            |
| -SH       | thiol groups  |
| Sulfo-MBS | m-maleimidobenzoyl-N-hydroxy-sulfosuccinimide ester     |
| Tx        | paclitaxel  |
| TCEP      | Tris (2-carboxyethyl)-phosphine hydrochloride           |

